NASA CONTRACTOR REPORT

NASA CR-7

C. 1

NASA CR-719

A THEORETICAL INVESTIGATION OF THE AERODYNAMICS OF SLENDER WING-BODY COMBINATIONS EXHIBITING LEADING-EDGE SEPARATION

by Alvin H. Sacks, Raymond E. Lundberg, and Charles W. Hanson

Prepared by
ITEK CORPORATION
Palo Alto, Calif.
for Ames Research Center

NATIONAL AERONAUTICS AND SPACE ADMINISTRATION • WASHINGTON, D. C. • MARCH 1967

NASA CR-719

A THEORETICAL INVESTIGATION OF THE AERODYNAMICS OF SLENDER WING-BODY COMBINATIONS EXHIBITING LEADING-EDGE SEPARATION

By Alvin H. Sacks, Raymond E. Lundberg,
and Charles W. Hanson

Prepared under Contract No. NAS 2-2620 by
ITEK CORPORATION
Palo Alto, Calif.

for Ames Research Center

NATIONAL AERONAUTICS AND SPACE ADMINISTRATION

For sale by the Clearinghouse for Federal Scientific and Technical Information
Springfield, Virginia 22151 – Price $3.00

TABLE OF CONTENTS

LIST OF SYMBOLS

a	local body radius
A	aspect ratio
B	$Va(da/dx)$
c_r	wing root chord
c_l	location of moment center
C_m	pitching-moment coefficient, $\frac{M}{\frac{1}{2}\rho V^2 S_r \ell_r}$
C_N	normal-force coefficient, $\frac{N}{\frac{1}{2}\rho V^2 S_r}$
C_{L_α}	lift curve slope
C.P.	center of pressure (percent of root chord)
$g(x)$	function related to lift per unit chord which is sought in Lawrence technique (see Eq. (8))
$g'(x)$	$\frac{d}{dx}\left[g(x)\right]$
$k(x)$	known function proportional to lift ahead of station x (see Eq. (11))
L	lift
ℓ	local loading
ℓ_r	reference length
M	pitching moment
n	number of vortex pairs shed up to the chordwise station in question
N	normal force, $N_{att} + N_s$
r_o	radius of transformed circle, $\frac{1}{2}\left(s + \frac{a^2}{s}\right)$
s	total local semispan
S_r	reference area

u	discontinuity in x component of the perturbation velocity across x-y plane
v	velocity component in the y direction
v_i	lateral velocity at the edge of the wing
v_k, w_k	velocity components of the k^{th} shed vortex
V	free-stream velocity
V_c	crossflow velocity at location of the wing edge
w	velocity component in the z direction
W	complex potential in the crossflow plane
W^1	$W - B \ell n \zeta$
x,y,z	body axes defined in sketch on page 10
α	angle of attack
γ	circulation per unit length of flat vortex-sheet segment shed at each chordwise station
Γ_i	circulation strength of i^{th} discrete shed vortex
δ	lateral distance from wing edge to position of n^{th} discrete shed vortex
δ_i	length of flat vortex-sheet segment in the transformed σ plane
Δs	length of flat vortex-sheet segment measured in the y direction
ΔL	incremental lift acting on a segment of the wing-body combination of length Δx
ζ	$y + iz$
ρ	fluid mass density
σ	complex coordinate in the transformed (circle) plane
ϕ	perturbation velocity potential

Subscripts and Special Notations

att	attached flow
ℓ	lower surface
Lawr.	Lawrence theory of Reference 16 or 27
n	pertaining to the vortex shed at that chordwise station
R	real part
s	separated flow
SB	slender-body theory
u	upper surface
xx,yy,zz	second derivatives with respect to x,y,z
$(\overline{\ })$	complex conjugate
96	96 vortex pairs used in calculation

A THEORETICAL INVESTIGATION OF THE AERODYNAMICS OF SLENDER WING-BODY COMBINATIONS EXHIBITING LEADING-EDGE SEPARATION

By A. H. Sacks, R. E. Lundberg
and C. W. Hanson
Vidya Division, Itek Corporation

SUMMARY

A theoretical analysis is presented for calculating the normal force and center of pressure on plane wing-body combinations exhibiting leading-edge separation. The mathematical model for the separated flow involves the shedding of a number of discrete vortex pairs along the wing leading edge, each pair satisfying the Kutta condition at the position of shedding. The subsequent lateral positions of these vortex filaments are calculated step by step, so that the rolling up of the vortex sheet is taken into account. Hence, the method predicts the chordwise normal-force distributions as well as the vortex sheet shapes over the configuration.

Two techniques are presented for predicting the rate of shedding of vorticity along the wing leading edge. A purely theoretical method is presented which predicts the shedding rate analytically but which is restricted to very slender configurations. An alternative semi-empirical method is also presented which utilizes delta-wing experimental data to predict the shedding rates on wings of general planform and on wing-body combinations.

Numerical calculations have been carried out for wings and wing-bodies in the range of aspect ratios 0.5 to 2.0. The semi-empirical method was well behaved in all cases, but convergence appeared to deteriorate for the theoretical method as the aspect ratio increased. The theoretical method overpredicts the nonlinear separated normal force, particularly for aspect ratios above 1.0. However, the semi-empirical technique yields satisfactory agreement with experiment for both normal force and center of pressure on the wings and wing-body combinations investigated.

INTRODUCTION

In aircraft which are designed for sustained flight at supersonic speeds, two general characteristics have evolved: the configurations are slender, having a narrow fuselage and highly swept wings; and the leading edges of the wings are sharpened. Both of these characteristics are prompted by an attempt to minimize aerodynamic drag during the supersonic cruise. When such aircraft are operated at low speeds and high angles of attack, as during the landing maneuver, the flow separates from the sharp leading edges and vortices form above the wing surface. Aerodynamically, the vortex formation results in an increase of the lift from that attained when the flow remains attached to the upper surface. Furthermore, the variation of lift coefficient with angle of attack becomes nonlinear.

A simplified, qualitative picture of the flow field about a sharp leading-edged delta wing is presented in Figure 1. The boundary layer separates at the sharp leading edge, forming a vortex sheet which rolls up into a spiral over the top surface of the wing. For delta wings, a sheet is shed from the leading edge on each side and the flow pattern is, in the absence of yaw, symmetric. This picture is, admittedly, an oversimplification; secondary and even tertiary vortices have been noted over the top surface of separated delta wings.

The objective of the present investigation is to develop methods for predicting the aerodynamic characteristics of slender aircraft when flow separation is present. The prediction of aerodynamic characteristics, as used here, is taken to mean the calculation of lift (or, more properly, normal force) coefficient and pitching-moment coefficient or aerodynamic center of pressure. Since the basic flow model considered is inviscid, and since leading-edge suction is precluded by flow separation, the chordwise force is zero, and the lift and drag are simply the vertical and horizontal components of the normal force.

PREVIOUS INVESTIGATIONS

Experimental

The aerodynamic behavior of swept wings has been a subject of considerable interest for a number of years, and numerous experimental investigations have been undertaken. These investigations have sought not only to

tabulate aerodynamic coefficients but to explore in detail the flow field about the wing. Because of their inherent simplicity, delta wings represent the planforms to which most attention has been devoted.

Jasslion and Trilling (Ref. 1) have made detailed probe measurements in the flow field over delta wings. Bergerson and Porter (Ref. 2) use smoke traces and a light slit technique to locate vortex core positions on an aspect ratio one delta wing and some studies of the flow field downstream of the trailing edge are also included. Recently, Hummel (Ref. 3) reported on the use of oil traces, tuft grids and smoke pictures, including some studies on the effects of yaw.

The basic flow pattern is illustrated by Figure 1. It will be noted that the details of the actual physical flow are somewhat more complicated (as pointed out, for example, by Ref. 2), and it is still unclear whether secondary flows are significant in determining performance. However, even for considerable yaw, the flow pattern is basically steady. At high angles of attack, an unstable phenomenon called "vortex bursting" occurs, in which the vortex field appears to decay to another state characterized by lower local rotational velocities but a larger extent of influence. This bursting phenomenon is not considered in the development presented herein.

For wing-body combinations far less effort has been made. Under certain flow conditions, the position of the vortex centers (or more accurately, centers of vorticity), which are low-pressure regions are visible due to moisture condensation, and no smoke or other visualization techniques are necessary. A considerable amount of work of this type has been conducted by Ames Research Center in connection with the tests of Reference 4 on a double delta wing-body combination. These studies indicate that more than one distinct vortex system can be formed if there are abrupt changes in wing leading-edge sweep. Wentz and McMahon (Ref. 5) have taken very detailed velocity probe measurements of the flow field around a double delta wing-body combination. It should be noted that Wentz' measurements do not reveal the dual vortex system illustrated by the Ames photos.

Most of the investigations referenced above also present some data on aerodynamic coefficients. In addition, LaVallee (Ref. 6) has taken data on sharp-edged delta wings, and Bartlett and Vidal (Ref. 7) present detailed lift and moment data for low aspect ratio wings with and without leading-edge separation.

Theoretical

The essence of classical aerodynamic theory is embodied in efforts to solve the linearized potential equation

$$(1 - M_o^2)\phi_{xx} + \phi_{yy} + \phi_{zz} = 0 \qquad (1)$$

where ϕ is the perturbation velocity potential and M_o is the free-stream Mach number. If an aircraft is sufficiently slender, then the axial variation of axial velocity is much smaller than the lateral variations of lateral velocities; that is,

$$\phi_{xx} << \phi_{yy} \text{ and } \phi_{zz}$$

and Equation (1) may be simplified to

$$\phi_{yy} + \phi_{zz} = 0 \qquad (2)$$

Hence, obtaining a mathematical description of the flow pattern reduces to finding solutions to Laplace's equation, satisfying appropriate boundary conditions in the y-z or crossflow plane. Any dependence of the resulting solution on axial shape variations is permitted to enter only through the boundary conditions.

The assumptions leading to Equation (2), and the application of these assumptions to a prediction of aerodynamic characteristics of a thin flat wing were described by Jones (Ref. 8). Since the flow field, under the slenderness assumption, can be described by a succession of two-dimensional flow fields, the concept of the complex potential and mapping techniques can be applied to generalize the approach of Jones. This generalization was first presented by Spreiter (Ref. 9), and was subsequently extended to include very general classes of wings and wing-body combinations (see Ref. 10).

Attached flow (low α).- Even if one can neglect the effects of separation and vorticity on the aerodynamic characteristics of aircraft, slender-body theory still exhibits a serious defect; it yields correct results only for vanishing aspect ratios. For thin flat-plate wings, slender-body theory predicts a linear lift curve having a slope, C_{L_α}, of $\pi A/2$. Figure 2a shows a comparison of the predicted values with experimental results for

flat-plate delta wings as reported by Lange/Wacke, Reference 11, and by Bartlett and Vidal, Reference 7. It can be seen that even at an aspect ratio of unity, slender-body theory overpredicts the linear (attached-flow) lift by 30 percent, and the discrepancy rapidly becomes greater as the aspect ratio increases. Basically, this difference occurs because, for the flow field around a finite-aspect-ratio wing, neglecting accelerations in the stream direction is simply not justified; that is, the flow field is truly three-dimensional except for vanishing aspect ratios.

For high-aspect-ratio wings, the classical lifting-line theory of Prandtl (Ref. 12) is quite successful in predicting lift up to the stall; however, the restrictions on wing shape are quite severe and no information regarding center of pressure is obtained. A generalization of lifting-line theory is the lifting-surface theory, which escapes some of the restrictions but results in considerable computational complexity. Two well-known examples of lifting-surface theory are the work of Multhopp and Truckenbrodt, References 13 and 14.

When the aircraft under consideration is reasonably slender, a considerable simplification can be effected in lifting-surface theory by incorporating certain features of slender-body theory. Two quite similar approaches to this "not-so-slender-body" theory are presented by Lomax and Sluder, Reference 15, and by Lawrence, Reference 16. Lift curve slope predictions from both of these methods are also shown in Figure 2. Either method is quite successful at predicting attached-flow lift for delta wings, for aspect ratios up to 3 or 4.

Separated flow (high α).- A number of theories have actually been developed for calculating the total lift on slender, flat-plate wings exhibiting leading-edge separation. However, most of these have been restricted to conical flows and are not readily extended to either arbitrary planforms or wing-body combinations.

The theory of Brown and Michael (Ref. 17) contains the essential elements of a number of recent papers (e.g., Refs. 18, 19, and 20). The analysis is confined to triangular wings of low aspect ratio and makes use of the slender-body approximation discussed on the previous page. With this approximation, the total lift is given by (see Ref. 17)

$$L = -\rho V \int_C \phi \, dy \qquad (3)$$

where the contour c encloses the trailing-edge cross section of the wing and the vortex sheets. Thus, the lift is linear in the potential ϕ and is therefore composed of two parts; one being the usual slender-body lift (which is linear in α), and one being the additional lift due to the potential associated with the separated vortices.

The model proposed by Brown and Michael is illustrated in the following sketch.

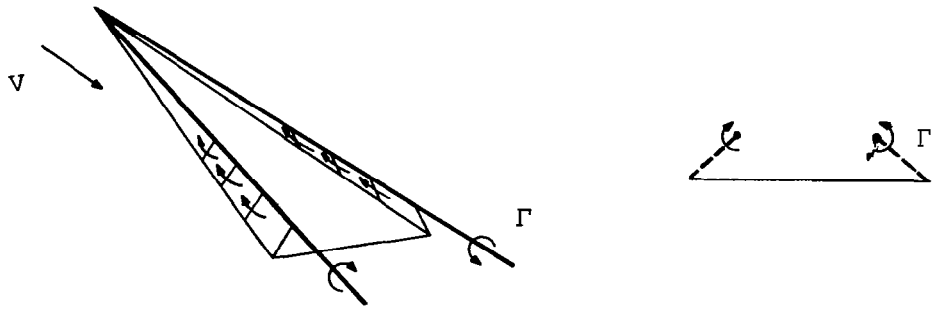

It is assumed that all of the trailing vorticity above the wing is concentrated in two fully rolled-up vortices whose strengths vary linearly in the chordwise direction. The contribution of the feeding vortex sheets (between the wing leading-edges and the rolled-up vortices) to the complex potential in the cross-flow plane is neglected. However, since the feeding vortices shed from the leading edge lie almost normal to the free stream (rather than along the streamlines) they must sustain a force. The condition that the shed vortex system be force-free everywhere is therefore approximated by requiring that the net force on the entire vortex system be zero. In this manner, with the Kutta condition imposed at the leading edges, Brown and Michael proceed to solve for the vortex strengths Γ and the vortex positions, and thereby calculate the total lift and drag, as well as the spanwise load distribution.

The lift curve calculated by the above method agrees well with experiment only for extremely low aspect ratios (small apex angles) and the predicted high peaks in the pressure distribution are not realized because the streamwise vorticity is actually distributed throughout the feeding sheet rather than being concentrated in two discrete vortices.

A somewhat more general treatment of the slender triangular wing with leading-edge separation has been developed by Mangler and Smith (Ref. 21) who consider a more realistic shape of the vortex sheets and calculate the lateral distribution of streamwise circulation within the sheet, accounting approximately for the requirement of no force on the sheet and no flow through it (see sketch).

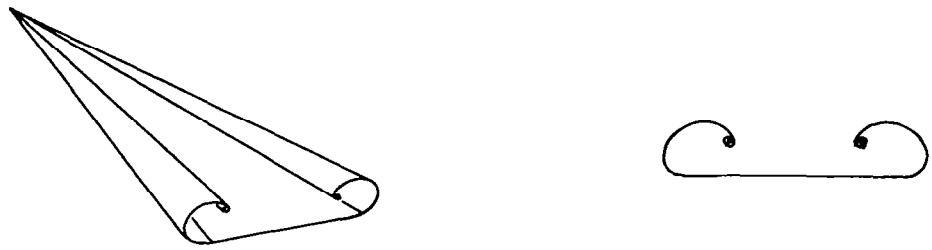

However, the flow is still assumed to be conical (resulting in a center of pressure at the two-thirds root chord position), and the severe limitation on aspect ratio remains.

More recently, two papers have appeared which attempt to treat swept-back wings of arbitrary aspect ratio and general planform with leading-edge separation. The first of these, by Gersten (Ref. 22) assumes that vortices are shed over the entire wing surface at an angle of $\alpha/2$ above the chord plane. This is the angle predicted by the theory of Bollay (Ref. 23) for rectangular wings of vanishing aspect ratio. By satisfying the boundary condition of no flow through the surface at a number of points along the span, Gersten solves for the loading distribution on a number of lifting lines representing the wing surface. In this manner, one can calculate the total normal force and pitching moment. Gersten's model effectively assumes that steady flow separation occurs over the entire upper surface of the wing. Although this assumption is difficult to justify, the results do show reasonably good agreement with experimental data for rectangular and delta wings of aspect ratios between about 0.5 and 3.0.

The two major objections to Gersten's theory are: (1) the assumption of separation over the entire upper surface, and (2) the assumption that the shedding angle is constant at $\alpha/2$. Both of these objections are overcome in the theory of Reference 24 in which separation is permitted only at the

wing edges, and the angle of shedding is calculated by requiring that the separation vortices lie along the local streamlines at the wing edges. Unfortunately, the calculated shedding angles do not agree well with experiment, and agreement with experiment on the normal force and center of pressure are obtained only by selecting the shedding angle which is a function of the aspect ratio, angle of attack, and planform. It should be mentioned that here again, even for high aspect ratios, the lift is found to be composed of a linear (attached-flow) solution and an additive nonlinear (separated-flow) solution.

Evidently, a major difficulty in the two mathematical treatments discussed above lies in the failure to allow the vortex sheets to roll up after they leave the wing. To be sure, this omission is intentional for reasons of mathematical tractability. However, it is known from experimental observations that the vortex sheets roll up quite rapidly, particularly for the lower aspect ratios. The low-aspect-ratio theories of Brown and Michael and Mangler and Smith attempt to account for this phenomenon by making simplifying assumptions regarding the nature of the rolled-up vortex sheets.

It would seem, then, that what is needed is a theoretical model which permits the vortex sheets to roll up freely without the restrictions of concentrated vortex cores or conical flows. This is the aim of the present theoretical analysis.

APPROACH TO THE PROBLEM

The preceding discussion indicates that there are two distinct facets to the prediction of the aerodynamic characteristics of low-aspect-ratio aircraft experiencing leading-edge separation; the prediction of the linear (attached-flow) lift characteristics, and the nonlinear (separated-flow) contribution to the resultant aerodynamic forces. The approach taken in the present work is to assume that these two contributions, linear lift and separated lift, are separable and additive. That is, we presume that

$$(C_L)_{\text{total}} = (C_L)_{\text{att}} + (C_L)_{\text{s}} \tag{4}$$

The idea of an additive component of lift, at finite angles of attack, to account for lift-curve nonlinearities was perhaps first presented by Betz

(Ref. 25), who introduced the concept of the "cross-flow drag coefficient." Within the assumptions of slender-body theory, for any number of discrete vortices in the flow field, Equation (4) results from a rigorous derivation of the body forces on a general aircraft (see Ref. 26).

The attached-flow lift characteristics are predicted using the integral equation method of Lawrence presented in References 16 and 27. A description of the method is given in the following section; the numerical technique for solving the integral equation is outlined in Appendix A.

The flow-field vorticity associated with separation is represented by a number of discrete line vortices using the concepts of slender-body theory to calculate the resultant forces. The flow model is described on page 13, and methods for determining the rate of addition (shedding) of vorticity to the flow field are discussed on pages 17 through 28.

THEORETICAL ANALYSIS

Attached Flow

The technique presented here for the linear (attached-flow) lifting characteristics of low-aspect-ratio wings is that due to Lawrence, Reference 16. The present discussion will be restricted to the wing-alone case, since the extension to wing-body combinations (presented by Lawrence in Ref. 27) results in only very minor changes in the computational procedure. It should be noted, however, that the method is not valid where the wing span is decreasing with x.

At low Mach numbers, the linearized potential equation (Eq. (1)) reduces to Laplace's equation in three dimensions. We are interested in a solution to Laplace's equation for the steady motion of a thin airfoil, lying in the $z = 0$ plane with local angle of attack α. The origin of the coordinate system is at the semi-root chord, as shown in the following sketch.

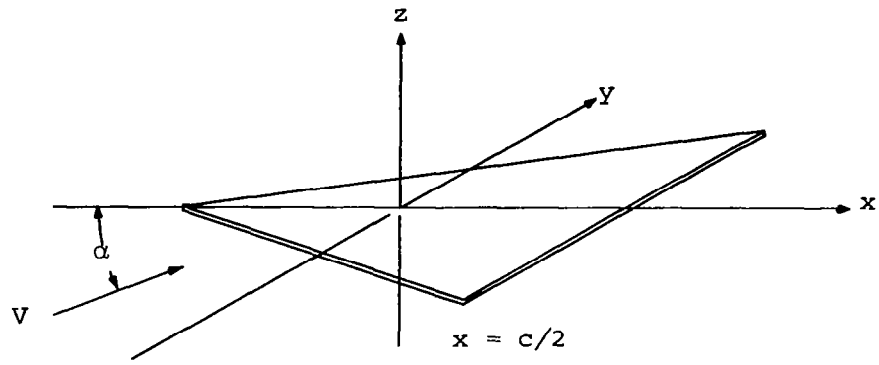

A solution to Laplace's equation can be written as (Ref. 28)

$$\phi_z(x,y,z) = -\frac{1}{2\pi}\frac{\partial}{\partial y}\int_{-\infty}^{\infty}\int_{-\infty}^{\infty} d\xi\, d\eta\, u(\xi,\eta)\left[\frac{y-\eta}{z^2+(y-\eta)^2}\left\{1 + \frac{(x-\xi)(r^2+z^2)}{r\left[z^2+(x-\xi)^2\right]}\right\}\right] \tag{5}$$

where

$$r^2 = (x-\xi)^2 + (y-\eta)^2 + z^2$$

and the quantity $u(\xi,\eta)$ is proportional to the discontinuity in the x component of the perturbation velocity across the x-y plane. In linear theory, this can be related to the wing loading through Bernoulli's equation as

$$\ell(x,y) = 2\rho V^2 u(x,y) \tag{6}$$

where $\ell(x,y)$ is the lift per unit area.

For a flat wing in steady flow, $\phi_z = -\alpha$ on the wing, and $u = 0$ everywhere else since the fluid cannot support a pressure difference. Hence, for points on the wing surface, we have the integral equation

$$\alpha = \frac{1}{2\pi}\frac{\partial}{\partial y}\left\{\iint_S d\xi\, d\eta\, \frac{u(\xi,\eta)}{y-\eta}\left[1 + \frac{\sqrt{(x-\xi)^2+(y-\eta)^2}}{x-\xi}\right]\right\} \tag{7}$$

where the double integral is carried out over the wing surface S. The two-dimensional integral equation above can be reduced to a one-dimensional integral equation by utilizing two successive steps. First, the lift per unit chord can be regarded as the independent variable; thus, let

$$g'(x) = \int_{-s}^{s} d\eta \; u(x,\eta) \tag{8}$$

where s is the local semi-span. This function is related to the lift per unit chord by

$$\frac{\partial L}{\partial x} = 2\rho V^2 g'(x) \tag{9}$$

Second, the explicit appearance of the variable y in Equation (7) can be eliminated by multiplying by an appropriate weighting factor and, with certain approximations, integrating on y across the span.

It should be noted that the use of Equation (8) to eliminate one integration means that no information regarding spanwise loading can be obtained. The choice of the weighting factor and the subsequent approximations represent the essence of Lawrence's contribution.

The weighting factor which Lawrence used is $\sqrt{s^2 - y^2}$, the spanwise distribution of surface potential which results from Jones' theory. Multiplying Equation (7) by this factor and integrating on y yields

$$\int_{-s}^{s} \alpha \sqrt{s^2 - y^2}\, dy = \frac{1}{2\pi} \int_{-c/2}^{c/2} \int_{-s}^{s} d\eta \; u(\xi,\eta) \cdot \int_{-s}^{s} \frac{y\, dy}{\sqrt{s^2 - y^2}} \left(\frac{1}{y - \eta}\right) \left[1 + \frac{\sqrt{(x-\xi)^2 + (y-\eta)^2}}{x - \xi} \right] \tag{10}$$

If we now denote

$$k(x) = \int_{-s}^{s} \alpha \sqrt{s^2 - y^2}\, dy \tag{11}$$

we find for a flat wing (α = constant),

$$k(x) = \frac{\alpha}{2} \pi s^2 \tag{12}$$

The quantity $k(x)$ is proportional to the lift of the section of the airfoil lying ahead of the station x, which is given by slender-body theory (see Ref. 8 or Ref. 10). For example, at the trailing edge of a delta wing,

$$k(x) = \frac{S_r}{4} (C_L)_{SB} \tag{13}$$

where S_r is the wing area and

$$(C_L)_{SB} = \frac{\pi}{2} A\alpha \tag{14}$$

the slender-body lift coefficient.

For sufficiently low aspect ratios, the quantity $\sqrt{(x-\xi)^2 + (y-\eta)^2}$ can be approximated by $\sqrt{(x-\xi)^2 + s^2}$. Utilizing this approximation in Equation (10), one obtains, after some manipulations

$$k(x) = \frac{1}{2} g(x) + \frac{1}{4} \int_{-c/2}^{c/2} d\xi \; g'(\xi) \left[1 + \frac{\sqrt{(x-\xi)^2 + s^2}}{x - \xi} \right] \tag{15}$$

where

$$g'(x) = \frac{d}{dx} \left[g(x) \right]$$

Equation (15) can be solved numerically for $g(x)$, and the aerodynamic coefficients are obtained from the expressions

$$C_L = \frac{4}{S_r} g(x) \Big|_{TE} \tag{16}$$

and

$$C_M = \int_{-c/2}^{c/2} \frac{C_L}{\ell_r} dx - \frac{C_L}{\ell_r} (c_r - c_1) \tag{17}$$

where ℓ_r is a reference length.

The numerical technique used to solve Equation (15) is, with minor modifications, that presented by Lawrence in Reference 16, and is presented in detail in Appendix B.

The success of the Lawrence method in predicting the linear lift characteristics of delta wings is well illustrated by Figure 2(a). Further comparisons are presented in Reference 15, and the computed attached-flow normal force and center of pressure for delta wings are shown in Figure 2(b).

The extension to include, approximately, the effect of a circular body of constant radius was made by Lawrence in Reference 27. For a circular body-planar midwing combination, the resulting integral equation is identical in form to Equation (15). However, the local semispan s under the radical in Equation (15) must be replaced by the exposed semispan, $s - a$, and, in place of Equation (12) we have

$$k(x) = \frac{\pi}{2} \alpha s^2 \left(1 - \frac{a^2}{s^2}\right)^2 \tag{18}$$

Separated Flow

For reasons of mathematical simplicity, the theoretical analysis of the lift due to separation will be restricted to small aspect ratios. This will permit the use of slender-body theory with all of the advantages of conformal mapping. That is, for calculating the flow field associated with the separated vortices, we shall assume that the flow is two-dimensional in planes normal to the plane of the wing. We shall further assume that separation occurs only along the wing leading edge. Body vortices are not considered.

Discrete vortex model.- In order to calculate the shape and strength of the vortex sheet shed from the wing leading edge, we shall represent the sheet by a finite number of discrete singularities representing vortex line filaments. We shall assume that a pair of filaments is shed at each of a number of chordwise positions just outside the wing leading edge, as shown in the following sketch.

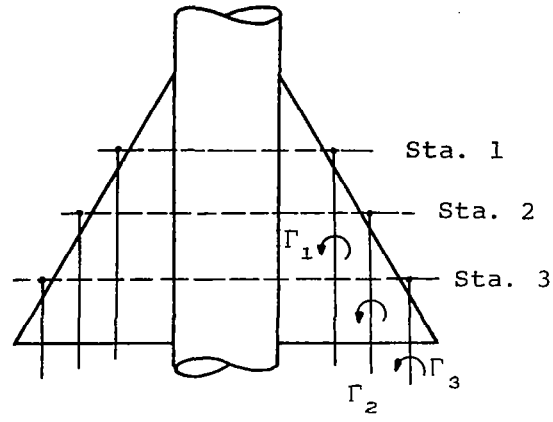

The strengths and positions of these vortices are to be determined at the instant of shedding by requiring that we satisfy the Kutta condition each time a new vortex is shed. The shed vortex will then be treated as a free vortex of constant strength whose subsequent positions will be computed step-by-step from the local induced velocities at the vortex.

Since the Kutta condition insures that the flow leaves the wing edge tangentially, it will be assumed that each discrete vortex lies in the plane of the wing at the instant of shedding. Hence, the initial position of each vortex at the instant of shedding can be described by a single variable δ, the lateral distance from the leading edge (side edge) of the wing to the vortex location.

We therefore have two unknowns at each shedding location (Γ_i and δ_i), and one equation given by the Kutta condition of finite velocity at the side edge. The remaining equation must be supplied by a determination of the shedding rate.

Satisfying the Kutta condition.- The Kutta condition requires that the velocity at the side edge of the wing remain finite. Hence, if we denote the complex potential in the cross-flow plane by W, we require that

$$\frac{dW}{d\zeta} = \frac{dW}{d\sigma}\frac{d\sigma}{d\zeta} \neq \infty \quad \text{at} \quad \zeta = s \tag{19}$$

where

$$\zeta = y + iz$$

and s is the local wing semispan. The transformation of the wing-body cross section to a circle of radius r_o (see sketch), is given by Reference 10.

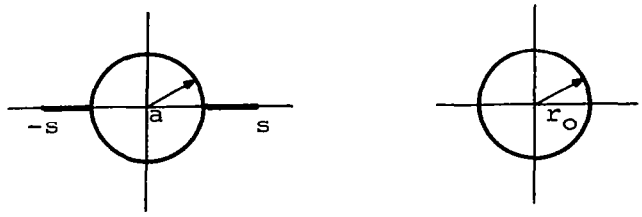

ζ plane σ plane

$$\sigma = \frac{1}{2}\left[\zeta + \frac{a^2}{\zeta} + \sqrt{\left(\zeta + \frac{a^2}{\zeta}\right)^2 - 4r_o^2}\right] \tag{20}$$

where

$$r_o = \frac{1}{2}\left(s + \frac{a^2}{s}\right) \tag{21}$$

Thus, since the derivative of the transformation $d\sigma/d\zeta$ is singular at $\zeta = s$, and since $\sigma = r_o$ at $\zeta = s$, we can express the Kutta condition of Equation (19) in the alternate form

$$\frac{dW}{d\sigma} = 0 \text{ at } \sigma = r_o \tag{22}$$

In other words, the Kutta condition is satisfied by requiring a stagnation point in the transformed plane at $\sigma = r_o$. For the present problem, with n free vortices shed from each side edge (see sketch), the complex potential can be expressed in the form (Ref. 26)

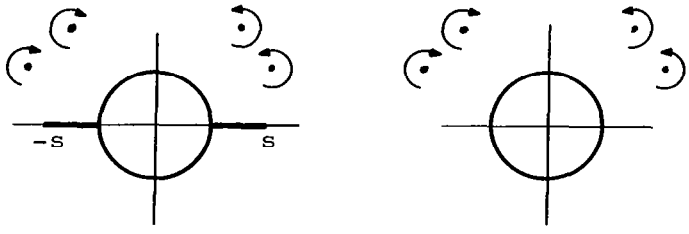

ζ plane σ plane

$$W(\sigma) = B \ln \zeta(\sigma) - iV\alpha \left(\sigma - \frac{r_o^2}{\sigma}\right) - \frac{i}{2\pi} \sum_{i=1}^{n} \Gamma_i \ln \frac{(\sigma - \sigma_i)\left(\sigma + \frac{r_o^2}{\sigma_i}\right)}{(\sigma + \bar{\sigma}_i)\left(\sigma - \frac{r_o^2}{\bar{\sigma}_i}\right)} \tag{23}$$

The first term represents the contribution of the source term for a growing body radius, the second represents the contribution of the cross-flow velocity at infinity, and the third represents the contribution of the discrete vortices and their images. We can now perform the operation indicated in Equation (22) by differentiating Equation (23) with respect to σ, setting $\sigma = r_o$, and equating the resulting expression to zero. The resulting equation is

$$\sum_{i=1}^{n} \Gamma_i \left(\frac{\sigma_i}{\sigma_i^2 - r_o^2} + \frac{\bar{\sigma}_i}{\bar{\sigma}_i^2 - r_o^2}\right) = 2\pi V\alpha \tag{24}$$

It is noted that the contribution of the source term vanishes at $\sigma = r_o$. This is expected, since its velocity contribution in the physical plane is finite. This, then, is the Kutta condition to be satisfied each time a new vortex pair is introduced. Further, since the Kutta condition insures that the flow leaves the wing edge tangentially, we shall assume that the n^{th} vortex pair lies in the plane of the wing at the instant of shedding. Hence, σ_n is real, so that $\sigma_n = \bar{\sigma}_n$, and Equation (24) becomes

$$\sum_{i=1}^{n-1} \Gamma_i \left(\frac{\sigma_i}{\sigma_i^2 - r_o^2} + \frac{\bar{\sigma}_i}{\bar{\sigma}_i^2 - r_o^2}\right) + \Gamma_n \left(\frac{2\sigma_n}{\sigma_n^2 - r_o^2}\right) = 2\pi V\alpha \tag{25}$$

Finally, σ_n is related to the lateral distance δ from the wing edge by the transformation Equation (20). Thus,

$$\sigma_n = \frac{1}{2}\left[s + \delta + \frac{a^2}{s + \delta} + \sqrt{\left(s + \delta + \frac{a^2}{s + \delta}\right)^2 - 4r_o^2}\right] \tag{26}$$

Therefore, Equation (25) furnishes one of the two necessary equations to solve for the two unknowns Γ_n and δ at a given chordwise station. The second equation is obtained from the shedding rate, for which two methods will be presented herein. In the first, or theoretical method, the shedding rate is determined directly from the lateral velocity at the edge of the wing. This velocity is used to calculate the lateral growth of a flat vortex sheet in the plane of the wing, whose strength is calculated to satisfy the Kutta condition. This sheet is then replaced by a single vortex of the same strength which is also placed to satisfy the Kutta condition.

In the second, or semi-empirical method, it will be assumed that the local shedding rate depends only upon the local sweep angle of the wing leading edge and the local cross-flow velocity. In particular, it is assumed that the wing in the presence of the body sheds at a rate corresponding to that of the wing alone at a higher angle of attack. The shedding rates are then obtained from delta-wing data by assuming that $d\Gamma/dx$ = constant and varying $d\Gamma/dx$ parametrically until the calculated lift and the experimental lift agree.

Both of the above methods for determining the shedding rate will be discussed in the following sections.

DETERMINATION OF THE SHEDDING RATE

Water Tank Studies

In order to study vortex positions experimentally and to attempt an experimental determination of leading-edge shedding rates, models of several delta and double-delta wings and wing-body combinations were fabricated for testing in the Vidya water tank. The wings were thin (0.090" thick) flat plates of 8 inch span with sharp leading edges (beveled on both surfaces), and the body was a body of revolution. Some of the models are shown in Figure 3. The models were tested by driving them vertically into the water by means of a motor-driven rack and gear arrangement, as shown in Figure 4.

The vortex sheets were made visible by applying white poster paint along the wing leading edges or at selected spots along the leading edges and over the body nose. Motion pictures of the flow patterns were then taken through a glass plate flush with the surface while the model traveled through the water. Enlargements of selected frames are shown in Figure 5.

One of the purposes of the preliminary water-tank studies was to determine the approximate sweep angles for which the flow becomes unsteady. That is, since a sharp-edged rectangular wing will shed a periodic wake from the leading edge (zero sweep) and a steady rolled-up vortex sheet from the side edges (90° sweep), there must be some minimum sweep angle for which the flow remains steady. It can be seen from Figure 5 that the rear portion of a double-delta wing produced periodic shedding for a 25° sweep and steady shedding for a 45° sweep. Since the configurations to be studied herein (both the double-delta and the F5D planform) have more than 45° sweep, it was concluded that a steady-flow analysis would be appropriate, so long as the aspect ratios treated remained below about 3.

It can be seen from Figure 5 that for 45° sweep of the rear portion of the double-delta wing, the leading edges appear to shed continuously and form a single pair of well-defined vortex cores which are nearly conical ahead of the wing break and curve outward thereafter. Figure 5 indicates that a second vortex filament may be formed at the wing break for certain sweep angles, as observed in the Ames 7- by 10-foot wind tunnel. For 25° sweep at certain angles of attack, the vortex cores become poorly defined aft of the wing break, as the vorticity shed from the rear portion is spread out in the chordwise direction as unsteady shedding is approached.

In order to gain some insight into the magnitude and distribution of shedding velocities and vorticity along the wing, some flat-plate delta wing models were made of lucite, so that short tufts mounted on the upper and lower surfaces of the wing leading edges could be observed simultaneously. For this purpose, it was necessary to take pictures nearly normal to the plane of the wing. This required a vertical window in the tank, as shown in Figure 4.

The theoretical basis for the experimental determination of the shedding velocity lies in the two-dimensional flow assumption of slender-body theory. The lateral velocity of the sheet at the wing leading edge is then given by the average lateral velocity immediately below and above the vortex sheet. These velocities, in turn, can be obtained directly from the directions of short tufts mounted on the lower and upper surfaces of the wing leading edges (see sketch).

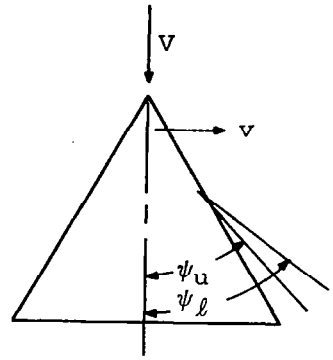

Thus

$$v_i = \frac{v_\ell + v_u}{2} \tag{27}$$

and, for small angles of the tufts relative to the free stream,

$$\left.\begin{aligned} v_\ell &= V\psi_\ell \\ v_u &= V\psi_u \end{aligned}\right\} \tag{28}$$

so that

$$v_i = \frac{V}{2}\left(\psi_\ell + \psi_u\right) \tag{29}$$

Furthermore, the vorticity being shed at any point along the leading edge is given by

$$\left.\begin{aligned} \gamma &= v_\ell - v_u \\ &= V\left(\psi_\ell - \psi_u\right) \end{aligned}\right\} \tag{30}$$

The shedding rate is then determined from the relation

$$\left.\begin{aligned} \frac{d\Gamma}{dt} = \frac{d\Gamma}{dx} \cdot V &= \gamma \cdot v_i \\ &= \frac{V^2}{2}\left(\psi_\ell{}^2 - \psi_u{}^2\right) \end{aligned}\right\}$$

or $$\frac{1}{V}\frac{d\Gamma}{dx} = \frac{1}{2}\left(\psi_\ell^2 - \psi_u^2\right) \tag{31}$$

Hence, the shedding rate itself could be determined directly if accurate measurements could be made of the local flow angles above and below the wing leading edge.

A number of attempts were made to determine the shedding rate experimentally in the Vidya water tank. For this purpose, a horizontally-mounted camera was used to look through the tank with the aid of a remote flash bulb located above the water surface. Short tufts of various materials and lengths were glued or taped to the upper and lower surfaces of the wing, but visual observations indicated that the tufts were not following the local flow directions above and below the vortex sheet. Dye streaks were also tried, but here the streamline curvature prevented accurate angle determinations at the leading edge. For these reasons, attempts to determine the leading-edge shedding rates experimentally were unsuccessful.

Theoretical Method

Since the shedding rate is the rate at which vorticity is fed into the vortex sheet at the leading edge, and since the portion of that sheet immediately adjacent to the wing has a large influence in satisfying the Kutta condition, it seems appropriate to treat each new amount of vorticity introduced as a continuous sheet rather than a discrete vortex. This is quite feasible, since the sheet leaves the wing tangentially and, therefore, we can treat the entire vortex system as made up of (1) a number of discrete vortices (those previously shed), and (2) a flat vortex sheet extending from each wing panel (those vortices being shed), as shown in the sketch.

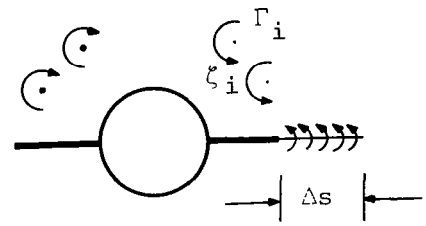

Once the length of the sheet Δs and its vorticity have been determined, we can then replace the sheet by a single dicrete vortex of the same total strength, which is again placed to satisfy the Kutta condition. We can then

proceed to calculate the subsequent positions until another sheet segment is shed. The shedding intervals, of course, are arbitrary, and the model should improve as the size of the intervals is decreased. For the present problem, with n-1 free vortices and a flat sheet shed from each side edge (see sketch), the complex potential can be expressed in the form (Ref. 26)

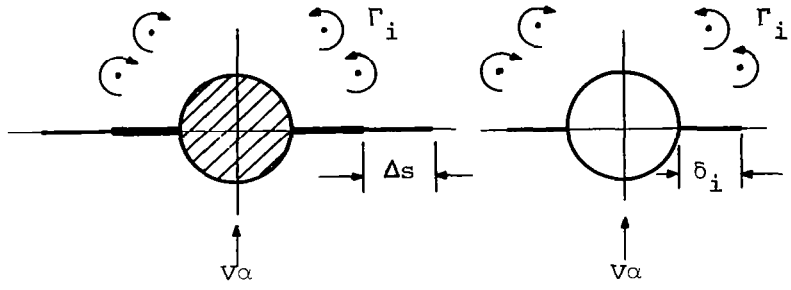

$$W(\sigma) = B\ell n\zeta(\sigma) - iV\alpha\left(\sigma - \frac{r_o^2}{\sigma}\right) - \frac{i}{2\pi}\sum_{i=1}^{n-1}\Gamma_i\,\ell n\,\frac{\left(\sigma-\sigma_i\right)\left(\sigma+\frac{r_o^2}{\sigma_i}\right)}{\left(\sigma+\bar{\sigma}_i\right)\left(\sigma-\frac{r_o^2}{\bar{\sigma}_i}\right)}$$

$$-\frac{i}{2\pi}\int_{\sigma_i=r_o}^{\sigma_i=r_o+\delta_i}\gamma\,dy\,\ell n\,\frac{\left(\sigma-\sigma_i\right)\left(\sigma+\frac{r_o^2}{\sigma_i}\right)}{\left(\sigma+\bar{\sigma}_i\right)\left(\sigma-\frac{r_o^2}{\bar{\sigma}_i}\right)} \qquad (32)$$

where γ is the vorticity (circulation per unit length) of the flat sheet. The first term represents the contribution of the source term for a growing body radius, the second represents the contribution of the cross-flow velocity at infinity, the third represents the contribution of the discrete (previously shed) vortices and their images, and the last represents the contribution of the (newly shed) flat sheet and its image system. At this point, we need the inverse transformation of the wing-body cross-section to the circle; that is, (see sketch):

ζ plane $\qquad$ σ plane

$$\zeta = \frac{1}{2}\left(\sigma + \frac{r_o^2}{\sigma}\right) + \frac{1}{2}\sqrt{\left(\sigma + \frac{r_o^2}{\sigma}\right)^2 - 4a^2} \tag{33}$$

where

$$r_o = \frac{1}{2}\left(s + \frac{a^2}{s}\right)$$

On the real axis we have $\zeta = y$ and differentiation with respect to σ_i yields

$$dy = \frac{1}{2}\, d\sigma_i \left(1 - \frac{r_o^2}{\sigma_i^2}\right)\left[1 + \frac{\sigma_i + \frac{r_o^2}{\sigma_i}}{\sqrt{\left(\sigma_i + \frac{r_o^2}{\sigma_i}\right)^2 - 4a^2}}\right] \tag{34}$$

Hence, by differentiating under the integral sign in Equation (32) and noting that $\sigma_i = \overline{\sigma}_i$ on the real axis, we find that the Kutta condition of Equation (22) can be expressed in the form

$$\sum_{i=1}^{n-1} \Gamma_i \left(\frac{\sigma_i}{\sigma_i^2 - r_o^2} + \frac{\overline{\sigma}_i}{\overline{\sigma}_i^2 - r_o^2}\right) + \int_{r_o}^{r_o+\delta_i} \gamma \frac{d\sigma_i}{\sigma_i}\left[1 + \frac{\sigma_i + \frac{r_o^2}{\sigma_i}}{\sqrt{\left(\sigma_i + \frac{r_o^2}{\sigma_i}\right)^2 - 4a^2}}\right] = 2\pi V\alpha \tag{35}$$

If we now assume that γ is constant over the short sheet segment at the instant of shedding, then the integral can be evaluated analytically. In the case of a wing alone ($a = 0$), the expression in the bracket reduces to 2 and Equation (35) becomes

$$\sum_{i=1}^{n-1} \Gamma_i \left(\frac{\sigma_i}{\sigma_i^2 - r_o^2} + \frac{\bar{\sigma}_i}{\bar{\sigma}_i^2 - r_o^2} \right) + 2\gamma \ \ell n \left(1 + \frac{\delta_i}{r_o} \right) = 2\pi V\alpha \qquad (36)$$

In the case of a wing-body combination ($a \neq 0$), the integration in Equation (35) yields (see Ref. 29)

$$\sum_{i=1}^{n-1} \Gamma_i \left(\frac{\sigma_i}{\sigma_i^2 - r_o^2} + \frac{\bar{\sigma}_i}{\bar{\sigma}_i^2 - r_o^2} \right) + \gamma \ \ell n \left(1 + \frac{\delta_i}{r_o} \right)$$

$$+ \frac{\gamma}{2} \left\{ \sinh^{-1} \left[\frac{\left(r_o + \delta_i \right)^2 + r_o^2 - 2a^2}{2a \sqrt{r_o^2 - a^2}} \right] - \sinh^{-1} \left[\frac{r_o^2 - a^2}{a \sqrt{r_o^2 - a^2}} \right] \right.$$

$$\left. - \sinh^{-1} \left[\frac{2r_o^4 + \left(2r_o^2 - 4a^2 \right) \left(r_o + \delta_i \right)^2}{4a \left(r_o + \delta_i \right)^2 \sqrt{r_o^2 - a^2}} \right] + \sinh^{-1} \left[\frac{r_o^4 + \left(r_o^2 - 2a^2 \right) r_o^2}{2ar_o^2 \sqrt{r_o^2 - a^2}} \right] \right\}$$

$$= 2\pi V\alpha \qquad (37)$$

These, then, are the two alternate forms of the Kutta condition to be satisfied for wings or wing-body combinations each time a vortex sheet segment of length δ_i (in the transformed plane) is introduced.

The length of the flat vortex sheet in the physical plane is obtained from the lateral velocity at the wing leading edge. That is, if the edge of the sheet moves outboard at a velocity v_i which is induced by all the free vortices and their images, then the length of the sheet a distance Δx downstream is given by

$$\Delta s = v_i \ \Delta t = \frac{v_i}{V} \Delta x \qquad (38)$$

The induced velocity v_i at the wing leading edge (the side edge) is obtained from the complex potential by satisfying the Kutta condition and determining the (finite) limiting value of the local velocity as the wing edge is approached. This procedure is given in Appendix C, and the resulting expression for v_i is

$$v_i = V \frac{a}{s} \frac{da}{dx} + \frac{is}{2\pi} \left(1 - \frac{a^4}{s^4}\right) \sum_{i=1}^{n-1} \Gamma_i \left[\frac{\sigma_i^2}{\left(\sigma_i^2 - r_o^2\right)^2} - \frac{\bar{\sigma}_i^2}{\left(\bar{\sigma}_i^2 - r_o^2\right)^2} \right] \tag{39}$$

The length δ_i of the vortex sheet in the transformed plane is related to the length Δs in the physical plane through the transformation Equation (20), so that

$$r_o + \delta_i = \frac{1}{2} \left[s + \Delta s + \frac{a^2}{s + \Delta s} + \sqrt{\left(s + \Delta s + \frac{a^2}{s + \Delta s}\right)^2 - 4r_o^2} \right] \tag{40}$$

This expression must be substituted into the Kutta condition of Equation (36) or Equation (37) which is then to be solved for the strength γ of the vortex sheet.

Having determined the size and strength of the newly shed sheet segment, we can then replace that segment with a single vortex of the same total strength

$$\Gamma_n = \gamma \cdot \Delta s \tag{41}$$

and require that this single vortex be located at a distance δ from the wing edge such that it, in turn, also satisfies the Kutta condition. This is done by applying Equation (25). One can then proceed to introduce subsequent vortices in the same manner, tracing the paths of each shed vortex by evaluating the vortex velocities at each chordwise station. The expressions for these velocities are developed in Appendix D.

Within the assumptions of slender-body theory, the lift on a length Δx of the wing-body combination in the presence of n discrete vortices is given by the change of the quantity (Ref. 26)

$$\Delta L = 2\rho V \sum_{i=1}^{n} \Gamma_i R \sqrt{\left(\zeta_i + \frac{a^2}{\zeta_i}\right)^2 - \left(s + \frac{a^2}{s}\right)^2} \qquad (42)$$

between x and $x + \Delta x$, where R refers to the real part of the square root. Similarly, for $n-1$ discrete vortices and a sheet of width Δs shed from the wing edges, the lift acting on a length Δx of the wing-body combination is

$$\Delta L = 2\rho V \sum_{i=1}^{n-1} \Gamma_i R \sqrt{\left(\zeta_i + \frac{a^2}{\zeta_i}\right)^2 - \left(s + \frac{a^2}{s}\right)^2}$$

$$+ 2\rho V \int_{s}^{s+\Delta s} \gamma \, dy \sqrt{\left(y + \frac{a^2}{y}\right)^2 - \left(s + \frac{a^2}{s}\right)^2} \qquad (43)$$

and the total separation lift on the configuration back to the wing trailing edge is given by this quantity evaluated at the wing trailing edge, since the initial value at the aircraft nose is zero. For configurations which extend aft of the point of maximum span, the reader is cautioned regarding the application of slender-body theory. For wings alone or wing-body combinations having cylindrical afterbodies, the attached flow lift contribution aft of the maximum span is zero. A correction to the attached-flow lift to account for the body boattail (a diminishing body radius) was presented by Adams and Sears in Reference 30. The separation lift must be calculated by continuing to follow the free vortices and calculating the above quantity. Furthermore, it must be borne in mind that an additional initially flat vortex sheet is shed from the wing trailing edge. This vortex sheet must also be allowed to roll up and should be included in the calculation. Such calculations were considered to be beyond the scope of the present investigation. Consequently, all of the calculations presented herein terminate at the last chordwise station at which the wing span is not decreasing. Finally, carrying out the integration indicated in Equation (43), we find that the total separated lift coefficient is given by

$$C_{L_s} = \frac{4}{S}\sum_{i=1}^{n-1}\frac{\Gamma_i}{V} R \sqrt{\left(\zeta_i + \frac{a^2}{\zeta_i}\right)^2 - \left(s + \frac{a^2}{s}\right)^2} + \frac{2}{S}\frac{\gamma}{V}\left\{\sqrt{(s+\Delta s)^4 - \left(s^2 + \frac{a^4}{s^2}\right)(s+\Delta s)^2 + a^4}\right.$$

$$- \frac{1}{2}\left(s^2 + \frac{a^4}{s^2}\right) \ell n \frac{\sqrt{(s+\Delta s)^4 - \left(s^2 + \frac{a^4}{s^2}\right)(s+\Delta s)^2 + a^4} + (s+\Delta s)^2 - \frac{1}{2}\left(s^2 + \frac{a^4}{s^2}\right)}{\frac{1}{2}\left(s^2 - \frac{a^4}{s^2}\right)}$$

$$\left. - a^2 \ell n \left[\frac{\sqrt{(s+\Delta s)^4 - \left(s^2 + \frac{a^4}{s^2}\right)(s+\Delta s)^2 + a^4} + a^2 - \frac{1}{2}\left(\frac{s^2}{a^2} + \frac{a^2}{s^2}\right)(s+\Delta s)^2}{\frac{1}{2}\left(\frac{a^2}{s^2} - \frac{s^2}{a^2}\right)(s+\Delta s)^2}\right]\right\} \qquad (44)$$

evaluated at the wing trailing edge.

The separation pitching moment is calculated from

$$M = \int_0^c \Delta L(c_1 - x)\,dx \qquad (45)$$

where ΔL is given by Equation (43) and c_1 is the distance from the wing apex or the wing-body juncture to the center of moments.

For the case of a wing alone ($a = 0$), it can be shown that Equation (44) reduces to

$$C_{L_s} = \frac{4}{S}\sum_{i=1}^{n-1}\frac{\Gamma_i}{V} R \sqrt{\left(\zeta_i + \frac{a^2}{\zeta_i}\right)^2 - \left(s + \frac{a^2}{s}\right)^2} + \frac{2}{S}\frac{\gamma}{V}\left[(s+\Delta s)\sqrt{2s\,\Delta s + \Delta s^2}\right.$$

$$\left. - s^2 \ell n \left(\frac{s + \Delta s + \sqrt{2s\,\Delta s + \Delta s^2}}{s}\right)\right] \qquad (46)$$

which is to be evaluated at the wing trailing edge.

Semi-Empirical Method

As was discussed in the section on Separated Flow, the basic separated flow model is restricted by the slender-body assumption to very low aspect

ratios. Therefore, in the absence of a three-dimensional theoretical method, an alternative semi-empirical method is presented here which can be used as a device to extend available delta-wing data to more general planforms and thus provide a method for lift prediction.

The basic assumption underlying the semi-empirical method is that the shedding rate depends only on the local sweep angle of the wing leading edge and on the local cross-flow velocity V_c; that is,

$$\frac{d\Gamma}{dx} = f\left(\frac{ds}{dx}, V_c\right) \tag{47}$$

For delta wings, which have a constant sweep angle, this results in a constant shedding rate.

Figure 6 presents a summary of the normal-force coefficients attributed to separated flow from References 6, 7, and 31. These curves are obtained by subtracting the attached flow C_N (or C_L) as given by the Lawrence method from the total measured normal-force coefficient. This figure illustrates that, within experimental uncertainty, the normal force per unit area produced by flow separation is independent of wing aspect ratio.

Utilizing the basic assumption represented by Equation (47), the shedding rates for various-aspect-ratio delta wings were varied systematically until the normal-force coefficients, calculated by the method given in the section on Separated Flow, matched the mean curve represented in Figure 6. The resulting shedding rates for this condition are summarized in Figure 7.

The procedure for constructing a solution for arbitrary planform wings is as follows. At each integration step, the slope of the wing leading edge is obtained; this and the angle of attack are used in a two-way table look-up to obtain $d\Gamma/dx$. A vortex pair (and an image pair) of strengths $d\Gamma/dx \cdot \Delta x$ is placed in the flow field on the real axis so as to satisfy the Kutta condition. Then the induced velocities at the locations of all the vortices now in the field are calculated and the positions of the vortex system at the next chord station are calculated. The process is repeated until the trailing edge of the wing is reached, and the lift and moment are calculated.

In the semi-empirical method, since all shed vortices are assumed to be discrete vortices (i.e., no vortex sheets), the calculation of lift is considerably simplified. Here, the expression of Equation (44) for the

separation lift coefficient reduces to (since $\gamma = 0$)

$$C_{L_s} = \frac{4}{S} \sum_{i=1}^{n} \frac{\Gamma_i}{V} R \sqrt{\left(\zeta_i + \frac{a^2}{\zeta_i}\right)^2 - \left(s + \frac{a^2}{s}\right)^2} \tag{48}$$

and the pitching-moment coefficient is again given by Equation (45) which reduces to

$$C_{m_s} = \frac{4}{Sc} \int_0^c (c_1 - x) \sum_{i=1}^{n} \frac{\Gamma_i}{V} R \sqrt{\left(\zeta_i + \frac{a^2}{\zeta_i}\right)^2 - \left(s + \frac{a^2}{s}\right)^2} \, dx \tag{49}$$

To illustrate the modification of the method to include the effects of the body, let us consider the two cases below.

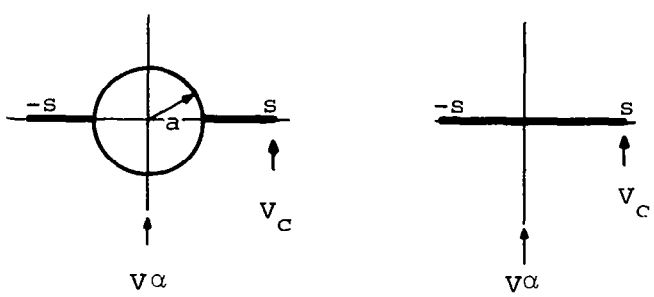

If the wing were not present for the case represented by the right-hand sketch, the velocity at the leading edges ($y = \pm s$) would be $V\alpha$. If the wing were not present in the case represented by the left-hand sketch, the velocity at $y = \pm s$ would be $V\alpha(1 + a^2/s^2)$ due to the presence of the body[1]. Therefore, when applying the semi-empirical method to a wing-body combination, the table look-up is performed at the equivalent angle of attack.

$$\alpha_e = \alpha \left(1 + \frac{a^2}{s^2}\right) \tag{50}$$

[1]This is obtained by differentiating the free stream part of the complex potential of Equation (32) with respect to σ and replacing σ by s and r_o by a.

NUMERICAL CALCULATIONS AND CONVERGENCE

Numerical Procedure

The procedure for calculating the attached-flow normal force and pitching moment consists of a straightforward solution of the integral Equation (15) for the function $g(x)$ using Equation (18) for the known function $k(x)$. The details of this procedure are outlined in Appendix B and the normal force and pitching moment are then given by Equations (16) and (17), respectively.

The procedure for calculating the separated-flow normal force and pitching moment is not quite so straightforward, since it involves the introduction and subsequent position-following of n pairs of free vortices shed from the wing leading edge. Two alternative techniques for calculating the separated-flow normal force distribution have been presented herein. The detailed procedures for these two methods are described below, and a detailed description of the computer program is given in Appendix E.

Theoretical method.- (1) Select the number of vortices to be carried in the calculation. This point is discussed, with regard to convergence, under the section, Convergence with Number of Vortices, and estimates of the computing time are given in Appendix E.

(2) Assume for first vortex sheet segment at $x = \Delta x$ that $v_i = V\alpha/2$.

(3) Calculate width of sheet segment from $\Delta s = (v_i/V)\Delta x$ where $\Delta x = c/N$, and N is the number of vortices to be introduced.

(4) Calculate width of sheet δ_i in the σ plane from Equation (40).

(5) Calculate the strength of the sheet segment from the Kutta condition by solving Equation (37) for γ. (Use Eq. (36) if $a = 0$.)

(6) Calculate strength of discrete shed vortex to replace the sheet by $\Gamma = \gamma \cdot \Delta s$.

(7) Determine position σ_n of this vortex in the transformed plane by applying the Kutta condition in the form of Equation (25).

(8) Determine the lateral distance δ from the vortex to the wing edge in the physical ζ plane by applying the transformation Equation (33) and setting $\zeta = s + \delta$ and $\sigma = \sigma_n$.

(9) Calculate the v and w velocity components of the shed vortex pair from Equation (D-8) of Appendix D.

(10) Calculate new lateral positions of shed vortices at next chordwise station by integrating Equation (D-8) over the interval Δx.

(11) Calculate shedding velocity at next station from Equation (39).

(12) Repeat steps 3 through 5.

(13) Calculate separation normal force on segment of length Δx by applying Equation (43) (see Eq. (44) for integration).

(14) Repeat steps 6 through 10 until trailing edge is reached. Note that method is not valid where the wing span is decreasing.

(15) Calculate separated pitching moment from Equations (45) and (43).

Semi-empirical method.- (1) Select the number of vortices to be carried in the calculation. See the following page for convergence requirements and Appendix E for estimates of computing time.

(2) For first aircraft segment of length Δx, evaluate leading-edge slope ds/dx and look up shedding rate for that slope using the equivalent angle of attack.

$$\alpha_e = \alpha\left(1 + \frac{a^2}{s^2}\right)$$

(3) Calculate strength of shed vortex pair from

$$\Gamma = \frac{d\Gamma}{dx}\Delta x$$

(4) Apply steps 7 through 10 of the Theoretical Method.

(5) Calculate separation normal force on segment of length Δx by applying Equation (43) with $\gamma = 0$, carrying the summation over n rather than $n-1$.

(6) Repeat steps 2 through 4 until trailing edge is reached. Here again, note that method is not valid where the wing span is decreasing.

(7) Calculate the separation normal-force and pitching-moment coefficients by applying Equations (48) and (49).

Convergence with Number of Vortices

The development in the section on separated flow indicates that the determination of the flow field consists of following the positions of a set of free vortices as they progress back along the wing chord. Regardless of the method of determining the shedding rate, this position tracing consists of solving a set of simultaneous differential equations. The number of equations in this set varies from two[2], as the first vortex pair is introduced, to twice the number of vortices, 2n, at the trailing edge of the wing.

The solution of the equation is effected with a fourth-order Runge-Kutta numerical integration technique (the Gill variation outlined in Ref. 32). For the present problem, this method has the advantage of ease of starting; it has the disadvantage of requiring an evaluation of the differential equations at axial positions intermediate to the integration interval. This difficulty is amplified for the flow model used here, since the method of placing vortices satisfies the Kutta condition only at discrete chord stations. At chord stations intermediate to the introduction of vortices, the wing leading edge is a singularity in the flow field and the evaluation of induced velocities near the singularity can create numerical difficulties. This problem was alleviated by requiring the chord increment, Δx, used to numerically integrate the differential equations to be equal to the chord increment at which vortices are introduced.

As the number of vortices introduced becomes larger and larger, the degree to which the discrete vortex model approximates a continuous sheet of vorticity should become better; that is, the method should converge with increasing number of vortices. However, when using numerical techniques, a demonstration of convergence is all that can be obtained, since it is possible that round-off and truncation errors will either mask or produce changes in computed results.

The approach to convergence is a function of both aspect ratio and angle of attack. In the range of interest in the present program, convergence of the theoretical method is most troublesome at high aspect ratios and low angles of attack. (At very low angles of attack, of course, linear

[2]Two equations are required to determine the y and z coordinates of the vortices. Because of symmetry, only two are required even though a pair of vortices is involved.

theory suffices.) A convergence demonstration was conducted for a flat-plate delta wing of aspect ratio 2 at 10° angle of attack, since this case appeared to be converging at the slowest rate. Figure 8 presents a plot of the separated-flow lift coefficient as a function of number of vortices for this case. The convergence of the method is less rapid than might be desired, but it does appear to converge at somewhere around 80 vortices. Fortunately, convergence is much more rapid for smaller aspect ratios. For comparison, Figure 8 also shows the approach to convergence of the separated-flow lift for aspect ratio 0.5 and aspect ratio 1.0 at 10° angle of attack. Although it is difficult to make rigorous conclusions from the limited number of cases run, a rough convergence rule would be

$$n = 30 + 30A \tag{51}$$

where n is the number of vortices required for convergence, and A is the aspect ratio. Usually, the value of n given by Equation (51) can be reduced by about 15 percent if answers within 10 percent of final values are acceptable. Equation (51) should be applied only for cases where $0.5 \leq A \leq 2.0$.

If one is to use experimentally-determined shedding rates in a calculative numerical procedure, it is essential that the procedure be a convergent one and that a sufficient number of vortices be used to insure consistent satisfactory results. Figure 9 presents the variation of separated flow normal-force coefficient with number of vortices for an aspect ratio 2 delta wing at 15° angle of attack, as calculated by the semi-empirical method. As indicated, the constant shedding-rate model appears to converge at somewhere around 100 vortices. However, for computational convenience, a smaller number of vortices was used, relying on an adjustment of apparent shedding rates to yield consistent numerical results. This was justified only by the fact that the adjustment was relatively small; that is, even if no adjustment was made, the resulting lift at the number of vortices used (24) was within 15 percent of the converged value (somewhere around 90 vortices), as seen from Figure 9. The shedding rates given in Figure 7 are based on a 24-vortex model. For the theoretical method, no adjustment can be made, and hence, the approach to convergence becomes much more critical from a computational standpoint.

RESULTS AND DISCUSSION

As discussed in the section on the Approach to the Problem, the normal force and pitching moment are assumed herein to be made up of the sum of a linear (attached-flow) component and a nonlinear (separated-flow) component. The linear normal force and pitching moment are calculated by the method of Lawrence (described in the section on Attached Flow), and the nonlinear contribution may be calculated by either the theoretical method or the semi-empirical method. Calculations have been carried out by both techniques for flat-plate wings of several planforms and for two different plane wing-body configurations for which experimental data are available. The flat-plate wings selected include delta wings of aspect ratios 1.0, 1.5, and 2.0, and a gothic wing of aspect ratio 1.0, all with sharp leading edges. The wing-body combinations selected are the double delta configuration (A = 1.45) and the so-called "Ogee modified" F5D configuration (A = 1.70). The planforms for these wings and the gothic wing are shown in Figures 10, 11, and 12.

Comparisons of the calculated and experimental values of normal force and center of pressure for flat-plate wings are presented in Figures 12, 13, and 14, and it can be seen that the semi-empirical technique yields better results in all cases. It should be noted that the theoretical results for the aspect-ratio-2 delta wing were not converged at 48 vortices and are therefore not presented. Since the theories of Brown and Michael (Ref. 17) and of Mangler and Smith (Ref. 21) are restricted to conical flows, comparisons with those theories are shown only for the delta wings. It can be seen from Figure 13 that the present theory gives about the same results as that of Mangler and Smith and gives substantially better results than the theory of Brown and Michael. However, all of these theories overpredict the normal force at high angles of attack. It should be noted that the theories of Brown and Michael and of Mangler and Smith have been used here to calculate only the separated normal force; that is, the slender-body theory restriction has been relaxed somewhat by modifying the attached-flow lift by the method of Lawrence (Ref. 16). Thus, the ordinate of the general curves presented in References 17 and 21 (see Fig. 15) has been interpreted as giving the sum $C_{N_s} + \frac{\pi}{2} A\alpha$ from which the separated normal force can be extracted. This is then added to the linear (attached-flow) normal force as given by Lawrence in order to obtain the total normal-force curves shown in Figure 13. This gives a more fair comparison with the methods presented herein than if the curves of References 17 and 21 were taken as predictions of the total normal force for all aspect ratios.

It can be seen from Figures 12 and 13 that the agreement between the theoretical and experimental normal force becomes poorer as the angle of attack increases. Likewise, the convergence of the present theoretical method also deteriorates with increasing aspect ratio. This is not too surprising, since the theoretical method presented herein for calculating the separated normal force is based upon the assumption that the flow field is two-dimensional. The risk of such an assumption is clearly pointed up by comparing the predictions for the attached-flow lift as given by slender-body theory with those given by the modified, quasi-three-dimensional theory of Lawrence. It can be seen from Figure 2 that close agreement exists only for low aspect ratios. Consequently, one might suspect that the theoretical method of the present report is likewise restricted, as are the methods of References 17 and 21.

The semi-empirical method presented herein is of course not restricted to very slender planforms, and agreement with experimental normal force is insured for delta wings. However, the lift distribution, and thus center of pressure, will depend on the resultant vortex pattern which develops. Hence, a check on the "reasonableness" of the basic flow model is provided by a comparison of the computed center of pressure with experimental values. Figure 14 is a comparison of both C_N and center of pressure for the semi-empirical method with the data of Bartlett and Vidal (Ref. 7) and Peckham (Ref. 31) for delta wings of aspect ratio 1.0, 1.5, and 2. The total normal force was obtained by adding the semi-empirical separated-flow normal force to the attached-flow normal force given in Figure 2(b). The agreement exhibited in Figure 14 is indeed encouraging.

As mentioned previously, the experimental separation normal force (total normal force minus Lawrence normal force) for delta wings is essentially independent of aspect ratio up to aspect ratios of about 2. A comparison of this mean curve (taken from Fig. 6) with points calculated by the theoretical method is shown in Figure 16, and the deterioration of convergence with aspect ratio is apparent.

In the absence of a three-dimensional correction for the separated flow, it is interesting to simply apply the same correction as was found by the Lawrence method for the attached flow in any particular case. Let us assume that the ratio of the correct normal force to that predicted by slender-body

theory is the same for the separated-flow component as for the attached-flow component. In that case, the total normal force is given by

$$C_N = \left(\frac{C_{N_{Lawr.}}}{C_{N_{SB}}} \right)_{att} \left(C_{N_{SB}} \right)_{total} \tag{52}$$

It must be noted that the Lawrence method is not really applicable to the separated-flow problem, since it is based upon a linear relationship between local pressure and the velocity potential (see Ref. 16). The pressure due to the separated flow, however, contains quadratic terms which do not cancel. Therefore, Equation (52) must be regarded as a crude "correction technique" rather than a valid theoretical method. Nevertheless, calculations have been carried out for delta wings of aspect ratios 1.0 and 1.5, in which case Equation (52) can be written as

$$C_N = \left(\frac{C_{N_{Lawr.}}}{C_{N_{SB}}} \right)_{att} \left[\left(C_{N_S} \right)_{SB} + \frac{\pi}{2} A\alpha \right] \tag{53}$$

and the resulting curves are shown in Figure 17. It can be seen that considerable improvement results in the agreement with experiment.

The calculated normal force and center of pressure for wing-body combinations are compared with experimental data in Figures 18 and 19 and here again the empirical method yields superior results at the higher angles of attack. Also shown on Figure 18 is the theory of Smith (Ref. 33) which is an extension of the theory of Brown and Michael to general planforms. It can be seen that the present theory gives considerably better agreement with experiment for this case.[3]

As a further check on the present analysis, the vortex positions above a delta wing as determined by both the theoretical and empirical methods have been plotted in Figure 20, and the lateral center of gravity of the separated vortex system is compared with water-tank observations for a double-delta wing in Figure 21. The detailed shape of the vortex sheets as

[3]For this calculation, the method of Reference 33 has been extended to wing-body combinations by conformal mapping.

predicted by the theoretical and semi-empirical methods are shown in Figures 22 and 23, and it can be seen that the shape becomes quite unrealistic for large numbers of vortices (owing to the discrete vortex approximation), although the lateral center-of-gravity positions agree very well with experiment (Fig. 21). It is interesting to note that the center-of-gravity location is predicted more accurately by the theoretical method than by the semi-empirical method, although for normal-force predictions the reverse is true. This would seem to indicate that the inaccuracy of the theoretical method lies in an overprediction of the shedding rate. It is further noted (Fig. 21) that the outboard trend of the lateral center of gravity with angle of attack is correctly predicted over the rearward portion of the double-delta wing by the present theory, while the theory of Smith (Ref. 33) predicts an inboard trend. It appears from Figures 20 and 21 that the lateral vortex positions are more accurately predicted by the semi-empirical method for the delta wing but not for the double-delta wing. All of this would seem to indicate that the theoretical method presented herein offers a reliable method for predicting the development of the vortex positions over general planforms, but tends to overpredict the shedding rate, particularly for aspect ratios above 1.0.

Figure 24 shows two photographs taken in the Ames 7- by 10-foot wind tunnel which illustrate an interesting experimental phenomenon in the vortex patterns for the double-delta configuration. In particular, it appears that a second vortex core is initiated at the break in the wing leading edge, and that the two cores interact in such a way as to produce the complex patterns shown in the photo. Such a phenomenon was clearly observed only for angles of attack of about 12° to 16°. Although the predicted vortex sheet shapes are very complex (see Fig. 25), no such phenomenon was evident in the vortex shapes calculated by the methods presented herein. On the other hand, the predicted center of gravity location for the entire vortex system from each wing panel seems to be in very reasonable agreement with experimental observations. The calculated lateral c.g. positions for the double delta configuration are presented in Figure 26, and it can be seen that a mean curve through the two visible traces of the photos in Figure 24 would come close to the predicted values. A mean curve cannot actually be drawn, however, since the strengths of the two visible vortex cores are unknown.

CONCLUSIONS

A method has been developed for predicting the normal force and center of pressure on reasonably slender wings and wing-body combinations exhibiting flow separation along the wing leading edges. The method is applicable to general plane-wing-body configurations and predicts the shape and location of the vortex sheets above the wing as well as the resulting loadings on the airplane. The calculation of the linear (attached-flow) normal force and pitching moment is performed by the method of Lawrence (Ref. 27), and two alternative methods are presented for calculating the loadings due to separation. One is a purely theoretical method based on slender-body theory in which the shedding rate is calculated at each point. The other is a semi-empirical method based on delta-wing data in which the shedding rate is assumed to depend only upon angle of attack and leading-edge sweep. The mathematical model employed to represent the separated flow field involves the use of a large number of free vortices which are shed at the wing edges so as to satisfy the Kutta condition there, and their subsequent motions are calculated. The model exhibits many of the features of the physical flow with regard to shedding rate, rolling up of the vortex sheets, and lateral travel of the vortex centers of gravity.

Calculations have been carried out by both the theoretical and semi-empirical techniques for several wing and wing-body configurations, and comparisons have been made between the calculated and measured normal force, center of pressure, vortex-sheet shape, and vortex center of gravity. Based on these calculations, the following conclusions are drawn:

(1) Both the theoretical and semi-empirical methods appear to converge with respect to the number of discrete vortices shed.

(2) Convergence of the theoretical method apparently deteriorates with increasing aspect ratio. The number of shed vortices required for convergence is approximately given by $n = 30\ (1+A)$.

(3) Convergence of the semi-empirical method appears to be considerably better. It was found that 24 vortices yielded satisfactory results for all cases calculated, provided the shedding rates used to match the delta wing data were also calculated using 24 vortices.

(4) Even the theoretical method yields results comparable with the conical-flow theory of Mangler and Smith for delta wings up to aspect ratios of 1.5 and is applicable to general planforms.

(5) The semi-empirical method appears to give satisfactory predictions of both normal force and center of pressure for all of the wing and wing-body configurations calculated over the angle of attack range of interest.

(6) The center of gravity positions of the vortex sheets as predicted by both the theoretical and semi-empirical techniques show good agreement (particularly the former) with observations made in the Vidya water tank.

(7) The theoretical method overpredicts the normal force due to separation, particularly at high angles of attack and high aspect ratios.

(8) It appears that the overprediction of the normal force due to separation stems from an overprediction of the shedding rate and is largely due to three-dimensional effects as is the case for the attached flow. An approximate "correction technique" has been presented which gives considerable improvement in the results.

Vidya Division, Itek Corporation
Palo Alto, California
June 30, 1966

APPENDIX A

LAWRENCE SLENDER APPROXIMATION TO THE LIFTING-SURFACE INTEGRAL EQUATION

Equation (10) of the section on Attached Flow can be written as

$$k(x) = \frac{1}{2\pi} \int_{-c}^{c} d\xi \; g'(\xi) \int_{-s}^{s} \frac{y \, dy}{\sqrt{s^2 - y^2}} \left(\frac{1}{y - \eta}\right) \left[1 + \frac{\sqrt{(x - \xi)^2 + (y - \eta)^2}}{x - \xi}\right] \tag{A-1}$$

Equation (A-1) can be written identically as

$$k(x) = \frac{1}{2\pi} \int_{-c}^{c} d\xi \; g'(\xi) \int_{-s}^{s} \frac{y \, dy}{\sqrt{s^2 - y^2}} \left(\frac{1}{y - \eta}\right) \left\{ \left[1 + \frac{|x - \xi|}{x - \xi}\right] + \left[\frac{\sqrt{(x - \xi)^2 + (y - \eta)^2} - |x - \xi|}{x - \xi}\right] \right\} \tag{A-2}$$

The first term in the braces in Equation (A-2) is independent of y enabling the integration on y to be carried out. It should be noted that[1]

$$\int_{-s}^{s} \frac{y \, dy}{(y - \eta)\sqrt{s^2 - y^2}} \equiv \pi \tag{A-3}$$

so long as $-s \leq \eta \leq s$! Hence,

[1] This can be demonstrated by interpreting the integral as a principal value.

$$k(x) = \frac{1}{2} \int_{-c}^{c} g'(\xi) \left[1 + \frac{|x - \xi|}{(x - \xi)} \right] d\xi$$

$$+ \frac{1}{2\pi} \int_{-c}^{c} g'(\xi)\, d\xi \int_{-S}^{S} \frac{y\, dy}{\sqrt{S^2 - y^2}} \frac{1}{(y - n)}$$

$$\left[\frac{\sqrt{(x - \xi)^2 + (y - n)^2} - |x - \xi|}{x - \xi} \right] \qquad \text{(A-4)}$$

The remaining integral on y in Equation (A-4) can be carried out by multiplying numerator and denominator by

$$\sqrt{(x - \xi)^2 + (y - n)^2} + |x - \xi|$$

and utilizing the approximation

$$\sqrt{(x - \xi)^2 + (y - n)^2} \simeq \sqrt{(x - \xi)^2 + S^2} \qquad \text{(A-5)}$$

Then Equation (A-4) reduces to

$$k(x) = \frac{1}{4} \int_{-c}^{c} g'(\xi) \left[1 + \frac{|x - \xi|}{(x - \xi)} \right] d\xi + \frac{1}{4} \int_{-c}^{c} g'(\xi) \left[1 + \frac{\sqrt{(x - \xi)^2 + S^2}}{(x - \xi)} \right] d\xi$$

(A-6)

But since

$$\left[1 + \frac{|x - \xi|}{(x - \xi)} \right] = 2 \quad \text{for} \quad \xi \leq x$$

$$= 0 \quad \text{for} \quad \xi \geq x,$$

Equation (A-6) becomes

$$k(x) = \frac{1}{2} g(x) + \frac{1}{4} \int_{-c}^{c} g'(\xi) \left[1 + \frac{\sqrt{(x - \xi)^2 + s^2}}{(x - \xi)} \right] d\xi \qquad \text{(A-7)}$$

which is the one-dimensional integral equation given by Lawrence.

APPENDIX B

DESCRIPTION OF COMPUTER PROGRAM FOR ATTACHED-FLOW LIFT PREDICTION

A computer program was developed for calculating the aerodynamic lift distribtuion for low aspect ratio wing-body combinations, following the method of H. R. Lawrence as detailed in References 6 and 27. A brief description of this FORTRAN IV computer program along with directions for its use are presented here.

The mathematical problem posed in the method of Lawrence is the solution of an integral equation of the following form:

$$k(x) = \frac{1}{2} g(x) + \frac{1}{4} \int_{-c}^{c} d\xi \; g'(\xi) \left[1 + \frac{\sqrt{(x - \xi)^2 + s^2(x)}}{(x - \xi)} \right] \qquad \text{(B-1)}$$

in which x is the chordwise variable, $k(x)$ and $s(x)$ are known functions which can be expressed analytically in terms of the wing semispan and body radius, and $g(x)$ is the unknown function related to the lift per unit chord. The method of solving this integral equation, recommended by Lawrence and followed in this program development was the method of collocation. This method involves expressing the solution as a truncated infinite series, substituting this series form into Equation (B-1) and performing the indicated operations. The series chosen by Lawrence was

$$g(x) = (\pi - \theta)(A_0 + A_1) + \sum_{r=1}^{N-1} (A_{r-1} - A_{r+1}) \left(\frac{\sin r\theta}{r} \right) \qquad \text{(B-2)}$$

where $\theta = \cos^{-1} x$. Substituting Equation (B-2) into Equation (B-1) results in an equation relating the unknown series coefficients, A_r, to the independent variable x.

This equation is then satisfied for specified values of x, using as many chord stations as there are unknown series coefficients, resulting in a set of simultaneous (and in this case, linear) equations in terms of the unknown series coefficients, which may be solved readily by established numerical techniques.

The organization of the computer program reflects a division of the effort into three tasks.

(1) Subroutine LOFT is concerned with the configuration of the wing. Specification of the wing and body shapes is input via LOFT. In addition, LOFT evaluates the functions $k(x)$ and $s(x)$ at the points called for by the collocation solution.

(2) Subroutine SMLSLV is used for solving the set of simultaneous linear equations resulting in the collocation solution.

(3) The main program controls the operation of the subroutines, sets up the simultaneous equations to be solved, and prints the answers.

The input to the program consists of a deck of cards which specify the wing and body dimensions and slopes at several chord stations, followed by one card with two numbers: n, the number of terms in the truncated series approximation, and m, the number of steps used in evaluating the integral in the above equation over the chord of the wing. The method used in evaluating this integral is the simple trapezoidal rule, as recommended by Lawrence and followed in this development. A more complicated and more accurate method (16-ordinate Gauss quadrature) was tried, but did not yield as satisfactory results as the trapezoidal rule with nearly the same interval size. (The nonuniform distribution of abscissae in the Gauss method was thought to be the cause of this anomalous behavior, as the collocation points were uniformly spaced.)

The output from the program is labeled and consists of the following items:

(1) The input data are listed for reference.

(2) The coefficients, A_r, of the series solution are presented.

(3) The lift and moment coefficients, for unit angle of attack, are presented along with the corresponding center of pressure.

(4) The distribution of the lift per unit chord ($\Delta C_L/\Delta x$) is indicated by listing local values of this quantity at each of the points of collocation.

The detailed input data format is as follows:

First Card

Seventy-nine columns of comments for the user to identify and label the job. These are printed at the head of the listing of the input data.

Second Card

Col. 1	Blank
Col. 2-15	±X·XXXXXXXE±YY, reference area of the wing, S_R, ft^2
Col. 16-29	±X·XXXXXXXE±YY, reference length for moments, ℓ_R, ft
Col. 30-43	±X·XXXXXXXE±YY, chord station of point about which moments are computed, c_1, ft
Col. 44-57	±X·XXXXXXXE±YY, forebody lift coefficient, C_{L-FB}, dimensionless
Col. 58-71	±X·XXXXXXXE±YY, forebody moment coefficient, C_{M-FB}, dimensionless

Third and Following Cards

Col. 1	Blank
Col. 2-15	±X·XXXXXXXE±YY, chord station, x, in ft
Col. 16-29	±X·XXXXXXXE±YY, wing semispan, s, in ft
Col. 30-43	±X·XXXXXXXE±YY, slope of wing semispan, ds/dx, dimensionless
Col. 44-57	±X·XXXXXXXE±YY, body radius, a, in ft
Col. 58-71	±X·XXXXXXXE±YY, slope of body radius, da/dx, dimensionless

Next Card

Indicates that specification of wing-body configuration is terminated. A negative value of s is used to indicate this condition. Thus, this card need only have -1. in columns 16, 17, and 18.

Last Card

Col. 1	Blank
Col. 2-5	KKKK, number of terms in series, n
Col. 6	Blank
Col. 7-10	KKKK, number of steps in trapezoid integration scheme, m

The input decks for several jobs may be stacked. The order of the cards in the group of "third and following" is critical. They must be in order of increasing chord station, x. The input deck for this program is compatible with the input requirements of the program for separated flow lift, except for the last card. Also, the separated flow lift program does not make use of the forebody lift and moment values of the second card.

The time and output line requirements may be estimated from the following approximations:

$$\text{TIME} < 1.5\times10^{-4}\ mn \text{ minutes}$$

$$\text{LINES} < 2n + 30$$

where

n number of terms in series

m number of steps in trapezoid rule

Values of $n = 12$ and $m = 23$, have been found to give adequate accuracy. (The quantity m should be about twice as big as n, but m and n should be incommensurable.)

The input deck for a sample case is listed below. The output from this case is reproduced on the following page. The remaining pages of this appendix contain a listing in FORTRAN IV of the three programs used for computing attached-flow lift from the method of Lawrence.

Input for sample case:

```
        S S T WING-BODY PLANFORM I      SAMPLE CASE
4.39      E+02 1.911     E+01 3.928     E+01 7.58      E-02 1.115     E-01
1.892     E+01 1.63      E+00 2.2719    E-01 1.63      E-00 4.64      E-02
3.448     E+01 5.17      E+00 2.2719    E-01 2.0       E-00 9.6       E-03
3.448     E+01 5.17      E+00 6.0086    E-01 2.0       E-00 9.6       E-03
4.842     E+01 1.364     E+01 6.0086    E-01 1.96      E-00-2.22      E-02
4.842     E+01 1.364     E+01 0.0       E-00 1.96      E-00-2.22      E-02
5.196     E+01 1.364     E+01 0.0       E-00 1.87      E-00-3.6       E-02
0.0       E-00-1.0       E-00
 12   23
```

LIFT DISTRIBUTION FROM THE METHOD OF LAWRENCE

INPUT DATA

S S T WING-BODY PLANFORM I SAMPLE CASE

S R	L R	C 1	C L FB	C M FB
0.4390000E 03	0.1911000E 02	0.3928000E 02	0.7580000E-01	0.1115000E-00

X	S	DS/DX	A	DA/DX
0.1892000E 02	0.1630000E 01	0.2271900E-00	0.1630000E 01	0.4640000E-01
0.3448000E 02	0.5170000E 01	0.2271900E-00	0.2000000E 01	0.9600000E-02
0.3448000E 02	0.5170000E 01	0.6008600E 00	0.2000000E 01	0.9600000E-02
0.4842000E 02	0.1364000E 02	0.6008600E 00	0.1960000E 01	-0.2220000E-01
0.4842000E 02	0.1364000E 02	0.	0.1960000E 01	-0.2220000E-01
0.5196000E 02	0.1364000E 02	0.	0.1870000E 01	-0.3600000E-01

S S T WING-BODY PLANFORM I SAMPLE CASE

NUMBER OF TERMS, N = 12 M = 23

LIST OF A SUB R, R=0,N-1

0.6306876E-02 0.1540563E-00 0.8980986E-01 -0.2766669E-01 -0.3390085E-01
-0.1580724E-01 0.1406449E-01 -0.8400617E-02 0.1250172E-02 -0.4460072E-02
0.1105976E-01 -0.8550003E-02

C L	C M	COP
0.2090983E 01	0.6287854E-01	0.3870534E 02

N	THETA(N)	X(N)	DCL/DX
0	0.	0.5196E 02	-0.
1	0.1500E 02	0.5140E 02	0.2256E-00
2	0.3000E 02	0.4975E 02	0.7440E 00
3	0.4500E 02	0.4712E 02	0.1483E 01
4	0.6000E 02	0.4370E 02	0.1982E 01
5	0.7500E 02	0.3972E 02	0.2018E 01
6	0.9000E 02	0.3544E 02	0.1452E 01
7	0.1050E 03	0.3116E 02	0.5467E 00
8	0.1200E 03	0.2718E 02	0.4324E-00
9	0.1350E 03	0.2376E 02	0.1448E-00
10	0.1500E 03	0.2113E 02	0.2272E-00
11	0.1650E 03	0.1948E 02	-0.1657E-00

```
C      CORRECTED SLENDER BODY THEORY - INTEGRAL METHOD OF LAWRENCE
C              FOR GENERAL WING-BODY COMBINATIONS
C
       DIMENSION CF(20,20),RF(20),A(20),HRN(21)
       DIMENSION XG(10),CTH(20),WG(20),TALK(20),XL(99)
       COMMON X,BETA,CLSBT,C,SR,ELR,CE1,CLFB,CMFB,TALK,XL,KIN,KO
C
  400  FORMAT(48H1  LIFT DISTRIBUTION FROM THE METHOD OF LAWRENCE///)
  401  FORMAT(1X,I4,I5,F10.5)
  402  FORMAT(/21H NUMBER OF TERMS, N =,I3,6H   M =,I3/)
  403  FORMAT(/29H     LIST OF A SUB R, R=0,N-1/)
  404  FORMAT(1X,5E15.7)
  405  FORMAT(5X,I5,4(2X,E11.4))
  406  FORMAT(//46H          N     THETA(N)        X(N)        DCL/DX/)
  407  FORMAT(//38H        C L            C M            COP/)
  408  FORMAT(//12H  INPUT DATA/)
  409  FORMAT(1X,A3,19A4)
       KIN=5
       KO=6
C
       TOPI=.63661977
       PI=3.1415927
   10  WRITE(KO,400)
   40  WRITE (KO,408)
       CALL LOFT(0)
       READ (KIN,401) NMAX,MG
   41  WRITE(KO,409) (TALK(I),I=1,20)
       WRITE (KO,402) NMAX,MG
       NP=NMAX+1
       ENMAX=NMAX
       MGP=MG+1
       EMG=MG
C
C      LOOP ON THETA N
       DO 27 N=1,NMAX
       EN=N-1
       THN=EN*PI/ENMAX
       COSTH=COS (THN)
       X=C*COSTH
       CALL LOFT(1)
       BETASQ=BETA*BETA
       RF(N)=0.5*TOPI*CLSBT
       DO 11 NR=1,NP
   11  HRN(NR)=0.
C
C      TRAPEZOID RULE FOR HRN
       DO 19 M=1,MGP
       EM=M-1
       TAU=PI*EM/EMG
       COST=COS (TAU)
       ARG=COST-COSTH
       IF(ABS (ARG)-0.001/EMG)12,12,13
   12  GRAND=0.
       GO TO 14
   13  GRAND=(SQRT (ARG*ARG+BETASQ)-BETA)/ARG
   14  FACTOR=2./EMG
       IF(M-1)16,16,15
   15  IF(M-MGP)17,16,16
   16  FACTOR=1./EMG
   17  DO 18  NR=1,NP
```

```
      ENR=NR-1
      COSRT=COS (ENR*TAU)
   18 HRN(NR)=HRN(NR)+COSRT*GRAND*FACTOR
   19 CONTINUE
C
C     FORM COEFFICIENT ARRAY FOR A SUB R
      HRN(1)=.5*HRN(1)+TOPI*THN-3.
      SINTH=SIN (THN)
      DO 26 NR=2,NP
      RN=NR-1
      IF(SINTH)21,21,22
   21 HRN(NR)=.5*HRN(NR)+TOPI/RN+BETA*RN
      GO TO 23
   22 SINRTH=SIN (RN*THN)
      HRN(NR)=.5*HRN(NR)+SINRTH*(TOPI/RN+BETA/SINTH)
   23 MR=NR-2
      IF(MR-1)24,25,25
   24 MR=1
   25 IR=NR-1
   26 CF(N,IR)=HRN(NR)-HRN(MR)
   27 CONTINUE
C
      CALL SMLSLV(NMAX,CF,RF,A,DET)
C
      WRITE (KO,403)
      WRITE (KO,404) (A(NR),NR=1,NMAX)
C
      CL=4.*PI*(A(1)+A(2))
      COP=C*(1.-.5*(A(1)-A(3))/(A(1)+A(2)))+XL(1)
      CM=CL*(CE1+XL(1)-COP)/ELR+CMFB
      CL=CL+CLFB
      COP=CE1+XL(1)-ELR*CM/CL
      WRITE (KO,407)
      WRITE (KO,404) CL,CM,COP
      WRITE (KO,406)
      DO 32 N=1,NMAX
      NM=N-1
      EN=NM
      THN=PI*EN/ENMAX
      XBAR=COS (THN)
      DCLDX=.5*A(1)*SIN (THN)/(1.+XBAR)
      DO 31 NR=2,NMAX
      ENR=NR-1
   31 DCLDX=DCLDX+A(NR)*SIN (ENR*THN)
      DCLDX=8.*DCLDX
      XBAR=C*(1.+XBAR)+XL(1)
      THN=180.*EN/ENMAX
   32 WRITE (KO,405) NM,THN,XBAR,DCLDX
C
      GO TO 10
      END
```

```
      SUBROUTINE LOFT(M)
C
      DIMENSION XW(99),R(25),DR(25),RA(25),DRA(25),TALK(20)
      COMMON X,BETA,CLSBT,C,SR,ELR,CE1,CLFB,CMFB,TALK,XW,KIN,KO
C
  410 FORMAT(20A4)
  411 FORMAT(1X,5E16.7)
  412 FORMAT(1X,5E14.7,3I3)
  413 FORMAT(/77H         S R              L R              C 1              C
     1 L FB            C M FB/)
  414 FORMAT(/76H          X                S               DS/DX
     1  A              DA/DX/)
      IF(M)1,11,1
C
C     SEARCH
    1 XN=X+XW(1)+C
      DO 2 I=2,IMAX
      IF(XN-XW(I))3,3,2
    2 CONTINUE
C
C     OUT OF RANGE
      A=RA(IMAX)
      S=R(IMAX)
      GO TO 4
C
C     HERMITE INTERPOLATION
    3 IM=I-1
      DX=XW(I)-XW(IM)
      XA=(XN-XW(IM))/DX
      XB=(XN-XW(I))/DX
      HA=(1.+XA+XA)*XB*XB
      HB=(1.-XB-XB)*XA*XA
      HC=DX*XB*XA*XB
      HD=DX*XA*XA*XB
      S=HA*R(IM)+HB*R(I)+HC*DR(IM)+HD*DR(I)
      A=HA*RA(IM)+HB*RA(I)+HC*DRA(IM)+HD*DRA(I)
    4 RAT=A*A/(S*S)
      BETA=(S-A)/C
      CLSBT=6.2831854*S*S*(1.-RAT)*(1.-RAT)/SR
      RETURN
C
C     INPUT WING-BODY CONFIGURATION
   11 READ (KIN,410) (TALK(I),I=1,20)
      WRITE(KO,410) (TALK(I),I=1,20)
      READ (KIN,412) SR,ELR,CE1,CLFB,CMFB
      WRITE(KO,413)
      WRITE (KO,411) SR,ELR,CE1,CLFB,CMFB
      WRITE (KO,414)
      DO 12 I=1,25
      READ(KIN,412)XW(I),R(I),DR(I),RA(I),DRA(I)
      IF(R(I))13,12,12
   12 WRITE(KO,411)XW(I),R(I),DR(I),RA(I),DRA(I)
   13 IMAX=I-1
      C=.5*(XW(IMAX)-XW(1))
      CE1=CE1-XW(1)
      RETURN
      END
```

```
      SUBROUTINE SMLSLV(N,A,C,X,DET)
      DIMENSION A(20,20),AL(20,20),C(20),CL(20),X(20),M(20)
      DET = 0.
      DO 2 I=1,N
      CL(I) = C(I)
      DO 1 J=1,N
    1 AL(I,J) = A(I,J)
    2 CONTINUE
      IR = 0
      PRD = 1.
      ALT = 1.
      DO 15 J=1,N
      ALTA = -ALT
      BIG = 0.
      DO 8 I=1,N
      IRHO = 1
      IF (IR) 21, 5, 3
    6 IRHO = IRHO + 1
    3 IF (I-M(IRHO) ) 4, 8, 4
    4 IF(IR-IRHO) 21, 5, 6
    5 ALTA = -ALTA
      V = ABS (AL(I,J))
      IF (V-BIG) 8, 8, 7
    7 BIG = V
      ALT = ALTA
      M(IR+1) = I
    8 CONTINUE
      IF (BIG) 21, 21, 9
    9 I = M(IR+1)
      PRD = PRD * AL(I,J)
      CL(I) = CL(I)/ AL(I,J)
      IF (J-N) 10, 16, 21
   10 L = J+1
      DO 11 K= L, N
   11 AL(I,K) = AL(I,K)/ AL(I,J)
      IR = IR + 1
      DO 14 IU= 1,N
      DO 12 IRHO = 1,IR
      IF (IU-M(IRHO) ) 12, 14, 12
   12 CONTINUE
      DO 13 K= L, N
   13 AL(IU,K) = AL(IU,K) - AL(IU,J)*AL(I,K)
      CL(IU) = CL(IU) - AL(IU,J)*CL(I)
   14 CONTINUE
   15 CONTINUE
      GO TO 21
   16 DET = ALT * PRD
      I = M(N)
      X(N) = CL(I)
   17 IF (J-1) 20, 21, 18
   18 L = J
      J = J-1
      I = M(J)
      X(J) = CL(I)
      DO 19 K= L, N
   19 X(J) = X(J) - AL(I,K)*X(K)
      GO TO 17
   20 DET = 0.
   21 RETURN
      END
```

APPENDIX C

LATERAL VELOCITY AT THE EDGE OF THE WING

The local velocity at the wing edge is found directly from the velocity potential by using the expression

$$v - iw\Big|_{\zeta=s} = \frac{dW}{d\zeta}\Big|_{\zeta=s} = \frac{dW}{d\zeta}\Big|_{\sigma=r_o} \tag{C-1}$$

Differentiation of Equation (D-1) of Appendix D yields

$$\frac{dW}{d\zeta} = \frac{B}{\zeta} + \frac{dW^1}{d\sigma}\,\frac{d\sigma}{d\zeta} \tag{C-2}$$

and

$$\frac{dW^1}{d\sigma} = \frac{i}{2\pi}\sum_{i=1}^{n}\Gamma_i\left(\frac{1}{\sigma-\sigma_i} + \frac{1}{\sigma+\frac{r_o^2}{\sigma_i}} - \frac{1}{\sigma+\bar{\sigma}_i} - \frac{1}{\sigma-\frac{r_o^2}{\bar{\sigma}_i}}\right) - iV\alpha\left(1+\frac{r_o^2}{\sigma^2}\right) \tag{C-3}$$

where

$$W^1 = W - B\,\ell n\,\zeta$$

Also, differentiation of the transformation Equation (20) yields, after simplification

$$\frac{d\sigma}{d\zeta} = \left(1-\frac{a^2}{\zeta^2}\right)\left(\frac{\sigma^2}{\sigma^2-r_o^2}\right) \tag{C-4}$$

Therefore, using the Kutta condition of Equation (24), we find from the above expressions that

$$v - iw = \frac{B}{\zeta} - \frac{i}{2\pi}\left(1 - \frac{a^2}{\zeta^2}\right)\left(\frac{\sigma^2}{\sigma^2 - r_o^2}\right)\sum_{i=1}^{n}\Gamma_i\left(\frac{1}{\sigma - \sigma_i} + \frac{1}{\sigma + \frac{r_o^2}{\sigma_i}} - \frac{1}{\sigma + \bar{\sigma}_i}\right.$$

$$\left. - \frac{1}{\sigma - \frac{r_o^2}{\bar{\sigma}_i}} + \frac{1 + \frac{r_o^2}{\sigma^2}}{\sigma_i - \frac{r_o^2}{\sigma_i}} + \frac{1 + \frac{r_o^2}{\sigma^2}}{\bar{\sigma}_i - \frac{r_o^2}{\bar{\sigma}_i}}\right) \qquad \text{(C-5)}$$

For points lying on the surface of the wing-body combination (i.e., on the transformed circle), we have

$$\sigma = r_o e^{i\theta} \qquad \text{(C-6)}$$

Substitution of this expression into Equation (C-5) yields, after algebraic manipulation,

$$v - iw = \frac{B}{\zeta} - \frac{i}{2\pi}\left(1 - \frac{a^2}{\zeta^2}\right)\sum_{i=1}^{n}\Gamma_i\frac{A}{C}$$

$$\left\{\frac{e^{2i\theta}\left(1+e^{2i\theta}\right)C+e^{2i\theta}\left(1+e^{-2i\theta}\right)\left[r_o^2\left(e^{2i\theta}-1\right)^2 + r_o e^{i\theta}\left(e^{2i\theta}-1\right)D + e^{2i\theta}E\right]}{r_o^2\left(e^{2i\theta}-1\right)^3 + r_o e^{i\theta}\left(e^{2i\theta}-1\right)^2 D + e^{2i\theta}\left(e^{2i\theta}-1\right)E}\right\} \qquad \text{(C-7)}$$

where

$$A = \sigma_i - \frac{r_o^2}{\sigma_i} + \bar{\sigma}_i - \frac{r_o^2}{\bar{\sigma}_i}$$

$$C = \left(\sigma_i - \frac{r_o^2}{\sigma_i}\right)\left(\bar{\sigma}_i - \frac{r_o^2}{\bar{\sigma}_i}\right)$$

$$D = \frac{r_o^2}{\sigma_i} - \sigma_i + \bar{\sigma}_i - \frac{r_o^2}{\bar{\sigma}_i}$$

$$E = \left(\frac{r_o^2}{\sigma_i} - \sigma_i\right)\left(\bar{\sigma}_i - \frac{r_o^2}{\bar{\sigma}_i}\right) = -C$$

Since Equation (C-7) reduces to the form zero over zero at $\theta = 0$, we apply L'Hospital's rule by differentiating the numerator and denominator in the braces with respect to θ and evaluate the resulting fraction at $\theta = 0$. Noting that $\xi = s$ at $\theta = 0$, we find that the resulting expression for the complex velocity at the wing edge, after simplification, is

$$\lim_{\theta \to 0} (v - iw) = V \frac{a}{s} \frac{da}{dx} + \frac{is}{2\pi}\left(1 - \frac{a^4}{s^4}\right) \sum_{i=1}^{n} \Gamma_i \left[\frac{\sigma_i^2}{\left(\sigma_i^2 - r_o^2\right)^2} - \frac{\bar{\sigma}_i^2}{\left(\bar{\sigma}_i^2 - r_o^2\right)^2}\right] \tag{C-8}$$

Since the expression in the brackets is the difference between a complex number and its conjugate, this quantity must be purely imaginary. Therefore, the right side of Equation (C-8) is real, and we conclude that w is identically zero at the wing leading edge. This must in fact be the case, since the Kutta condition is satisfied and the flow leaves the wing tangentially.

It is further noted that vortices lying in the plane of the wing (i.e., on the real axis) do not contribute to v_i since for such vortices $\sigma_i = \bar{\sigma}_i$ and the expression in the brackets vanishes identically. Hence, v_i can be calculated at each chordwise station without regard to the new flat sheet being shed there. The upper limit on the summation can therefore be replaced by n-1, as in Equation (34).

APPENDIX D

TRANSVERSE VELOCITIES OF THE SHED VORTICES

The complex potential for a system of n vortex pairs and their images in the circle plane with a free stream of magnitude $V\alpha$ upward at infinity is given by (see Ref. 26)

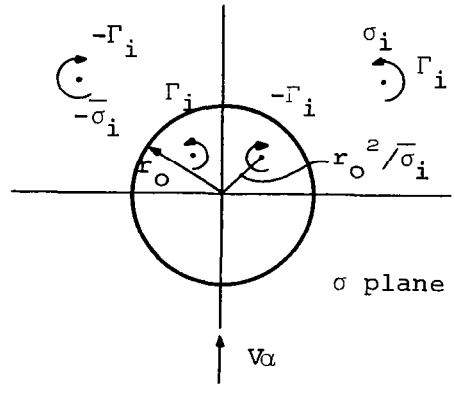

$$W(\sigma) = B\ell n\zeta(\sigma) - iV\alpha\left(\sigma - \frac{r_o^2}{\sigma}\right) - \frac{i}{2\pi}\sum_{i=1}^{n}\Gamma_i\,\ell n\,\frac{\left(\sigma - \sigma_i\right)\left(\sigma + \frac{r_o^2}{\sigma_i}\right)}{\left(\sigma + \bar{\sigma}_i\right)\left(\sigma - \frac{r_o^2}{\bar{\sigma}_i}\right)} \qquad \text{(D-1)}$$

and the complex velocity (in the physical ζ plane) of the k^{th} vortex can be written in the form (see Ref. 34)

$$v_k - iw_k = \frac{dW}{d\bar{\zeta}}\bigg|_{\zeta=\zeta_k} + \frac{d}{d\bar{\zeta}}\left[\frac{i\Gamma_k}{2\pi}\,\ell n\,(\zeta - \zeta_k)\right]_{\zeta=\zeta_k}$$

$$= \frac{dW}{d\sigma}\cdot\frac{d\sigma}{d\bar{\zeta}}\bigg|_{\zeta=\zeta_k} + \frac{i\Gamma_k}{2\pi}\cdot\frac{1}{\zeta - \zeta_k}\bigg|_{\zeta=\zeta_k} \qquad \text{(D-2)}$$

Therefore, we must carry out the indicated differentiations and separate out that part of the first term which removes the singularity of the second term.

Differentiation of Equation (D-1) with respect to σ yields (omitting the first term for convenience)

$$\left.\frac{dW^1}{d\sigma}\right|_{\zeta=\zeta_k} = -\frac{i}{2\pi}\sum_{\substack{i=1\\ i\neq k}}^{n}\Gamma_i\left(\frac{1}{\sigma_k-\sigma_i}+\frac{1}{\sigma_k+\frac{r_o^2}{\sigma_i}}\right)\frac{i}{2\pi}\sum_{i=1}^{n}\Gamma_i\left(\frac{1}{\sigma_k+\bar{\sigma}_i}+\frac{1}{\sigma_k-\frac{r_o^2}{\bar{\sigma}_i}}\right)$$

$$-iV\alpha\left(1+\frac{r_o^2}{\sigma_k^2}\right)-\frac{i\Gamma_k}{2\pi}\cdot\frac{1}{\sigma_k+\frac{r_o^2}{\sigma_k}}-\frac{i\Gamma_k}{2\pi}\cdot\left.\frac{1}{\sigma-\sigma_k}\right|_{\sigma=\sigma_k} \qquad \text{(D-3)}$$

where $W^1 = W - B\ell n\zeta$. Now we have from the Kutta condition of Equation (24)

$$iV\alpha = \frac{i}{2\pi}\sum_{i=1}^{n}\Gamma_i\left(\frac{\sigma_i}{\sigma_i^2-r_o^2}+\frac{\bar{\sigma}_i}{\bar{\sigma}_i^2-r_o^2}\right) \qquad \text{(D-4)}$$

Hence, substitution of these expressions into Equation (D-2) yields

$$v_k - iw_k = \frac{B}{\zeta_k}+\frac{i}{2\pi}\left[\frac{d\sigma}{d\zeta}\right]_{\zeta=\zeta_k}\left[-\sum_{\substack{i=1\\ i\neq k}}^{n}\Gamma_i\left(\frac{1}{\sigma_k-\sigma_i}+\frac{1}{\sigma_k+\frac{r_o^2}{\sigma_i}}\right)\right.$$

$$+\sum_{i=1}^{n}\Gamma_i\left(\frac{1}{\sigma_k+\bar{\sigma}_i}+\frac{1}{\sigma_k-\frac{r_o^2}{\bar{\sigma}_i}}\right)-\left(1+\frac{r_o^2}{\sigma_k^2}\right)\sum_{i=1}^{n}\Gamma_i\left(\frac{\sigma_i}{\sigma_i^2-r_o^2}\right.$$

$$\left.\left.+\frac{\bar{\sigma}_i}{\bar{\sigma}_i^2-r_o^2}\right)-\frac{\Gamma_k}{\sigma_k+\frac{r_o^2}{\sigma_k}}-\left.\frac{\Gamma_k}{\sigma-\sigma_k}\right|_{\sigma=\sigma_k}\right]+\left.\frac{i\Gamma_k}{2\pi}\cdot\frac{1}{\zeta-\zeta_k}\right|_{\zeta=\zeta_k} \qquad \text{(D-5)}$$

The sum of the last two terms can be written as

$$\frac{-i\Gamma_k}{2\pi} \cdot \frac{1}{\sigma - \sigma_k} \cdot \frac{d\sigma}{d\zeta}\bigg|_{\sigma=\sigma_k} + \frac{i\Gamma_k}{2\pi} \cdot \frac{1}{\zeta - \zeta_k}\bigg|_{\zeta=\zeta_k}$$

$$= \frac{i\Gamma_k}{2\pi}\left[\frac{1}{\zeta - \zeta_k} - \frac{\frac{d\sigma}{d\zeta}}{\sigma - \sigma_k}\right]_{\zeta=\zeta_k} = \frac{i\Gamma_k}{2\pi}\left[\frac{\left(\sigma - \sigma_k\right) - \left(\zeta - \zeta_k\right)\frac{d\sigma}{d\zeta}}{\left(\zeta - \zeta_k\right)\left(\sigma - \sigma_k\right)}\right]_{\zeta=\zeta_k} \qquad \text{(D-6)}$$

and we note that this quantity is of the form zero over zero. By applying L'Hospital's rule twice, we find that the limit as ζ approaches ζ_k is given by

$$\lim_{\zeta \to \zeta_k}\left[\frac{\left(\sigma - \sigma_k\right) - \left(\zeta - \zeta_k\right)\frac{d\sigma}{d\zeta}}{\left(\zeta - \zeta_k\right)\left(\sigma - \sigma_k\right)}\right] = -\frac{\frac{d^2\sigma}{d\zeta^2}}{2\left(\frac{d\sigma}{d\zeta}\right)}\bigg|_{\zeta=\zeta_k} \qquad \text{(D-7)}$$

Substitution of this form into Equation (D-5) therefore yields for the complex velocity of the k^{th} vortex

$$v_k - iw_k = \frac{B}{\zeta_k} + \frac{i}{2\pi}\left(\frac{d\sigma}{d\zeta}\right)_{\zeta=\zeta_k}\Bigg[-\sum_{\substack{i=1\\ i\neq k}}^{n}\Gamma_i\left(\frac{1}{\sigma_k - \sigma_i} + \frac{1}{\sigma_k + \frac{r_o^2}{\sigma_i}}\right) + \sum_{i=1}^{n}\Gamma_i\left(\frac{1}{\sigma_k + \bar{\sigma}_i}\right.$$

$$\left. + \frac{1}{\sigma_k - \frac{r_o^2}{\bar{\sigma}_i}}\right) - \left(1 + \frac{r_o^2}{\sigma_k^2}\right)\sum_{i=1}^{n}\Gamma_i\left(\frac{\sigma_i}{\sigma_i^2 - r_o^2} + \frac{\bar{\sigma}_i}{\bar{\sigma}_i^2 - r_o^2}\right)$$

$$\left. - \frac{\Gamma_k}{\sigma_k + \frac{r_o^2}{\sigma_k}}\right] - \frac{i\Gamma_k}{4\pi} \cdot \left(\frac{\frac{d^2\sigma}{d\zeta^2}}{\frac{d\sigma}{d\zeta}}\right)_{\zeta=\zeta_k} \qquad \text{(D-8)}$$

and we recall that $B = Va(da/dx)$. The first and second derivatives appearing in this expression are obtained by differentiating the transformation Equation (20). Thus,

$$\left.\frac{d\sigma}{d\zeta}\right|_{\zeta=\zeta_k} = \frac{1}{2}\left[1 - \frac{a^2}{\zeta_k^2} + \frac{\left(\zeta_k + \frac{a^2}{\zeta_k}\right)\left(1 - \frac{a^2}{\zeta_k^2}\right)}{\sqrt{\left(\zeta_k + \frac{a^2}{\zeta_k}\right)^2 - \left(s + \frac{a^2}{s}\right)^2}}\right] \qquad \text{(D-9)}$$

and

$$\left.\frac{d^2\sigma}{d\zeta^2}\right|_{\zeta=\zeta_k} = \frac{1}{2}\left\{\frac{2a^2}{\zeta_k^3} + \frac{2a^2\left(1 + \frac{a^2}{\zeta_k^2}\right)^3 - 8r_o^2a^2\left(1 + \frac{a^2}{\zeta_k^2}\right)\left(\frac{1}{\zeta_k^2}\right) - 4r_o^2\left(1 - \frac{a^2}{\zeta_k^2}\right)^2}{\left[\left(\zeta_k + \frac{a^2}{\zeta_k}\right)^2 - \left(s + \frac{a^2}{s}\right)^2\right]^{3/2}}\right\}$$

D-10)

APPENDIX E

DESCRIPTION OF A COMPUTER PROGRAM FOR SEPARATED-FLOW LIFT PREDICTION

As an implementation of the analysis presented in the sections on Theoretical Analysis and Determination of the Shedding Rate, a computer program was developed to calculate the aerodynamic lift distirbution due to separated flow by following the positions of multiple discrete vortices introduced at uniformly spaced chord stations along the leading edge of a wing. A description and listing of this FORTRAN IV program are presented here. Also, directions for the use of the program are furnished along with two sample cases.

As seen from the analysis of the aforementioned section, the essential mathematical problem to be treated is to solve a set of simultaneous first-order differential equations - the equations of motion of the discrete vortices. Since the treatment of the vortices was conveniently accomplished with the notation of complex numbers, it was convenient to use the complex arithmetic feature of FORTRAN IV in developing the computer program.

The program is organized in four parts, the main program and three subroutines. The main program functions to control the subroutines, numerically integrate the differential equations of motion and to output the results of the calculation. The numerical integration scheme adopted for this program is the Gill variation of the Runge-Kutta method, which is convenient for computer usage, although less efficient than predictor-corrector techniques of the same order.

The subroutine BODY is used for the input of the wing-body configuration by specifying values of wing semispan and body radius along with their chordwise derivatives at selected chord stations. In addition, it is used to interpolate for values of these quantities as they are required in solving the equations of motion.

Subroutine DERIV is used to calculate the derivatives of the vortex positions, that is, the vortex lateral and vertical velocity components, which are then numerically integrated in the main program to trace the path of each vortex as it spirals rearward over the wing. This subroutine is also used to calculate the elements of the lift distribution.

Two versions of subroutine VORTX are provided. The function of both is the same - to calculate the initial strength and position of each new vortex as it is being introduced. In one version, the theoretical method for introducing each new vortex, described in the section on Theoretical Method, is programed. In the other version, a semi-empirical approach was used. A table of vorticity, γ, as a function of two variables, angle of attack, α, and wing leading-edge slope, ds/dx, was obtained from available experimental results for delta wings from aspect ratio 0.5 to 2.0, and an angle of attack range from 5 to 20°. This second version of VORTX obtains the value of γ as it is required by two-dimensional interpolation from local values of α and ds/dx. The strength Γ of the discrete vortex is then determined, and the position is solved for so as to locally satisfy the Kutta condition. Hollerith statements within each program, which serve to distinguish the two versions, are printed in the heading before the answers are printed on each output listing. The user selects whichever of the two methods he desires to employ by combining the appropriate subroutine deck in the program deck that he submits for each series of calculations.

The input to the program consists of a deck of cards which specify the wing and body dimensions and slopes at selected chord stations, followed by a series of cards with two numbers: n, the number of vortices to be used, and α, the angle of attack to be considered.

The output from the program is labeled, and consists of the following quantities:

(1) The input data are listed for reference.

(2) A Hollerith statement is printed to identify which version of subroutine VORTX is being used.

(3) The chordwise lift distribution is given by listing the cumulative values of C_L and C_M for each of the chord stations where a new vortex was introduced.

(4) The positions and strengths of the discrete vortex elements are listed for the last chord station considered.

The detailed input-data format is as follows:

First Card

Seventy-nine columns of comments for the user to lable and identify the job. These are printed at the head of the listing of the input data, and again in the heading for the output answers for each case.

Second Card

Col. 1	Blank
Col. 2-15	±X·XXXXXXXE±YY, reference area of the wing, S_R, ft^2
Col. 16-29	±X·XXXXXXXE±YY, reference length for moments, ℓ_R, ft
Col. 30-43	±X·XXXXXXXE±YY, chord station of point about which moments are computed, c_1, ft

Third and Following Cards

Col. 1	Blank
Col. 2-15	±X·XXXXXXXE±YY, chord station, x, ft
Col. 16-29	±X·XXXXXXXE±YY, wing semispan, s, ft
Col. 30-43	±X·XXXXXXXE±YY, slope of wing semispan, ds/dx, dimensionless
Col. 44-57	±X·XXXXXXXE±YY, body radius, a, ft
Col. 58-71	±X·XXXXXXXE±YY, slope of body radius, da/dx, dimensionless

Next Card

Indicates that specification of wing-body configuration is terminated. A negative value of S is used to indicate this condition. Thus, this card need only heave -1. in columns 16, 17, and 18.

Last Few Cards

Col. 1	Blank
Col. 2-5	KKKK, the number of vortices, n
Col. 6-19	±X·XXXXXXXE±YY, angle of attack, α, in degrees

The number of these "last few" is the number of cases desired for the specified wing-body combinations. The input decks for several jobs (each job for one wing-body with any number of cases) may be stacked if a blank card is inserted after tha last card of each job. (The program senses zero angle of attack in the blank card as an indication to return to the input

of a new wing-body configuration.) As in the program for attached-flow lift, the order of the cards in the group "third and following" must be in order of increasing values of chord station, x. The input deck for this program is compatible with the input requirements of the program for attached-flow lift, except for the "last few cards." Also, this program does not make use of the forebody lift and moment values which may be additionally specified on the second card for the attached-flow program.

The time and output line requirements for each case may be estimated from the following approximate formulae:

$$\text{TIME} \approx \left(\frac{n}{24}\right)^2 \left(\frac{n + 12}{36}\right) \quad \text{minutes}$$

$$\text{LINES} \approx 2n + 100$$

Values of $n = 24$ for the semi-empirical method (gamma by table lookup) and $n = 48$ for the theoretical have been used satisfactorily, although for small angles of attack (10°), larger values are desirable in the theoretical method.

The input deck for both sample cases (same for both) is listed below. The output from each of these sample cases is reproduced on the following pages. The last pages of this appendix present the listing, in FORTRAN IV, of the five parts of the program, including the two versions of subroutine VORTX.

Input for the sample cases.

```
        S S T WING-BODY PLANFORM I      SAMPLE CASE
4.39      E+02 1.911     E+01 3.928     E+01 7.58      E-02 1.115     E-01
1.892     E+01 1.63      E+00 2.2719    E-01 1.63      E-00 4.64      E-02
3.448     E+01 5.17      E+00 2.2719    E-01 2.0       E-00 9.6       E-03
3.448     E+01 5.17      E+00 6.0086    E-01 2.0       E-00 9.6       E-03
4.842     E+01 1.364     E+01 6.0086    E-01 1.96      E-00-2.22      E-02
4.842     E+01 1.364     E+01 0.0       E-00 1.96      E-00-2.22      E-02
5.196     E+01 1.364     E+01 0.0       E-00 1.87      E-00-3.6       E-02
0.0       E-00-1.0       E-00
 24 1.5       E+01
```

MULTIPLE VORTEX MODEL

INPUT DATA
S S T WING-BODY PLANFORM 1 SAMPLE CASE

S R	L R	C 1
0.4390000E 03	0.1911000E 02	0.3928000E 02

X	S	DS/DX	A	CA/DX
0.1892000E 02	0.1630000E 01	0.2271900E-00	0.1630000E 01	0.4640000E-01
0.3448000E 02	0.5170000E 01	0.2271900E-00	0.2000000E 01	0.9600000E-02
0.3448000E 02	0.5170000E 01	0.6008600E 00	0.2000000E 01	0.9600000E-02
0.4842000E 02	0.1364000E 02	0.6008600E 00	0.1960000E 01	-0.2220000E-01
0.4842000E 02	0.1364000E 02	0.	0.1960000E 01	-0.2220000E-01
0.5196000E 02	0.1364000E 02	0.	0.1870000E 01	-0.3600000E-01

MULTIPLE VORTEX MODEL

S S T WING-BODY PLANFORM 1 SAMPLE CASE

24 VORTICES, ALPHA = 0.1500000E 02

NEW VORTEX INTRODUCED USING THEORETICAL METHOD

LIFT DISTRIBUTION

X	C L	C M
0.2029 7E 02	0.16901E-02	0.18007E-02
0.2167 3E 02	0.23349E-02	0.23696E-02
0.2305 0E 02	0.30831E-02	0.31151E-02
0.2442 7E 02	0.40407E-02	0.38083E-02
0.2580 3E 02	0.55268E-02	0.50604E-02
0.2718 0E 02	0.75266E-02	0.62420E-02
0.2855 7E 02	0.10192E-01	0.81106E-02
0.2993 3E 02	0.13461E-01	0.95429E-02
0.3131 0E 02	0.17698E-01	0.11939E-01
0.3268 7E 02	0.23083E-01	0.13501E-01
0.3406 3E 02	0.29668E-01	0.16327E-01
0.3544 0E 02	0.32786E-01	0.16316E-01
0.3681 7E 02	0.34571E-01	0.17462E-01
0.3819 3E 02	0.37934E-01	0.16904E-01
0.3957 0E 02	0.42731E-01	0.18087E-01
0.4094 7E 02	0.48606E-01	0.16690E-01
0.4232 3E 02	0.55535E-01	0.17253E-01
0.4370 0E 02	0.63266E-01	0.14317E-01
0.4507 7E 02	0.71940E-01	0.13830E-01
0.4645 3E 02	0.81691E-01	0.86763E-02
0.4783 0E 02	0.92743E-01	0.64893E-02
0.4920 7E 02	0.11508E-00	-0.68023E-02
0.5058 3E 02	0.15597E-00	-0.25281E-01
0.5196 0E 02	0.20276E-00	-0.58946E-01

VORTEX PROPERTIES AT X = 0.5196 0E 02

I	Y(I)	Z(I)	GAMMA(I)
1	0.79909E 01	0.12659E 01	0.38169E-00
2	0.10076E 02	0.17860E 01	0.30810E-00
3	0.83021E 01	0.58507E 00	0.29068E-00
4	0.93897E 01	0.10543E 01	0.30124E-00
5	0.72154E 01	0.92250E 00	0.31503E-00
6	0.96324E 01	0.74455E 00	0.33854E-00
7	0.84419E 01	0.11556E 01	0.36505E-00
8	0.89498E 01	0.15299E 01	0.39344E-00
9	0.96912E 01	0.14918E 01	0.42317E-00
10	0.10115E 02	0.10679E 01	0.45344E-00
11	0.10660E 02	0.57806E 00	0.47679E-00
12	0.10400E 02	0.25901E-00	0.54042E 00
13	0.86538E 01	0.34576E-00	0.54651E 00
14	0.72100E 01	0.41205E-00	0.54288E 00
15	0.65173E 01	0.96924E 00	0.55468E 00
16	0.70672E 01	0.17140E 01	0.57225E 00
17	0.81812E 01	0.20962E 01	0.59414E 00
18	0.94299E 01	0.22711E 01	0.61955E 00
19	0.10788E 02	0.21270E 01	0.64729E 00
20	0.11784E 02	0.18400E 01	0.67770E 00
21	0.12540E 02	0.14834E 01	0.71046E 00
22	0.13291E 02	0.10251E 01	0.76628E 00
23	0.13810E 02	0.96180E 00	0.81039E 00
24	0.13745E 02	0.	0.79016E 00
0	0.10142E 02	0.12331E 01	0.12420E 02

X = 0.5196 0E 02 CL = 0.2027 6E-00 CM =-0.5894 6E-01 COP = 0.4483 6E 02

```
      MULTIPLE  VORTEX  MODEL


 INPUT DATA
     S S T WING-BODY PLANFORM I       SAMPLE CASE

     S R             L R             C 1
 0.4390000E 03   0.1911000E 02   0.3928000E 02

       X               S              DS/DX             A              DA/DX
 0.1892000E 02   0.1630000E 01   0.2271900E 00   0.1630000E 01   0.4640000E-01
 0.3448000E 02   0.5170000E 01   0.2271900E 00   0.2000000E 01   0.9600000E-02
 0.3448000E 02   0.5170000E 01   0.6008600E 00   0.2000000E 01   0.9600000E-02
 0.4842000E 02   0.1364000E 02   0.6008600E 00   0.1960000E 01  -0.2220000E-01
 0.4842000E 02   0.1364000E 02   0.0000000E-38   0.1960000E 01  -0.2220000E-01
 0.5196000E 02   0.1364000E 02   0.0000000E-38   0.1870000E 01  -0.3600000E-01


      MULTIPLE  VORTEX  MODEL

      S S T WING-BODY PLANFORM I       SAMPLE CASE

24 VORTICES,  ALPHA = 0.1500000E 02

NEW VORTEX INTRODUCED USING THEORETICAL METHOD

           LIFT DISTRIBUTION
         X              C L             C M
     0.20297E 02    0.14090E-02     0.15012E-02
     0.21673E 02    0.24426E-02     0.24445E-02
     0.23050E 02    0.33137E-02     0.33057E-02
     0.24427E 02    0.43581E-02     0.40629E-02
     0.25803E 02    0.59191E-02     0.53809E-02
     0.27180E 02    0.80143E-02     0.66157E-02
     0.28557E 02    0.10792E-01     0.85667E-02
     0.29933E 02    0.14190E-01     0.10051E-01
     0.31310E 02    0.18586E-01     0.12542E-01
     0.32687E 02    0.24159E-01     0.14153E-01
     0.34063E 02    0.30929E-01     0.17068E-01
     0.35440E 02    0.34275E-01     0.17078E-01
     0.36817E 02    0.35996E-01     0.18247E-01
     0.38193E 02    0.39301E-01     0.17650E-01
     0.39570E 02    0.44138E-01     0.18869E-01
     0.40947E 02    0.50090E-01     0.17433E-01
     0.42323E 02    0.57128E-01     0.18022E-01
     0.43700E 02    0.64995E-01     0.15019E-01
     0.45077E 02    0.73829E-01     0.14537E-01
     0.46453E 02    0.83767E-01     0.92724E-02
     0.47830E 02    0.95033E-01     0.70546E-02
     0.49207E 02    0.11793E 00    -0.65735E-02
     0.50583E 02    0.15971E 00    -0.25441E-01
     0.51960E 02    0.20701E 00    -0.59526E-01

    VORTEX PROPERTIES AT X = 0.51960E 02
 I      Y(I)            Z(I)          GAMMA(I)
 1   0.79909E 01     0.12858E 01     0.38169E 00
 2   0.10076E 02     0.17860E 01     0.30810E 00
 3   0.83022E 01     0.58510E 00     0.29068E 00
 4   0.93897E 01     0.10543E 01     0.30124E 00
 5   0.72155E 01     0.92249E 00     0.31503E 00
 6   0.96335E 01     0.74455E 00     0.33854E 00
 7   0.84419E 01     0.11556E 01     0.36505E 00
 8   0.89498E 01     0.15299E 01     0.39344E 00
 9   0.96912E 01     0.14919E 01     0.42317E 00
10   0.10115E 02     0.10679E 01     0.45344E 00
11   0.10660E 02     0.57806E 00     0.47679E 00
12   0.10200E 02     0.25951E 00     0.54042E 00
13   0.86538E 01     0.34574E 00     0.54651E 00
14   0.72099E 01     0.41205E 00     0.54288E 00
15   0.65173E 01     0.96924E 00     0.55468E 00
16   0.70872E 01     0.17140E 01     0.57225E 00
17   0.81812E 01     0.20962E 01     0.59414E 00
18   0.94599E 01     0.22711E 01     0.61955E 00
19   0.10788E 02     0.21270E 01     0.64729E 00
20   0.11784E 02     0.18400E 01     0.67770E 00
21   0.12540E 02     0.18340E 01     0.71046E 00
22   0.13291E 02     0.18251E 01     0.76628E 00
23   0.13810E 02     0.96180E 00     0.81039E 00
24   0.13745E 02     0.00000E-38     0.79016E 00

 0   0.10142E 02     0.12331E 01     0.12420E 02


 X = 0.51960E 02     CL = 0.20701E 00     CM =-0.59526E-01     COP = 0.44775E 02
```

Figure 2. - Sample case with correction to VORTX(M) (appearing on page 62.)

MULTIPLE VORTEX MODEL

INPUT DATA
S S T WING-BODY PLANFORM I SAMPLE CASE

S R	L R	C I
0.4390000E 03	0.1911000E 02	0.3928000E 02

X	S	DS/DX	A	DA/DX
0.1892000E 02	0.1630000E 01	0.2271900E-00	0.1630000E 01	0.4640000E-01
0.3448000E 02	0.5170000E 01	0.2271900E-00	0.2000000E 01	0.9600000E-02
0.3448000E 02	0.5170000E 01	0.6008600E 00	0.2000000E 01	0.9600000E-02
0.4842000E 02	0.1364000E 02	0.6008600E 00	0.1960000E 01	-0.2220000E-01
0.4842000E 02	0.1364000E 02	0.	0.1960000E 01	-0.2220000E-01
0.5196000E 02	0.1364000E 02	0.	0.1870000E 01	-0.3600000E-01

MULTIPLE VORTEX MODEL

S S T WING-BODY PLANFORM I SAMPLE CASE

24 VORTICES, ALPHA = 0.1500000E 02

NEW VORTEX INTRODUCED USING TABLE LOOK-UP

LIFT DISTRIBUTION

X	C L	C M
0.2029?E 02	0.36609E-02	0.39004E-02
0.21673E 02	0.67245E-02	0.67086E-02
0.23650E 02	0.93220E-02	0.92633E-02
0.24427E 02	0.11587E-01	0.10854E-01
0.25603E 02	0.14128E-01	0.13107E-01
0.27180E 02	0.17?.2E-01	0.14861E-01
0.28557E 02	0.20910E-01	0.17554E-01
0.29933E 02	0.25257E-01	0.19283E-01
0.31210E 02	0.30562E-01	0.22484E-01
0.32687E 02	0.36076E-01	0.23785E-01
0.34063E 02	0.42122E-01	0.26737E-01
0.35440E 02	0.49959E-01	0.27489E-01
0.36817E 02	0.52583E-01	0.29215E-01
0.38193E 02	0.57568E-01	0.28356E-01
0.39570E 02	0.64494E-01	0.30130E-01
0.40947E 02	0.72422E-01	0.28079E-01
0.42323E 02	0.81672E-01	0.29011E-01
0.43700E 02	0.91567E-01	0.24995E-01
0.45077E 02	0.10219E-00	0.24741E-01
0.46453E 02	0.11369E-00	0.18246E-01
0.47830E 02	0.12613E-00	0.16310E-01
0.49207E 02	0.14475E-00	0.40541E-02
0.50583E 02	0.17165E-00	-0.64409E-02
0.51960E 02	0.19674E-00	-0.26613E-01

VORTEX PROPERTIES AT X = 0.51960E 02

I	Y(I)	Z(I)	GAMMA(I)
1	0.11211E 02	0.18397E 01	0.56175E 00
2	0.92627E 01	0.19474E 01	0.50685E 00
3	0.88654E 01	0.17385E 01	0.46841E-00
4	0.10033E 02	0.20118E 01	0.44016E-00
5	0.11668E 02	0.5898CE-01	0.41865E-00
6	0.10556E 02	0.42404E-00	0.40178E-00
7	0.85303E 01	0.12167E 01	0.38826E-00
8	0.88619E 01	0.96271E 00	0.37722E-00
9	0.73242E 01	0.66164E 00	0.36807E-00
10	0.10015E 02	0.15036E 01	0.36039E-00
11	0.11132E 02	0.75462E 00	0.35388E-00
12	0.97084E 01	0.10259E 01	0.74724E 00
13	0.10410E 02	0.10833E 01	0.73684E 00
14	0.94589E 01	0.44582E-00	0.72974E 00
15	0.82363E 01	0.63407E 00	0.72438E 00
16	0.75637E 01	0.14082E 01	0.71988E 00
17	0.80747E 01	0.22064E 01	0.71568E 00
18	0.94529E 01	0.26594E 01	0.71146E 00
19	0.10795E 02	0.26274E 01	0.70699E 00
20	0.12006E 02	0.23951E 01	0.70211E 00
21	0.12849E 02	0.24751E 01	0.69672E 00
22	0.13007E 02	0.32563E 01	0.99074E-01
23	0.13508E 02	0.25279E 01	0.98969E-01
24	0.13641E 02	0.	0.98834E-01
0	0.99541E 01	0.15225E 01	0.12133E 02

X = 0.51960E 02 CL = 0.19674E-00 CM =-0.26613E-01 COP = 0.41865E 02

```
C          MULTIPLE  VORTEX  MODEL   SEPARATED  LIFT  DISTRIBUTION
C
C
      COMPLEX ZTA,DZT,SGM,DSG,DDSG,DSGX,Q,C,VW
      DIMENSION ZTA(99),DZT(99),SGM(99),DSG(99),DDSG(99),DSGX(99),C(10),
     1Q(99),GAM(99),XEPS(10),EPS(10),TALK(20)
      DIMENSION AA(4),BB(4),CC(4)
      COMMON /COM1/ ZTA,DZT,SGM,DSG,DDSG,DSGX,Q;C
      COMMON /COM2/ TALK,
     1A,S,DA,DS,RZ,DRZ,SR,ELR,CE,GAM,JMAX,X,AOS,ASQ,RZSQ,DXEPS,CL,TOL,
     2CAL,SAL,TALF,IEMAX,IEPS,WOVIN,XEPS,EPS,DXIN,XBODY,KIN,KO,XINIT,DD
C
  400 FORMAT(33H1          MULTIPLE  VORTEX  MODEL///)
  401 FORMAT(1X)
  402 FORMAT(1X,5E14.7)
  403 FORMAT(1X,I4,2E14.7)
  404 FORMAT(/15H     INPUT DATA)
  406 FORMAT(1X,I4,19H VORTICES,  ALPHA =,E14.7)
  407 FORMAT(//15X,17HLIFT DISTRIBUTION)
  410 FORMAT(1X,I4,5(3X,E12.5))
  411 FORMAT(45H              X              C L             C M)
  412 FORMAT(5X,5(3X,E12.5))
  413 FORMAT(/  8X,24HVORTEX PROPERTIES AT X =,E12.5)
  414 FORMAT(47H    I       Y(I)             Z(I)          GAMMA(I))
  415 FORMAT(20A4)
  416 FORMAT(///7H     X =,E12.5,5X,4HCL =,E12.5,4X,4HCM =,E12.5,4X,5HCOP
     1 =,E12.5)
C
      C(10)=CMPLX(0.,0.)
      NOUT=1
      AA(1)=.5
      AA(2)=.29289322
      AA(3)=1.7071068
      AA(4)=.16666667
      BB(1)=2.
      BB(2)=1.
      BB(3)=1.
      BB(4)=2.
      CC(1)=.5
      CC(2)=AA(2)
      CC(3)=AA(3)
      CC(4)=.5
      TOPI=6.2831853
      KIN=5
      KO=6
C
C     INPUT
  101 WRITE(KO,400)
      WRITE(KO,404)
      CALL BODY(0)
  102 READ(KIN,403) NVORT,ALFA
      IF(ALFA)101,101,103
  103 WRITE(KO,400)
      WRITE(KO,415)(TALK(I),I=1,20)
      WRITE(KO,401)
      WRITE(KO,406)NVORT,ALFA
      WRITE(KO,401)
C
C     SET UP
      JMAX=1
```

```
      IEMAX=4
      TOL=.001
      DZT(1)=CMPLX(0.,0.)
      SAL=TOPI*SIN(ALFA/57.29578)
      CAL=TOPI*COS(ALFA/57.29578)
      TALF=SAL/CAL
      ZTA(1)=CMPLX(0.,0.)
      LAST=0
      EN=NOUT
      ENVOR=NVORT
      XSV=(XBODY-XINIT)/ENVOR
      DD=XSV
      XS=XSV/3.
      DXIN=XSV/EN
      X=XINIT+XSV
      DCM=0.
      SIG=-1.
      CALL BODY(1)
      DO 5 J=1,99
    5 Q(J)=CMPLX(0.,0.)
    6 CALL VORTX(0)
      WRITE(KO,407)
      WRITE(KO,411)
      GO TO 33
C
   11 DELX=DXIN
C
C     INTEGRATION LOOP
   21 DO 28 KI=1,NOUT
   23 DO 27 KRK=1,4
      GO TO (24,25,24,25),KRK
   24 X=X+.5*DELX
      CALL BODY(1)
   25 DO 26 J=2,JMAX
      VW=AA(KRK)*(DZT(J)-BB(KRK)*Q(J))
      ZTA(J)=ZTA(J)+DELX*VW
   26 Q(J)=Q(J)+3.*VW-CC(KRK)*DZT(J)
   27 CALL DERIV
   28 CONTINUE
C
C     CHECK LOOP TERMINAL
   32 CALL VORTX(1)
   33 SIG=-SIG
      DCM=DCM+(3.+SIG)*XS*CL
      CM=(DCM-(X-CE+XS)*CL)/ELR
      WRITE(KO,412) X,CL,CM
      IF(X-XBODY+TOL*DXIN) 55,57,57
   55 IF(X+DXIN*(EN-TOL)-XBODY) 11,11,56
   56 DELX=(XBODY-X)/(EN-TOL)
      GO TO 21
C
   57 WRITE(KO,413) X
      WRITE(KO,414)
      GAM(1)=0.
      ZTA(1)=CMPLX(0.,0.)
      DO 34 J=2,JMAX
      GAM(1)=GAM(1)+GAM(J)
      ZTA(1)=ZTA(1)+ZTA(J)*GAM(J)
      JM=J-1
   34 WRITE(KO,410) JM,ZTA(J),GAM(J)
```

```
ZTA(1)=ZTA(1)/GAM(1)
WRITE (KO,401)
WRITE(KO,410)LAST,ZTA(1),GAM(1)
COP=CE-CM*ELR/CL
WRITE(KO,416)X,CL,CM,COP
GO TO 102
END
```

```
      SUBROUTINE BODY(M)
C
      COMPLEX ZTA,DZT,SGM,DSG,DDSG,DSGX,Q,C,VW
      DIMENSION ZTA(99),DZT(99),SGM(99),DSG(99),DDSG(99),DSGX(99),C(10),
     1Q(99),GAM(99),XEPS(10),EPS(10),TALK(20)
      DIMENSION XW(25),R(25),DR(25),RA(25),DRA(25)
      COMMON /COM1/ ZTA,DZT,SGM,DSG,DDSG,DSGX,Q,C
      COMMON /COM2/ TALK,
     1A,S,DA,DS,RZ,DRZ,SR,ELR,CE,GAM,JMAX,X,AOS,ASQ,RZSQ,DXEPS,CL,TOL,
     2CAL,SAL,TALF,IEMAX,IEPS,WOVIN,XEPS,EPS,DXIN,XBODY,KIN,KO,XINIT,DD
C
  410 FORMAT(20A4)
  411 FORMAT(1X,5E16.7)
  412 FORMAT(1X,5E14.7,3I3)
  413 FORMAT(/43H         S R              L R              C 1/)
  414 FORMAT(/76H          X                S              DS/DX
     1  A              DA/DX/)
      IF(M)1,11,1
C
C     SEARCH
    1 DO 2 I=2,IMAX
      IF(X-XW(I))3,3,2
    2 CONTINUE
C
C     OUT OF RANGE
      A=RA(IMAX)
      DA=DRA(IMAX)
      S=R(IMAX)
      DS=DR(IMAX)
      AOS=A/S
      GO TO 4
C
C     HERMITE INTERPOLATION
    3 IM=I-1
      DX=XW(I)-XW(IM)
      XB=(X-XW(I))/DX
      XA=(X-XW(IM))/DX
      HA=(1.+XA+XA)*XB*XB
      HB=(1.-XB-XB)*XA*XA
      HC=DX*XB*XA*XB
      HD=DX*XA*XA*XB
      GA=(XB+XB)*(1.+XA+XA+XB)/DX
      GB=(XA+XA)*(1.-XB-XB-XA)/DX
      GC=XB*(XB+XA+XA)
      GD=XA*(XA+XB+XB)
      S=HA*R(IM)+HB*R(I)+HC*DR(IM)+HD*DR(I)
      A=HA*RA(IM)+HB*RA(I)+HC*DRA(IM)+HD*DRA(I)
      DS=GA*R(IM)+GB*R(I)+GC*DR(IM)+GD*DR(I)
      DA=GA*RA(IM)+GB*RA(I)+GC*DRA(IM)+GD*DRA(I)
      AOS=A/S
    4 RZ=0.5*(S+AOS*A)
      DRZ=.5*(1.-AOS*AOS)*DS+AOS*DA
      ASQ=A*A
      RZSQ=RZ*RZ
      RETURN
C
C     INPUT WING-BODY CONFIGURATION
   11 READ (KIN,410) (TALK(I),I=1,20)
      WRITE(KO,410) (TALK(I),I=1,20)
      READ (KIN,412) SR,ELR,CE
```

```
      WRITE(KO,413)
      WRITE(KO,411) SR,ELR,CE
      WRITE (KO,414)
      DO 12 I=1,25
      READ(KIN,412)XW(I),R(I),DR(I),RA(I),DRA(I)
      IF(R(I))13,12,12
   12 WRITE(KO,411)XW(I),R(I),DR(I),RA(I),DRA(I)
   13 IMAX=I-1
      XINIT=XW(1)
      XBODY=XW(IMAX)
      RETURN
      END
```

```
      SUBROUTINE DERIV
C
      COMPLEX ZTA,DZT,SGM,DSG,DDSG,DSGX,Q,C,VW
      DIMENSION ZTA(99),DZT(99),SGM(99),DSG(99),DDSG(99),DSGX(99),C(10),
     10(99),GAM(99),XEPS(10),EPS(10),TALK(20)
      COMMON /COM1/ ZTA,DZT,SGM,DSG,DDSG,DSGX,Q,C
      COMMON /COM2/ TALK,
     1A,S,DA,DS,RZ,DRZ,SR,ELR,CE,GAM,JMAX,X,AOS,ASQ,RZSQ,DXEPS,CL,TOL,
     2CAL,SAL,TALF,IEMAX,IEPS,WOVIN,XEPS,EPS,DXIN,XBODY,KIN,KQ,XINIT,DD
C
C     GET SIGMAS
      DO 11 J=2,JMAX
      C(1)=(ZTA(J)+ASQ/ZTA(J))*.5
      C(2)=C(1)*C(1)-RZSQ
      C(3)=CSQRT(C(2))
      C(4)=A/ZTA(J)
      C(5)=C(4)*C(4)
      C(6)=.5*(1.-C(5))
      SGM(J)=C(1)+C(3)
      DSG(J)=C(6)*(1.+C(1)/C(3))
   11 DDSG(J)=(C(5)/ZTA(J)+(C(2)*C(1)*C(5)/ZTA(J)-RZSQ*C(6)*C(6))/
     1(C(2)*C(3)))/DSG(J)*.5/DSG(J)
C
C     DERIVATIVES
      CL=0.
      DO 27 K=2,JMAX
      VW=DDSG(K)*GAM(K)
      DO 23 I=2,JMAX
      IF(I-K) 21,22,21
   21 VW=VW+GAM(I)/(SGM(K)-SGM(I))
   22 C(1)=CONJG(SGM(I))
   23 VW=VW+(SGM(I)/(SGM(I)*SGM(K)+RZSQ)-1./(SGM(K)+C(1))-C(1)/(C(1)*SGM
     1(K)-RZSQ))*GAM(I)
      VW=CMPLX(0.,-1.)*(VW/CAL+TALF*(1.+RZSQ/(SGM(K)*SGM(K))))*DSG(K)
     1+A*DA/ZTA(K)
      DZT(K)=CONJG(VW)
      C(1)=CONJG(SGM(K))
      IF(K-JMAX)26,24,24
   24 IF(WOVIN)25,26,25
   25 CL=CL+WOVIN
      GO TO 27
   26 CL=CL+REAL(SGM(K)-RZSQ/C(1))*GAM(K)
   27 CONTINUE
      CL=25.132741/CAL*CL/SR
      RETURN
      END
```

```
      SUBROUTINE VORTX(M)
C
      COMPLEX ZTA,DZT,SGM,DSG,DDSG,DSGX,Q,C,VW
      DIMENSION ZTA(99),DZT(99),SGM(99),DSG(99),DDSG(99),DSGX(99),C(10),
     1Q(99),GAM(99),XEPS(10),EPS(10),TALK(20)
      DIMENSION XW(10)
      COMMON /COM1/ ZTA,DZT,SGM,DSG,DDSG,DSGX,Q,C
      COMMON /COM2/ TALK,
     1A,S,DA,DS,RZ,DRZ,SR,ELR,CE,GAM,JMAX,X,AOS,ASQ,RZSQ,DXEPS,CL,TOL,
     2CAL,SAL,TALF,IEMAX,IEPS,WOVIN,XEPS,EPS,DXIN,XBODY,KIN,KO,XINIT,DD
C
  400 FORMAT(/49H   NEW VORTEX INTRODUCED USING THEORETICAL METHOD)
C
      JM=JMAX
      IF(M) 102,101,102
  101 WRITE (KO,400)
  102 JMAX=JMAX+1
      VI=0.
      SNA=SAL/6.2831853
      IF(JM-1) 10,10,11
   10 VOLD=.5*SNA
      VI=.5*SNA
      GO TO 15
   11 DO 12 J=2,JM
      C(3)=SGM(J)-RZSQ/SGM(J)
      C(3)=C(3)*C(3)
   12 VI=VI+GAM(J)*AIMAG(1./C(3))
      VI=-S*VI/3.1415927
   13 FAC=AOS*AOS
      VI=(1.-FAC*FAC)*VI+AOS*DA
   15 VAV=.5*(VI+VOLD)
      C(10)=CMPLX(VI,0.)
      VOLD=VI
      DLS=DD*VAV
   18 WN1=S+DLS
      WN2=WN1+ASQ/WN1
      DLI=.5*(WN2+SQRT(WN2*WN2-4.*RZSQ))/RZ
      DLI=DLI*DLI
      WN1=DLI*DLI
      WN2=1.-2.*ASQ/RZSQ
      WN3=SQRT(1.+2.*WN2+WN1)
      CON=2.*DLS/ALOG(WN1*(WN3+DLI+WN2)/(WN3+1.+DLI*WN2))
      SUM=.5*SAL
      IF(JM-2)3,1,1
    1 DO 2 J=2,JM
    2 SUM=SUM-REAL(GAM(J)/(SGM(J)-RZSQ/SGM(J)))
    3 GAM(JMAX)=CON*(SUM+SUM)
   31 WN1=.5*(S*S+ASQ/S*ASQ/S)
      WN2=(S+DLS)*(S+DLS)
      WN3=SQRT(WN2*WN2+2.*WN1*WN2+ASQ*ASQ)
      WN4=S*S-WN1
      WN5=ABS((WN1*WN2-ASQ*(WN3+ASQ))/WN4*WN2)
      WOVIN=WN3-WN1*ALOG((WN3+WN2-WN1)/WN4)-ASQ*ALOG(WN5)
      WOVIN=.5*WOVIN*GAM(JMAX)/DLS
      YS=CON+SQRT(RZSQ+CON*CON)
      SUM=.5*(YS+RZSQ/YS)
      YZ=SUM+SQRT(SUM*SUM-ASQ)
      ZTA(JMAX)=CMPLX(YZ,0.)
    4 CALL DERIV
      RETURN
```

```
      SUBROUTINE VORTX(M)
C
      COMPLEX ZTA,DZT,SGM,DSG,DDSG,DSGX,Q,C,VW
      DIMENSION ZTA(99),DZT(99),SGM(99),DSG(99),DDSG(99),DSGX(99),C(10),
     1Q(99),GAM(99),XEPS(10),EPS(10),TALK(20)
      DIMENSION XW(10)
      COMMON /COM1/ ZTA,DZT,SGM,DSG,DDSG,DSGX,Q,C
      COMMON /COM2/ TALK,
     1A,S,DA,DS,RZ,DRZ,SR,ELR,CE,GAM,JMAX,X,AOS,ASQ,RZSQ,DXEPS,CL,TOL,
     2CAL,SAL,TALF,IEMAX,IEPS,WOVIN,XEPS,EPS,DXIN,XBODY,KIN,KO,XINIT,DD
C
  400 FORMAT(/49H   NEW VORTEX INTRODUCED USING THEORETICAL METHOD)
C
      JM=JMAX
      IF(M) 102,101,102
  101 WRITE (KO,400)
  102 JMAX=JMAX+1
      VI=0.
      SNA=SAL/6.2831853
      IF(JM-1) 10,10,11
   10 VOLD=.5*SNA
      VI=.5*SNA
      GO TO 15
   11 DO 12 J=2,JM
      C(3)=SGM(J)-RZSQ/SGM(J)
      C(3)=C(3)*C(3)
   12 VI=VI+GAM(J)*AIMAG(1./C(3))
      VI=-S*VI/3.1415927
   13 FAC=AOS*AOS
      VI=(1.-FAC*FAC)*VI+AOS*DA
   15 VAV=.5*(VI+VOLD)
      C(10)=CMPLX(VI,0.)
      VOLD=VI
      DLS=DD*VAV
   18 WN1=S+DLS
      WN2=WN1+ASQ/WN1
      DLI=.5*(WN2+SQRT(WN2*WN2-4.*RZSQ))/RZ
      DLI=DLI*DLI
      WN1=DLI*DLI
      WN2=1.-2.*ASQ/RZSQ
      WN3=SQRT(1.+2.*WN2+WN1)
      CON=2.*DLS/ALOG(WN1*(WN3+DLI+WN2)/(WN3+1.+DLI*WN2))
      SUM=.5*SAL
      IF(JM-2)3,1,1
    1 DO 2 J=2,JM
    2 SUM=SUM-REAL(GAM(J)/(SGM(J)-RZSQ/SGM(J)))
    3 GAM(JMAX)=CON*(SUM+SUM)



   31 WN1=.5*(S*S+ASQ/S*ASQ/S)
      WN2=(S+DLS)*(S+DLS)
      WN3=SQRT(WN2*WN2-2.*WN1*WN2+ASQ*ASQ)<-------1
      WN4=S*S-WN1
      WN5=ABS((WN1*WN2-ASQ*(WN3+ASQ))/(WN4*WN2))<-------2
      WOVIN=WN3-WN1*ALOG((WN3+WN2-WN1)/WN4)-ASQ*ALOG(WN5)
      WOVIN=.5*WOVIN*GAM(JMAX)/DLS
      YS=CON+SQRT(RZSQ+CON*CON)
      SUM=.5*(YS+RZSQ/YS)
      YZ=SUM+SQRT(SUM*SUM-ASQ)
      ZTA(JMAX)=CMPLX(YZ,0.)
    4 CALL DERIV
      RETURN
      END
```

Figure 1. - Corrected version of subroutine VORTX(M) (appearing on page 70.)

```
      SUBROUTINE VORTX(M)
C
      COMPLEX ZTA,DZT,SGM,DSG,DDSG,DSGX,Q,C,VW
      DIMENSION ZTA(99),DZT(99),SGM(99),DSG(99),DDSG(99),DSGX(99),C(10),
     1Q(99),GAM(99),XEPS(10),EPS(10),TALK(20)
      DIMENSION TGAM(6,5)
      COMMON /COM1/ ZTA,DZT,SGM,DSG,DDSG,DSGX,Q,C
      COMMON /COM2/ TALK,
     1A,S,DA,DS,RZ,DRZ,SR,ELR,CE,GAM,JMAX,X,AOS,ASQ,RZSQ,DXEPS,CL,TOL,
     2CAL,SAL,TALF,IEMAX,IEPS,WOVIN,XEPS,EPS,DXIN,XBODY,KIN,KO,XINIT,DD
      COMMON /COM3/ TGAM,DELA,JALF,JALP,DALF
C     TGAM(I,1)=5 VALUES OF DS/DX FOR I=2,6
C     TGAM(1,J)=4 VALUES OF TANAL FOR J=2,5
C
  400 FORMAT(/44H   NEW VORTEX INTRODUCED USING TABLE LOOK-UP)
C
      JM=JMAX
      WOVIN=0.
      IF(M)102,101,102
  101 WRITE (KO,400)
      TGAM(1,1)=0.
      TGAM(1,2)=0.08749
      TGAM(1,3)=0.17633
      TGAM(1,4)=0.26795
      TGAM(1,5)=0.36397
      TGAM(2,1)=0.0
      TGAM(3,1)=0.125
      TGAM(4,1)=0.25
      TGAM(5,1)=0.375
      TGAM(6,1)=0.5
      TGAM(2,2)=0.0038
      TGAM(2,3)=0.0152
      TGAM(2,4)=0.0335
      TGAM(2,5)=0.0583
      TGAM(3,2)=0.0374
      TGAM(3,3)=0.0882
      TGAM(3,4)=0.1514
      TGAM(3,5)=0.2196
      TGAM(4,2)=0.0690
      TGAM(4,3)=0.1466
      TGAM(4,4)=0.2332
      TGAM(4,5)=0.3278
      TGAM(5,2)=0.1200
      TGAM(5,3)=0.2174
      TGAM(5,4)=0.3180
      TGAM(5,5)=0.4284
      TGAM(6,2)=0.1760
      TGAM(6,3)=0.2970
      TGAM(6,4)=0.4170
      TGAM(6,5)=0.5374
  102 JMAX=JMAX+1
      SNA=SAL/6.2831853
      DO 41 J=3,5
      DELA=TALF*(1.+AOS*AOS)-TGAM(1,J)
      IF(DELA) 42,41,41
   41 CONTINUE
   42 JALF=J-1
      JALP=J
      DELA=TALF*(1.+AOS*AOS)-TGAM(1,JALF)
      DALF=TGAM(1,JALP)-TGAM(1,JALF)
```

```
      DO 43 I=4,6
      DELS=DS-TGAM(I,1)
      IF(DELS) 44,43,43
   43 CONTINUE
   44 IDS=I-1
      IDP=I
      DELS=DS-TGAM(IDS,1)
      DDS=TGAM(IDP,1)-TGAM(IDS,1)
      FO=TGAM(IDS,JALF)
      GAMA=(TGAM(IDS,JALP)-FO)/DALF
      GAMB=(TGAM(IDP,JALF)-FO)/DDS
      GAMC=((TGAM(IDP,JALP)-FO)/DALF-GAMA)/DDS-GAMB/DALF
      GAM(JMAX)=DD*(FO+DELA*GAMA+DELS*(GAMB+DELA*GAMC))
C
C     EVALUATE YZ
      SUM=.5*SAL
      IF(JM-2) 3,1,1
    1 DO 2 J=2,JM
    2 SUM=SUM-REAL(GAM(J)/(SGM(J)-RZSQ/SGM(J)))
    3 CON=GAM(JMAX)/(SUM+SUM)
      YS=CON+SQRT(RZSQ+CON*CON)
      SUM=.5*(YS+RZSQ/YS)
      YZ=SUM+SQRT(SUM*SUM-ASQ)
      ZTA(JMAX)=CMPLX(YZ,0.)
      CALL DERIV
      RETURN
      END
```

REFERENCES

1. Jasslion, Ivan and Trilling, Leon: An Experimental Study of the Flow Field About Swept and Delta Wings with Sharp Leading Edges. AFOSR TN 58-6, Oct. 1957.

2. Bergesen, Andrew J. and Porter, J. D.: An Investigation of the Flow Around Slender Delta Wings with Leading-Edge Separation. Princeton University, Dept. of Aeronautical Engineering, Rpt. No. 510, May 1960.

3. Hummel, D.: Sichtbarmachung der Strömung an einem schlanken Deltaflügel. Institut für Strömungsmechanik Bericht 64/22, May 6, 1964.

4. Corsiglia, V. R. and Koenig, D. G.: Large-Scale Wind-Tunnel Tests of a Low Aspect Ratio Delta-Winged Model Equipped with Sharp-Edged Strakes. NASA TN D3621, Aug. 1966.

5. Wentz, W. H., Jr. and McMahon, M. C.: An Experimental Investigation of the Flow Fields About Delta and Double-Delta Wings at Low Speeds. Wichita State University Rpt. No. AR 65-2, Aug. 1965.

6. LaVallee, R. S.: Wind-Tunnel Tests on Wedge-Shaped Wings. United Aircraft Corp., Research Dept., Rpt. R-5503-2, Jan. 1947.

7. Bartlett, G. E. and Vidal, R. J.: Experimental Investigation of Influence of Edge Shape on the Aerodynamic Characteristics of Low-Aspect-Ratio Wings at Low Speeds. J. Aeron. Sci., vol. 22, no. 8, Aug. 1955, pp. 517-533.

8. Jones, R. T.: Properties of Low-Aspect-Ratio Pointed Wings at Speeds Below and Above the Speed of Sound. NACA Rpt. 835, 1946.

9. Spreiter, John R.: The Aerodynamic Forces on Slender Plane- and Cruiciform-Wing and Body Combinations. NACA Rpt. 962, 1950.

10. Sacks, Alvin H.: Aerodynamic Forces, Moments, and Stability Derivatives for Slender Bodies of General Cross Section. NACA TN 3283, Nov. 1954.

11. Lange/Wacke: Test Report on Three- and Six-Component Measurements on a Series of Tapered Wings of Small Aspect Ratio (Partial Rpt: Triangular Wing). NACA TM 1176, May 1948.

12. Von Karman, Theo. and Burgers, J. M.: General Aerodynamic Theory-Perfect Fluids. Chap. 3, Div. E., Vol. II of Aerodynamic Theory, W. F. Durand, ed., Springer, Berlin, 1935.

13. Multhopp, H.: Methods for Calculating the Lift Distribution of Wings (Subsonic Lifting Surface Theory). RAE Rpt. No. Aero. 2353, Jan. 1950.

14. Truckenbrodt, E. and Feindt, E. G.: Investigations on the Stalling Characteristics of Delta Wings in Incompressible Flow. AFOSR TN 57-538, June 4. 1957.

15. Lomax, H. and Sluder, L.: Chordwise and Compressibility Corrections to Slender Wing Theory. NACA Rpt. 1105, 1952.

16. Lawrence, H. R.: The Lift Distribution on Low Aspect Ratio Wings at Subsonic Speeds. J. Aeron. Sci., vol. 18, no. 10, Oct. 1951, pp. 638-695.

17. Brown, C. E. and Michael, W. H.: On Slender Delta Wings with Leading-Edge Separation. NACA TN 3430, Apr. 1955.

18. Legendre, R.: Écoulement au Voisinage de la Pointe Avant d'une Aile Forte Fleche Aux Incidences Moyennes. La Recherche Aéronautique (ONERA) No. 31, 1952, and No. 35, 1953.

19. Adams, M. C.: Leading-Edge Separation from Delta Wing at Supersonic Speeds. Readers' Forum, J. Aeron. Sci., vol. 20, no. 6, June 1953, p. 430.

20. Edwards, R. H.: Leading-Edge Separation from Slender Delta Wing. Readers' Forum, J. Aeron. Sci., vol. 21, no. 2, Feb. 1954, pp. 134-135.

21. Mangler, K. W. and Smith, J. H. B.: Calculation of the Flow Past Slender Delta Wings with Leading-Edge Separation. RAE Rpt. No. Aero. 2593, May 1957.

22. Gersten, K.: Nonlinear Airfoil Theory for Rectangular Wings in Compressible Flow. NASA RE 3-2-59W, Feb. 1959.

23. Bollay, W.: A Nonlinear Wing Theory and Its Application to Rectangular Wings of Small Aspect Ratio. Z. Angew., Math. Mech. Bd. 19 Nr., Feb. 1, 1939.

24. Sacks, A. H., Nielsen, J. N., and Goodwin, F. K.: A Theory for the Low-Speed Aerodynamics of Straight and Swept Wings with Flow Separation. Vidya Rpt. No. 91, Mar. 31, 1963.

25. Betz, A.: Applied Airfoil Theory. Div. J., Chap. III, vol. IV, Aerodynamic Theory, W. F. Durand, ed., Springer, Berlin, 1935, pp. 69-70.

26. Sacks, A. H.: Vortex Interference on Slender Airplanes. NACA TN 3525, Nov. 1955.

27. Lawrence, H. R.: The Aerodynamic Characteristics of Low Aspect Ratio Wing-Body Combinations in Steady Subsonic Flow. J. Aeron. Sci., Aug. 1953.

28. Reissner, Eric: On the General Theory of Thin Airfoils for Nonuniform Motion. NACA TN 946, Aug. 1944.

29. Pierce, B. O.: A Short Table of Integrals. Third Revised Edition, Ginn and Company, Boston, 1929.

30. Adams, M. C. and Sears, W. R.: Slender-Body Theory - Review and Extension. J. Aeron. Sci., vol. 20, no. 2, Feb. 1953, pp. 85-98.

31. Peckham. D. H.: Low-Speed Wind-Tunnel Tests on a Series of Uncambered Slender Pointed Wings with Sharp Edges. ARC Tech. Rpt. R&M No. 3186, 1961.

32. Ralston, A. and Wilf, H.(ed.): Mathematical Methods for Digital Computers. John Wiley & Sons, New York, 1960.

33. Smith, J. H. B.: A Theory of the Separated Flow from the Curved Leading Edge of a Slender Wing. ARC Tech. Rpt. R&M 3116, 1959.

34. Villat, H.: Lecons sur la Theorie des Tourbillons. Gauthier-Villars, Paris, France, 1930.

TABLE I

MULTIPLE VORTEX MODEL

INPUT DATA

S S T WING-BODY PLANFORM I MARCH 11, 1966

S R	L R	C 1
0.4390000E 03	0.1911000E 02	0.3928000E 02

X	S	DS/DX	A	DA/DX
0.1892000E 02	0.1630000E 01	0.2271900E-00	0.1630000E 01	0.4640000E-01
0.3448000E 02	0.5170000E 01	0.2271900E-00	0.2000000E 01	0.9600000E-02
0.3448000E 02	0.5170000E 01	0.6008600E 00	0.2000000E 01	0.9600000E-02
0.4842000E 02	0.1364000E 02	0.6008600E 00	0.1960000E 01	-0.2220000E-01
0.4842000E 02	0.1364000E 02	0.	0.1960000E 01	-0.2220000E-01
0.5196000E 02	0.1364000E 02	0.	0.1870000E 01	-0.3600000E-01

$(C_N)_{forebody} = 0.0758$

$(-C_M)_{forebody} = 0.1115$

Attached Flow

$(C_N)_\alpha = 2.103$/radian

$(C_M)_\alpha = 0.0691$/radian

Note that attached flow includes the forebody.

TABLE II

MULTIPLE VORTEX MODEL

INPUT DATA

OGEE MODIFIED F 5 D WING MAY 5, 1966

S R	L R	C 1
0.6610000E 03	0.2259000E 02	0.2713000E 02

X	S	DS/DX	A	DA/DX
0.1362500E 02	0.4416000E 01	0.2200000E-00	0.1837000E 01	0.
0.1592500E 02	0.5000000E 01	0.2750000E-00	0.1837000E 01	0.
0.1863300E 02	0.5833000E 01	0.3530000E-00	0.1837000E 01	0.
0.2079100E 02	0.6667000E 01	0.4280000E-00	0.1837000E 01	0.
0.2258300E 02	0.7500000E 01	0.4950000E-00	0.1837000E 01	0.
0.2414200E 02	0.8333000E 01	0.5560000E 00	0.1837000E 01	0.
0.2558300E 02	0.9167000E 01	0.6100000E 00	0.1837000E 01	0.
0.2693300E 02	0.1000000E 02	0.6460000E 00	0.1837000E 01	0.
0.2816600E 02	0.1083300E 02	0.6690000E 00	0.1837000E 01	0.
0.2947500E 02	0.1166700E 02	0.6810000E 00	0.1837000E 01	0.
0.3063300E 02	0.1250000E 02	0.6670000E 00	0.1837000E 01	0.
0.3149100E 02	0.1333300E 02	0.6130000E 00	0.1837000E 01	0.
0.3291600E 02	0.1416600E 02	0.6150000E 00	0.1837000E 01	0.
0.3485000E 02	0.1500000E 02	0.4740000E-00	0.1837000E 01	0.
0.3693300E 02	0.1583300E 02	0.3270000E-00	0.1837000E 01	0.
0.4208300E 02	0.1669100E 02	0.	0.1837000E 01	0.

$(C_L)_{forebody} = 0.0649$

$(C_M)_{forebody} = 0.0768$

Attached Flow

$(C_N)_\alpha = 2.053$/radian

$(C_M)_\alpha = 0.090$/radian

Note that the attached flow results include the forebody.

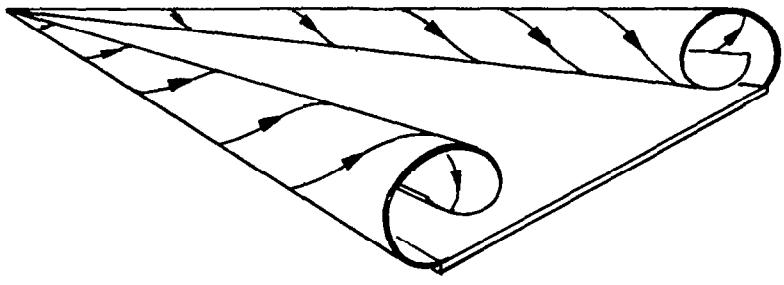

Figure 1.- Simplified flow pattern on sharp-edged delta wings.

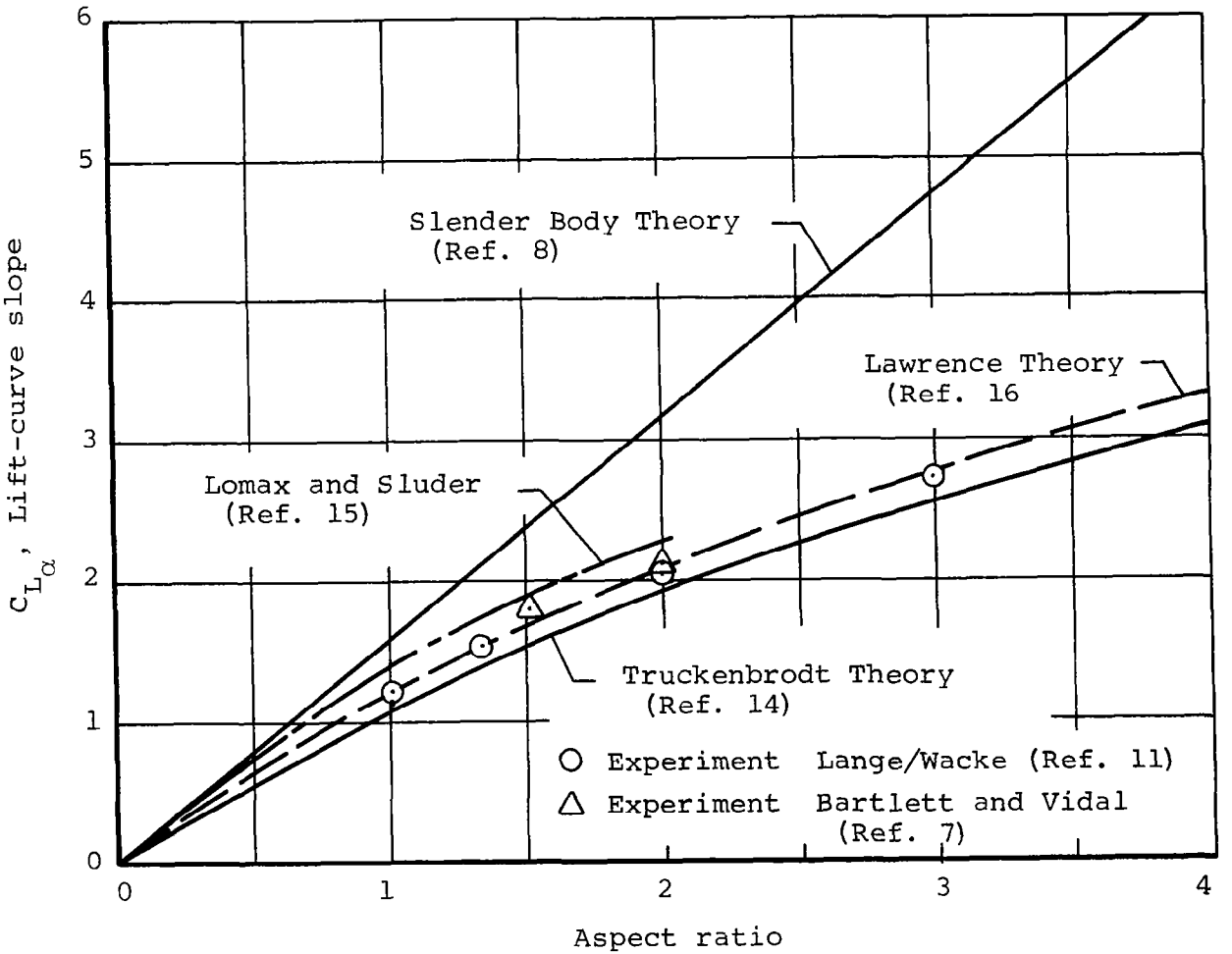

(a) Comparison of lift-curve slope with other theories and experiment.

Figure 2.- Linear (attached flow) aerodynamic characteristics of delta wings by the method of Lawrence (Ref. 16).

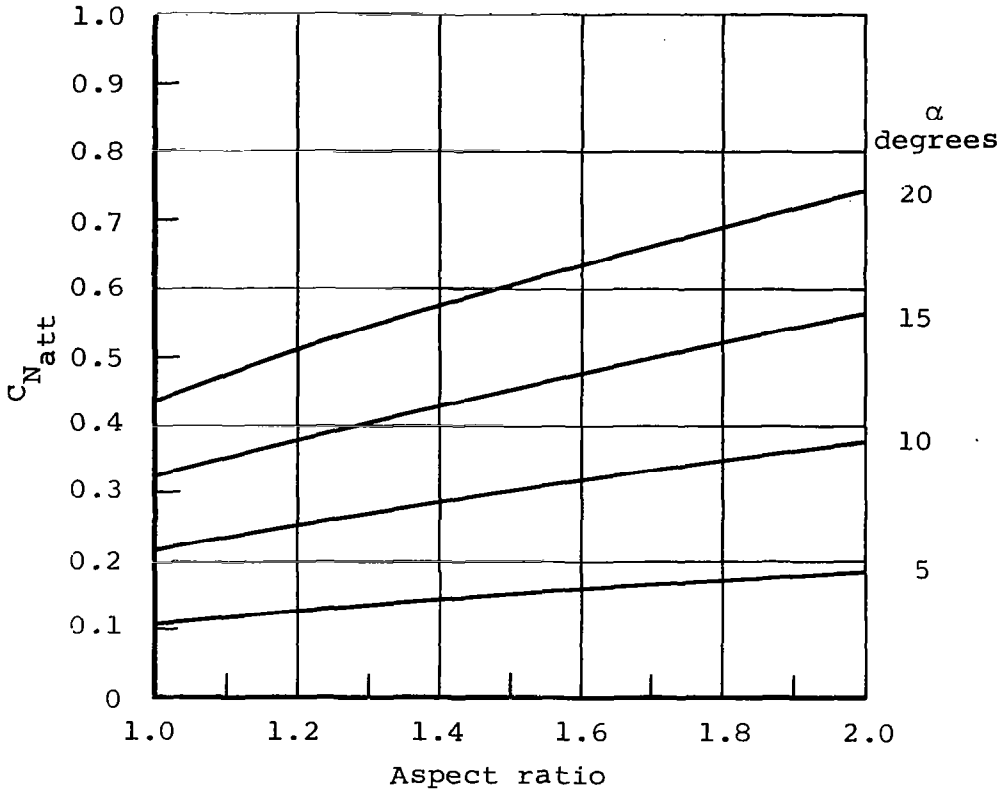

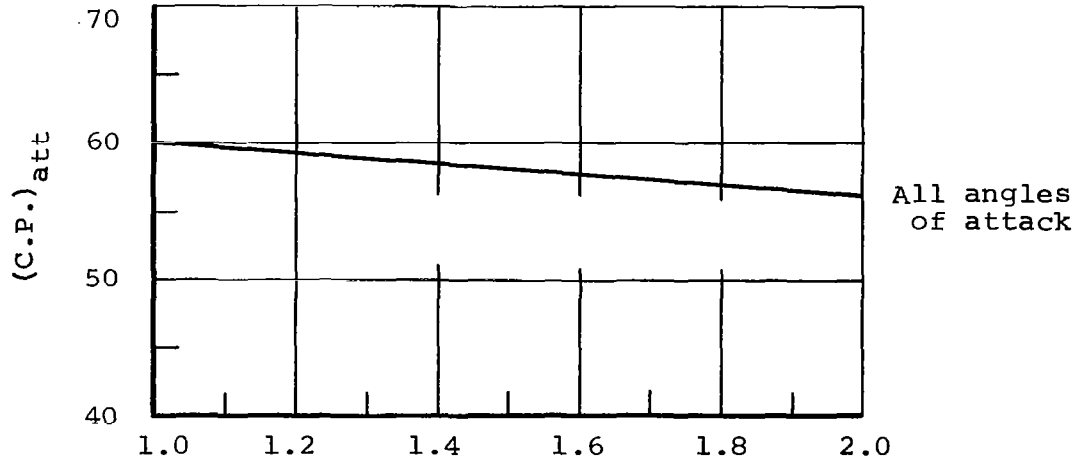

(b) Predicted normal force and center of pressure.

Figure 2.- Concluded.

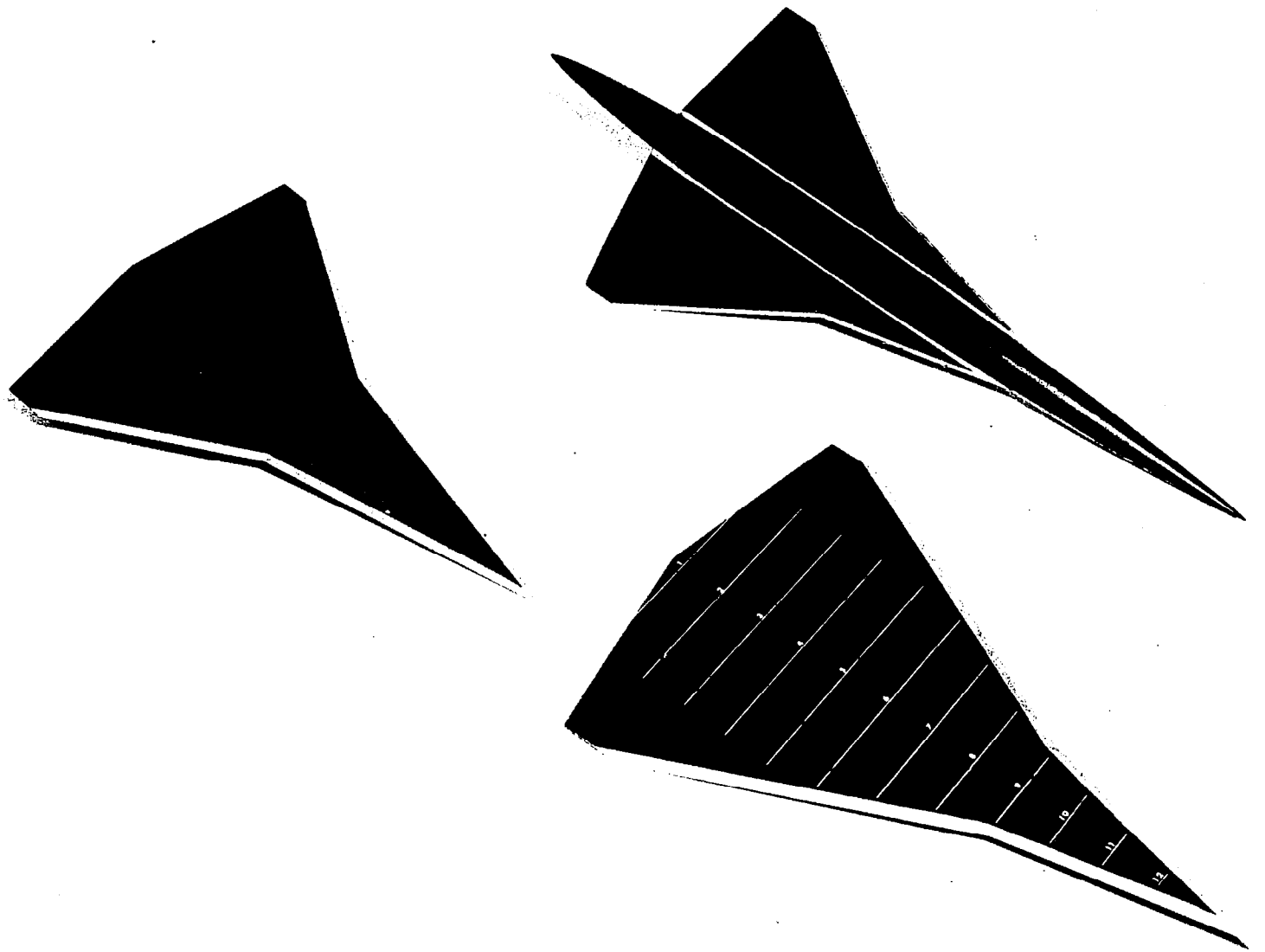

Figure 3.- Models tested in water tank.

Figure 4.- Water tank arrangement for surface and underwater photography.

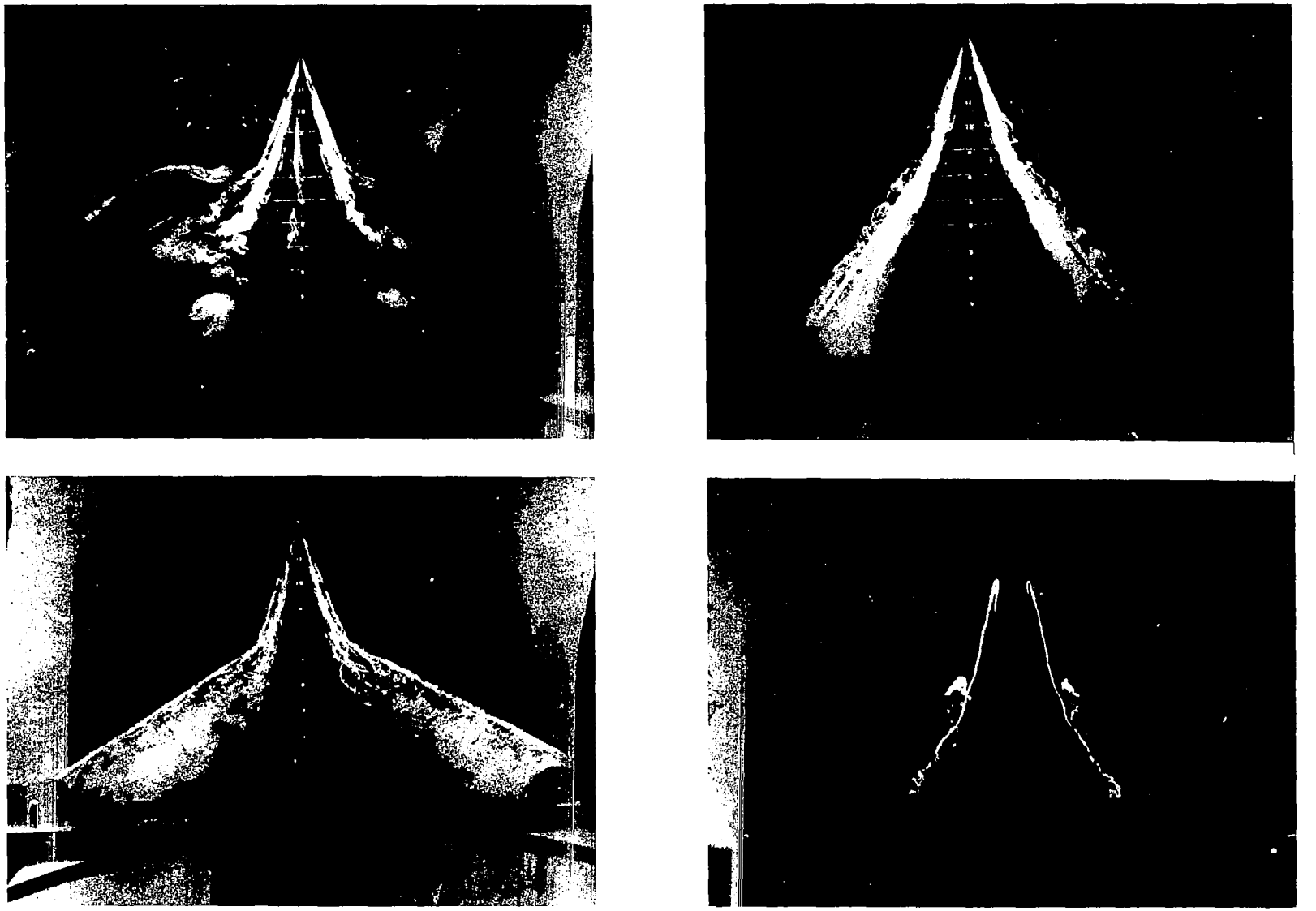

25° sweep of aft section

45° sweep of aft section

Figure 5.- Selected movie frames of double delta wing in water tank.

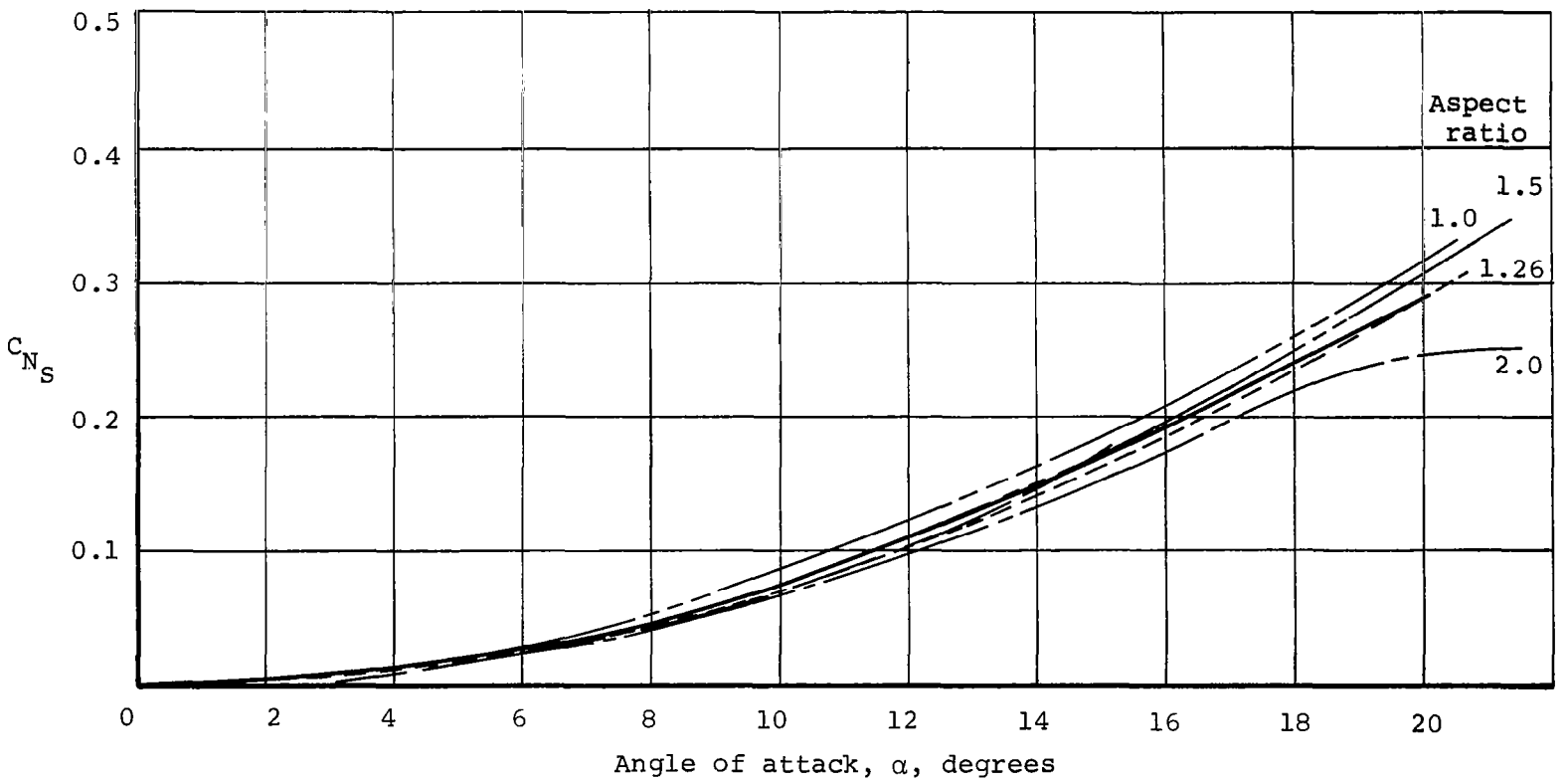

Figure 6.- Experimental values of separation normal force (measured minus attached) for delta wings from Refs. 2, 6, 7, and 31).

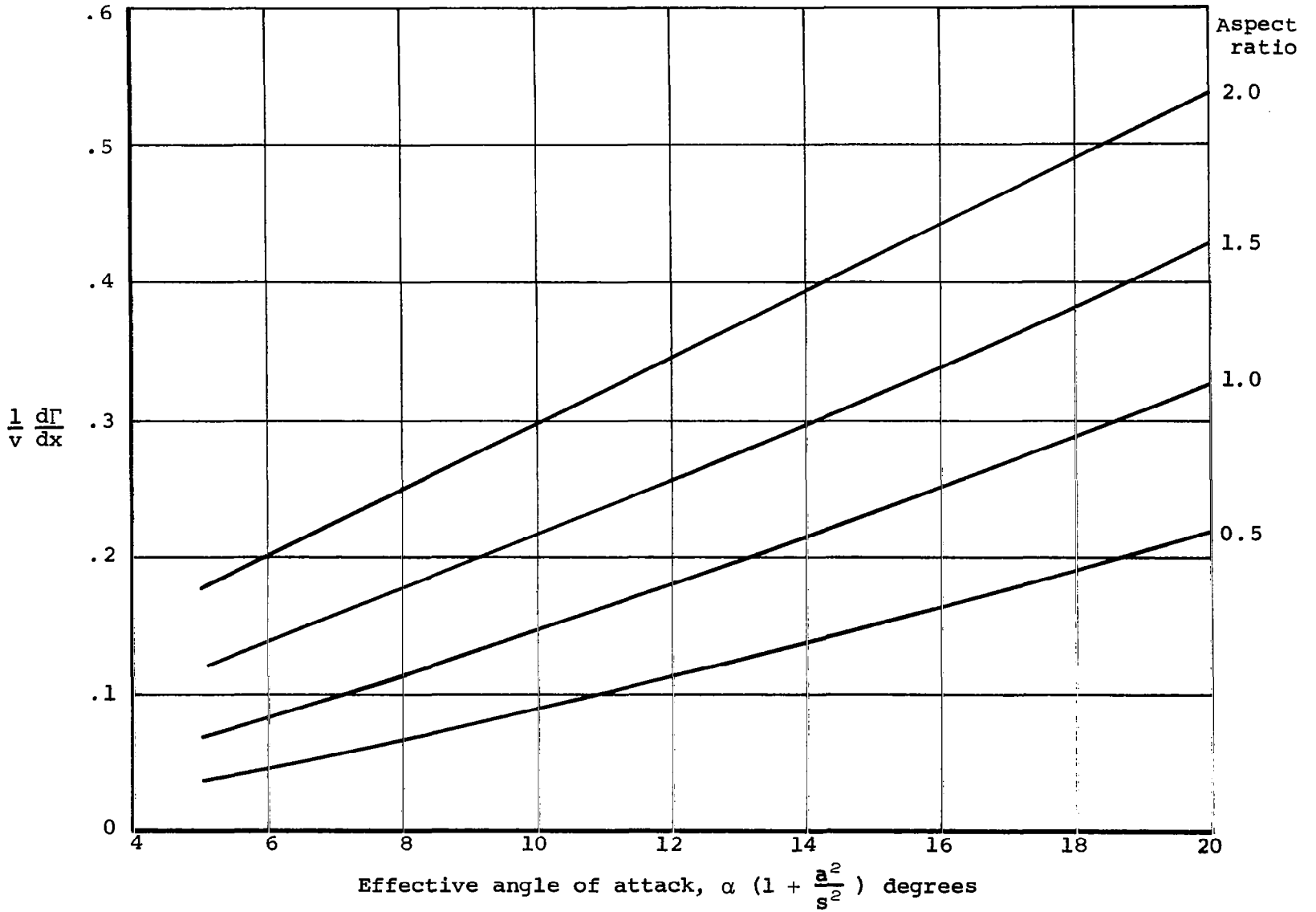

Figure 7.- Calculated shedding rates for use in semi-empirical method.

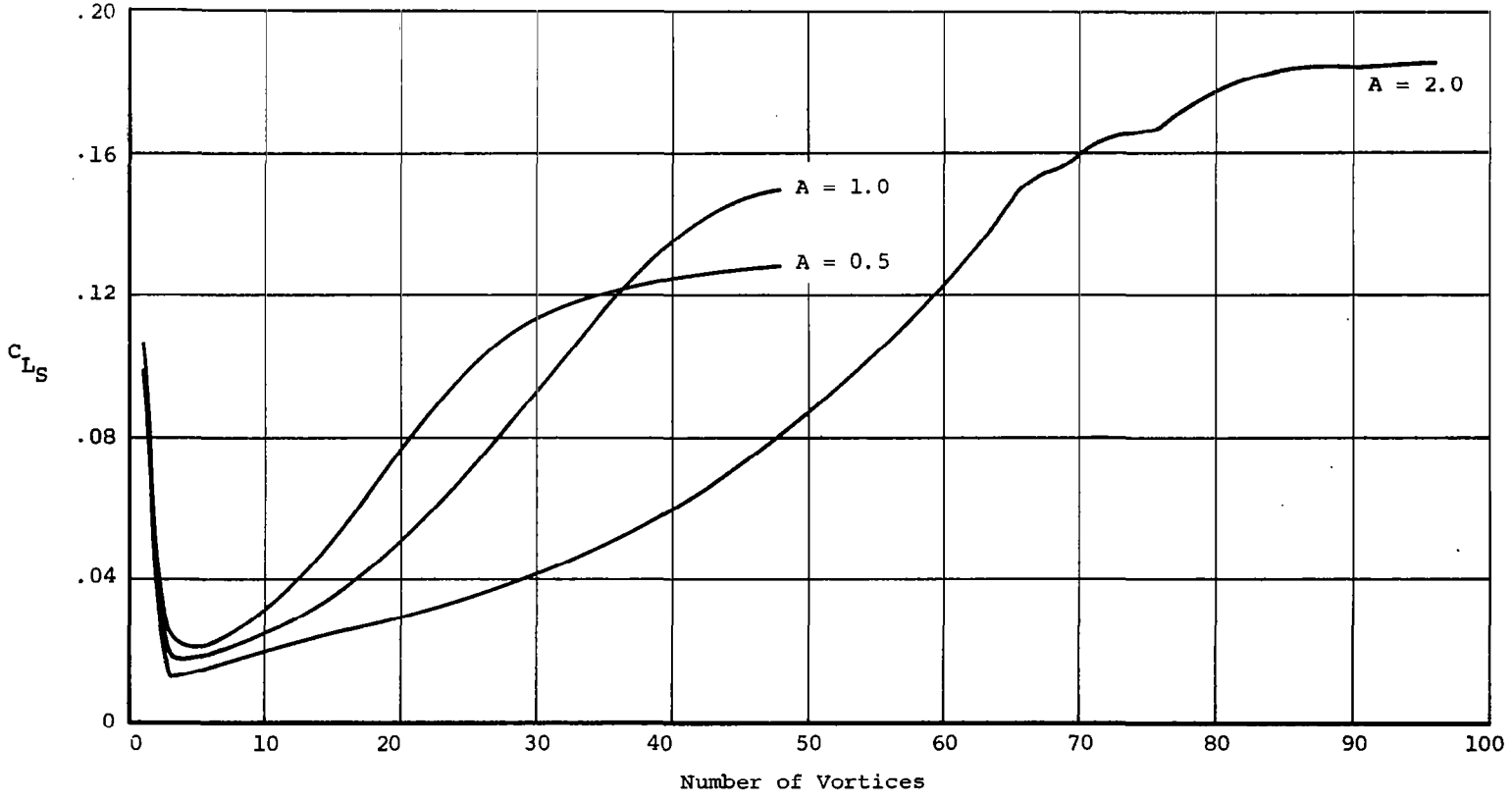

Figure 8.- Theoretical method convergence check for delta wings ($\alpha = 10^{\circ}$).

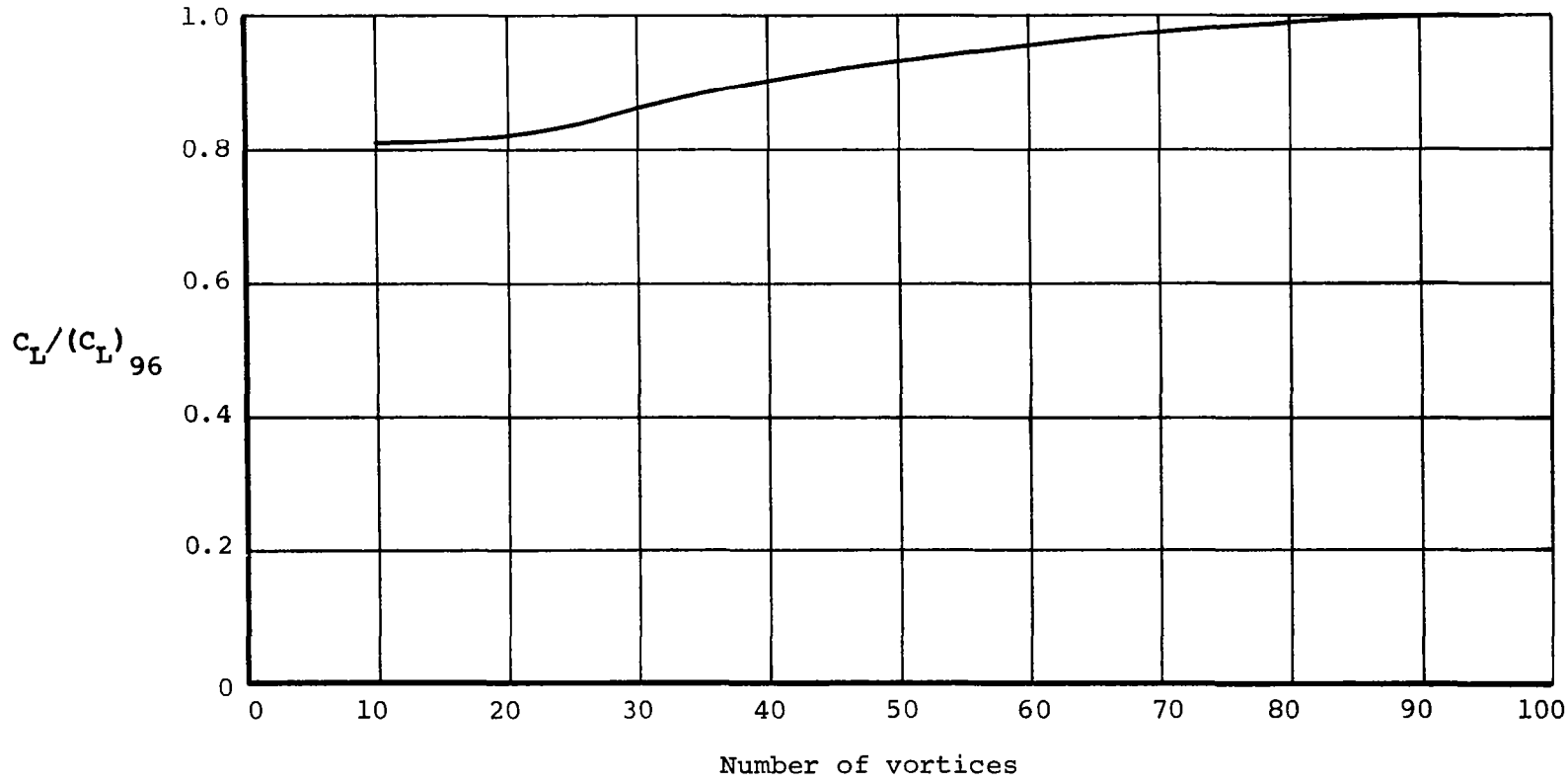

Figure 9.- Semi-empirical method convergence check for delta wing of aspect ratio 2.

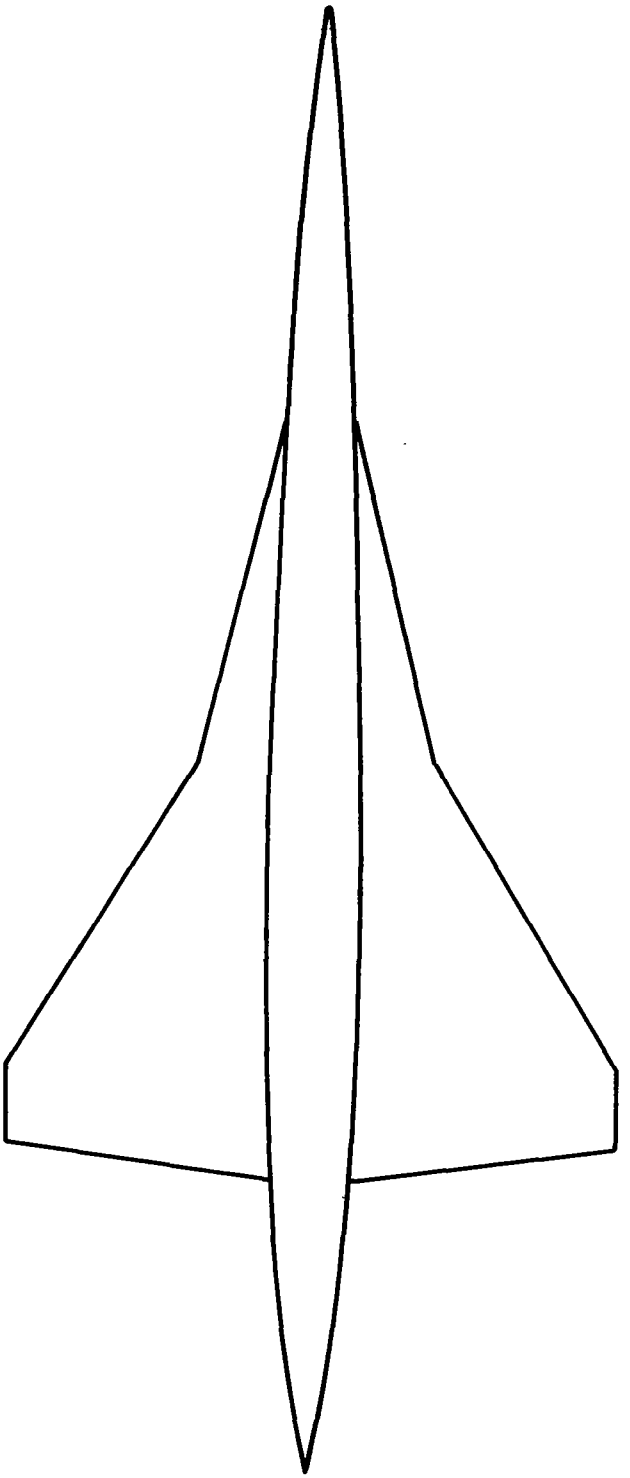

Figure 10.- Double-delta wing-body configuration.
(See Table I for dimensions.)

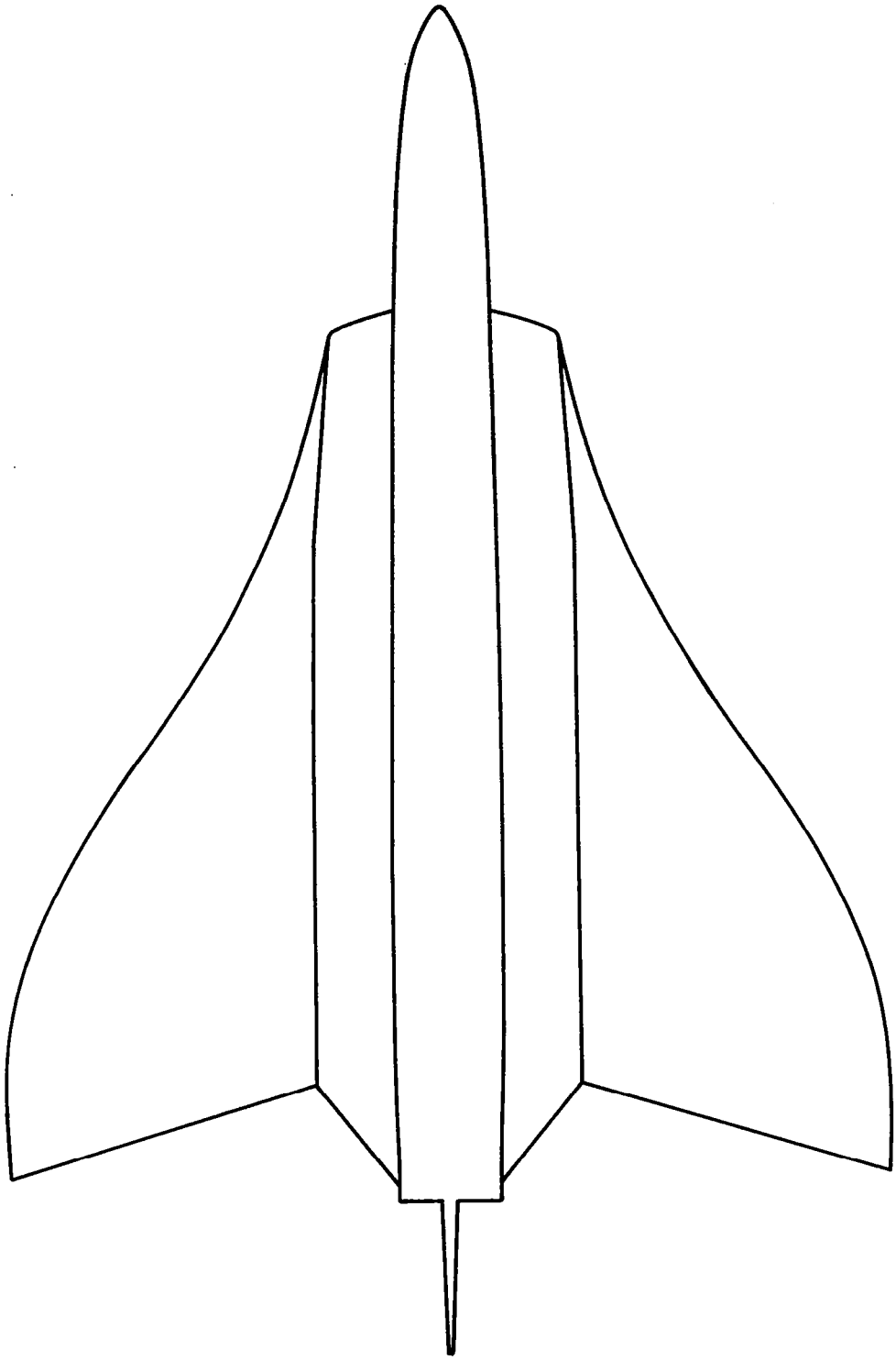

Figure 11.- OGEE modified F5D wing-body configuration.
(See Table II for dimensions)

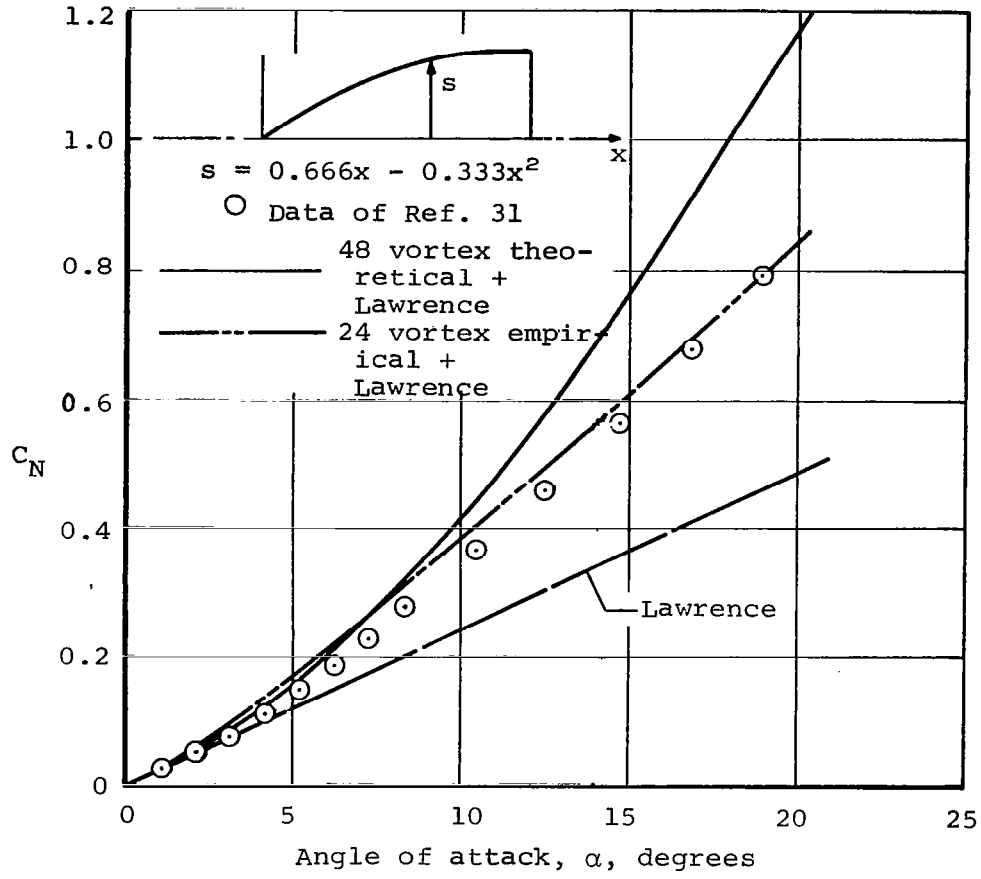

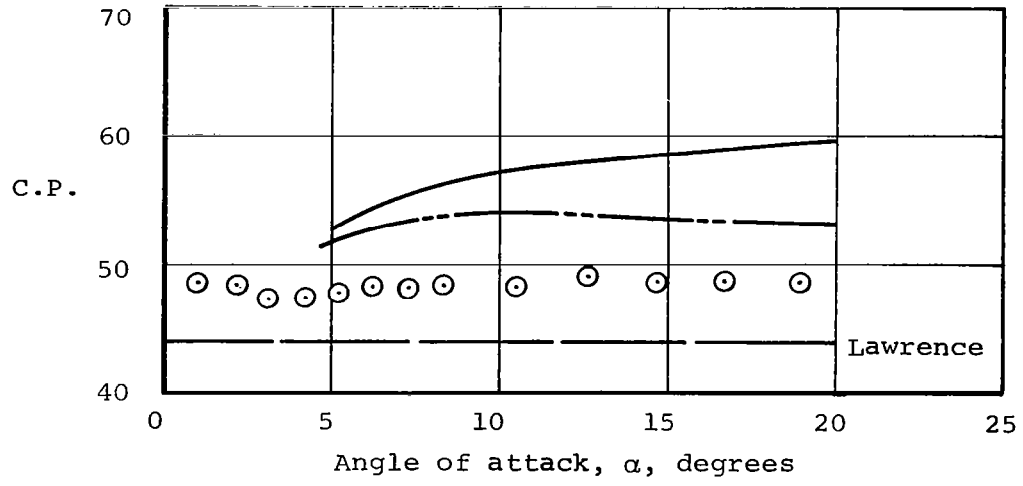

Figure 12.- Calculated and experimental normal force and center of pressure for gothic wing of aspect ratio 1.0.

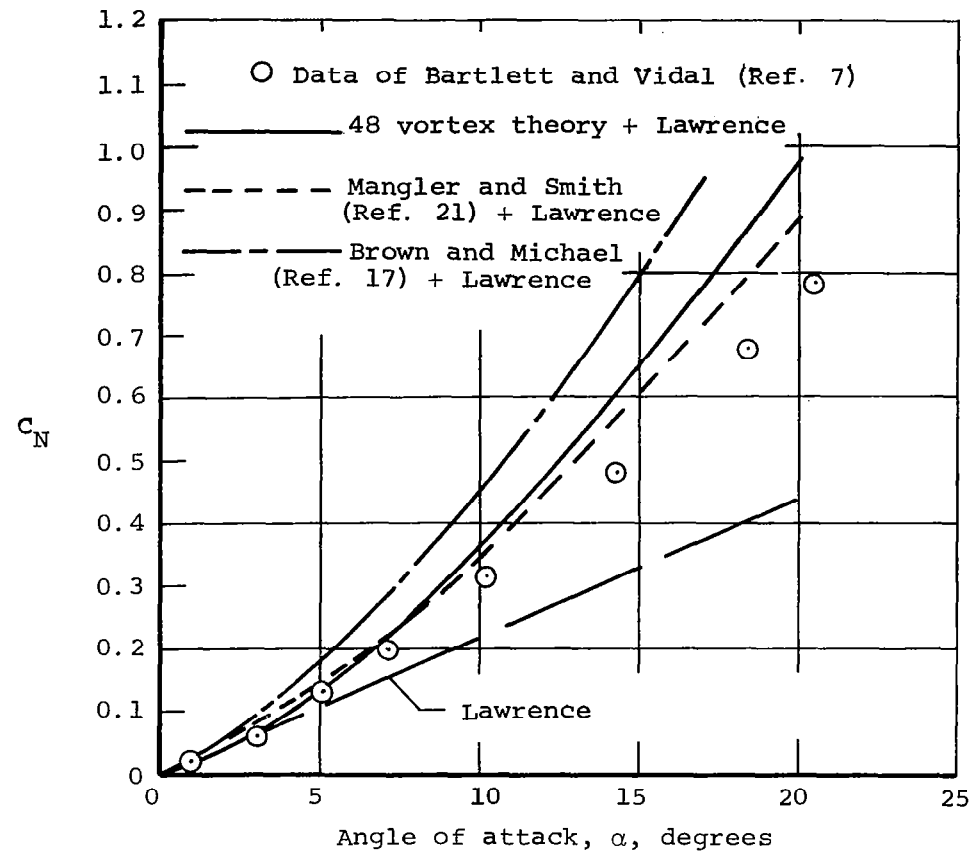

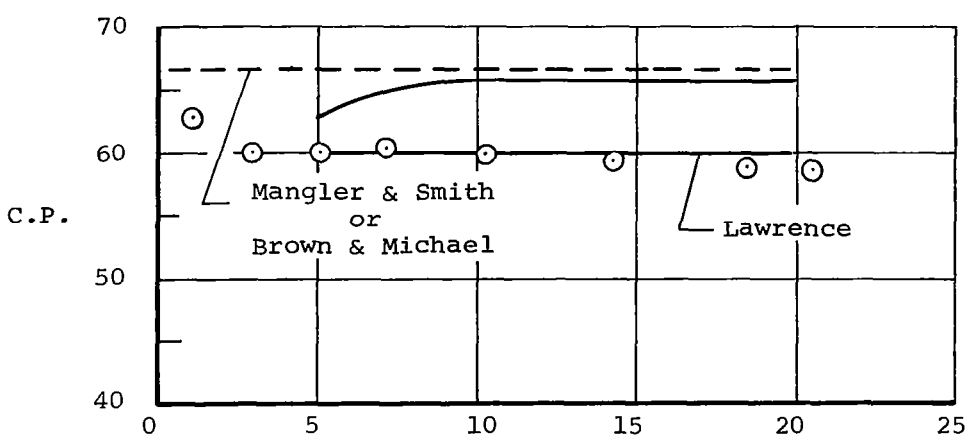

(a) Aspect ratio 1.0

Figure 13.- Comparison of theoretical methods with experimental measurements of normal force and center of pressure on delta wings.

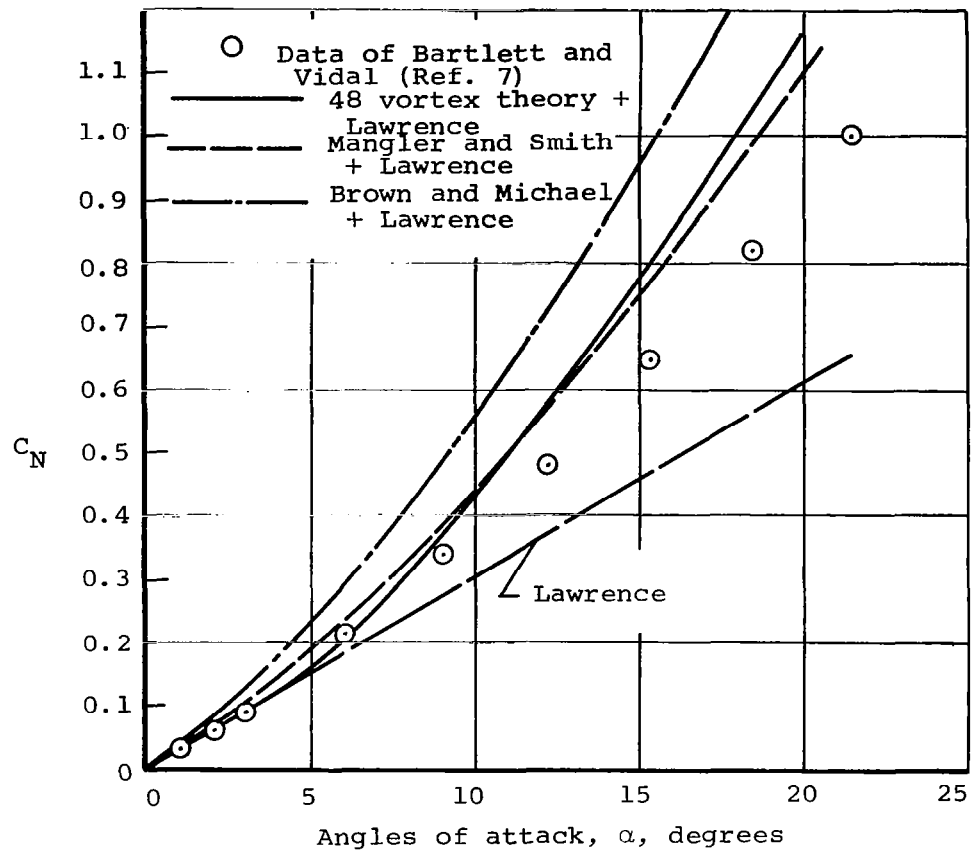

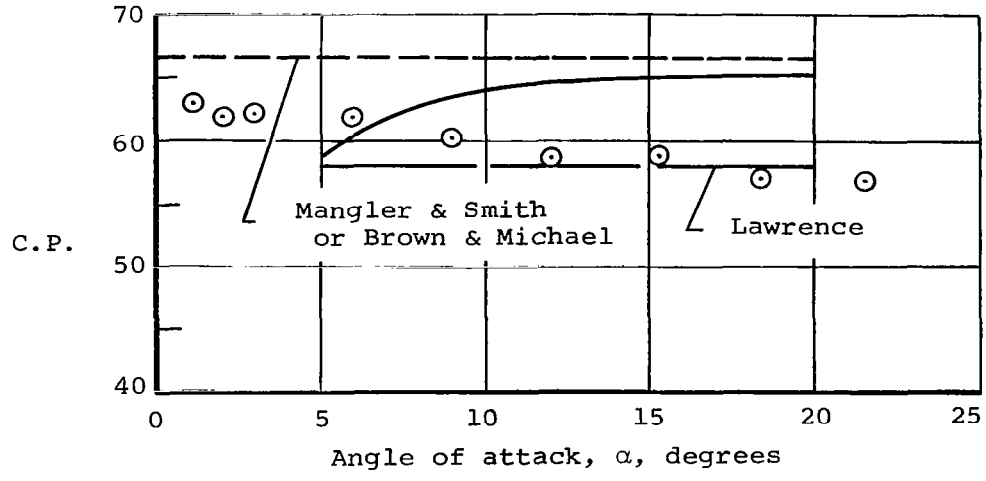

(b) Aspect ratio 1.5

Figure 13.- Concluded.

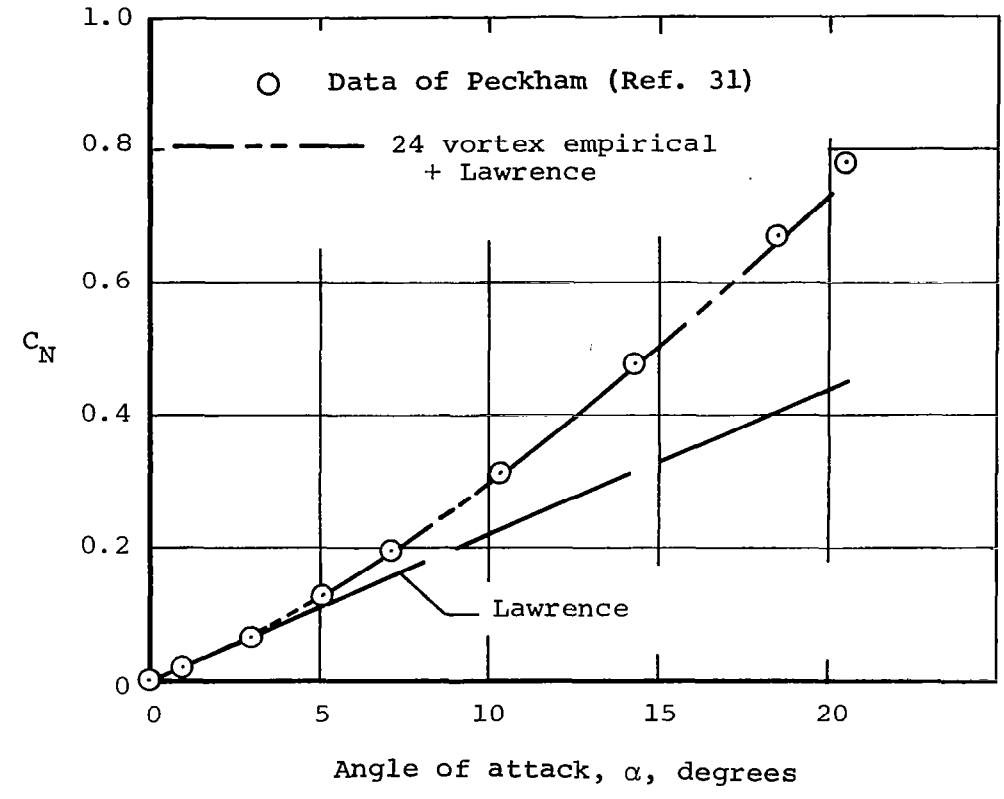

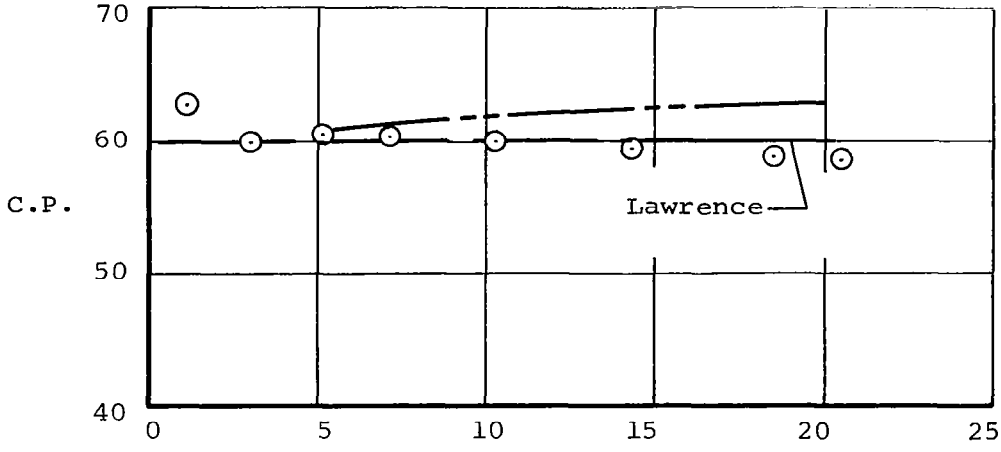

(a) Aspect ratio 1.0

Figure 14.- Comparison of semi-empirical method with experimental measurements of normal force and center of pressure on delta wings.

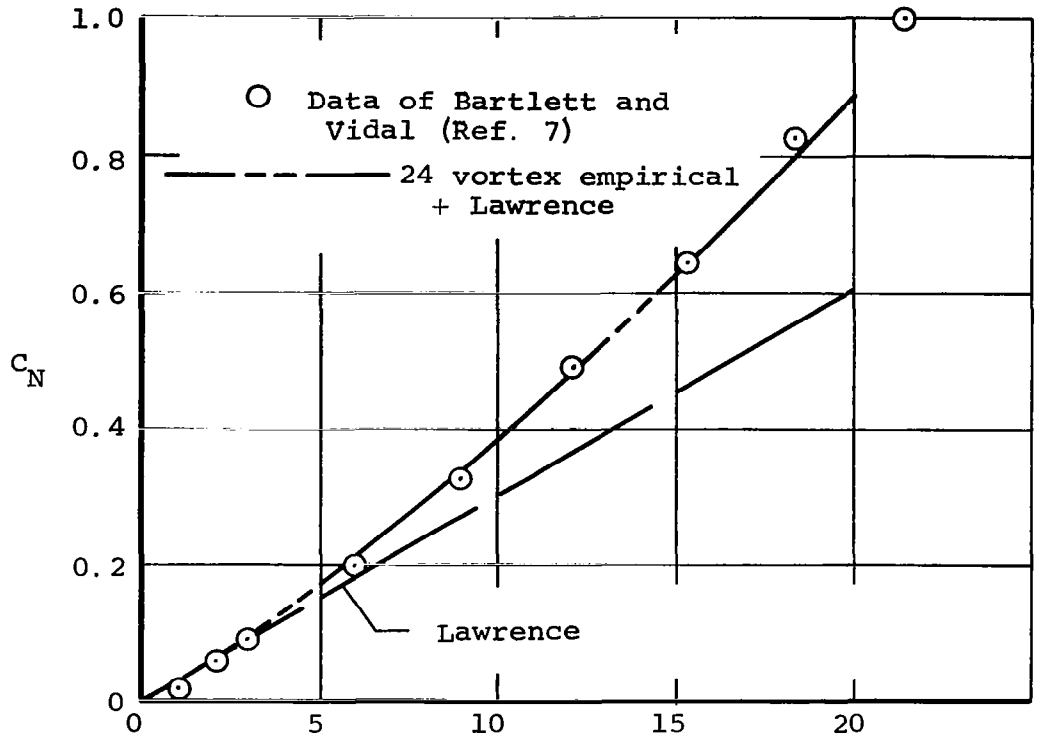

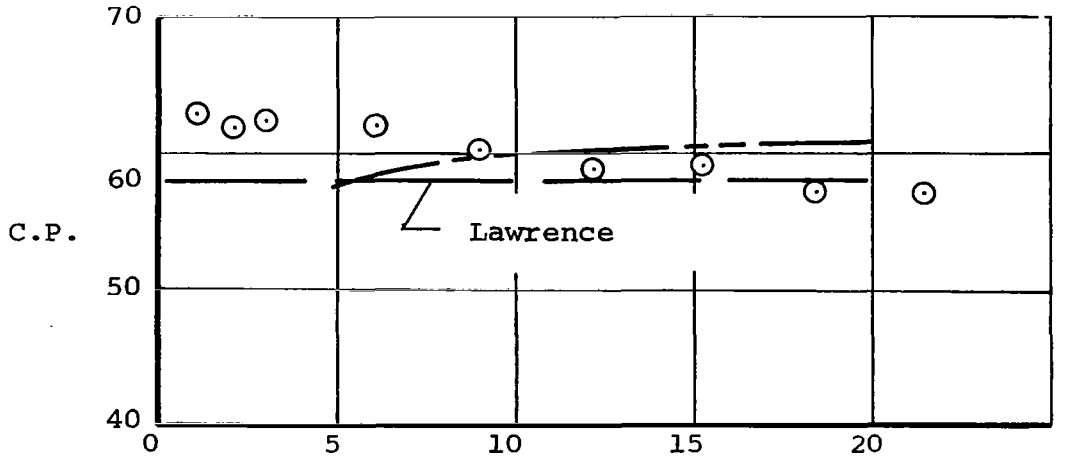

(b) Aspect ratio 1.5

Figure 14.- Continued.

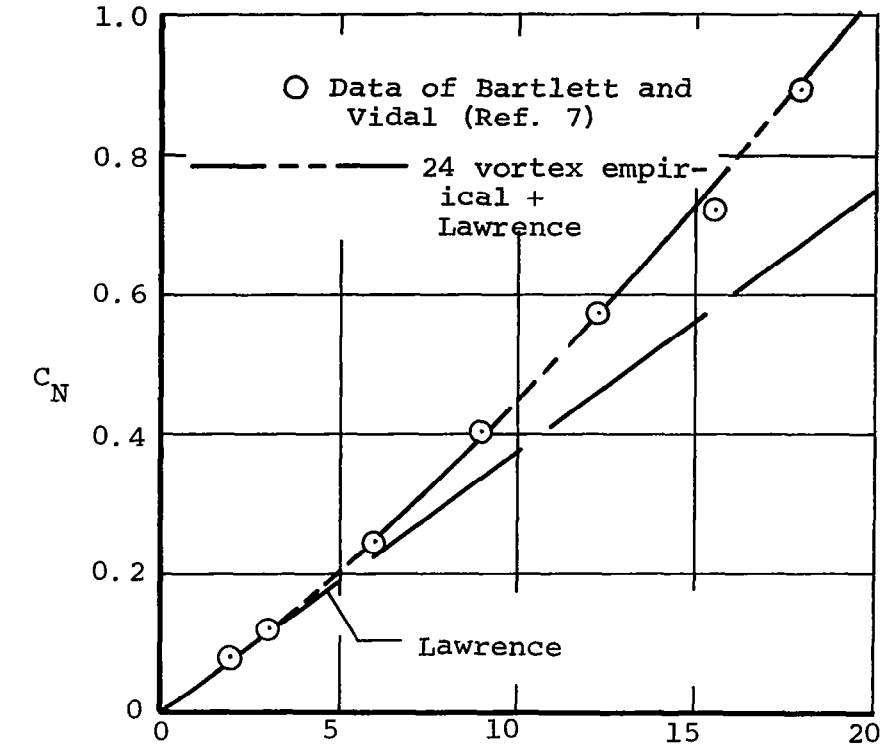

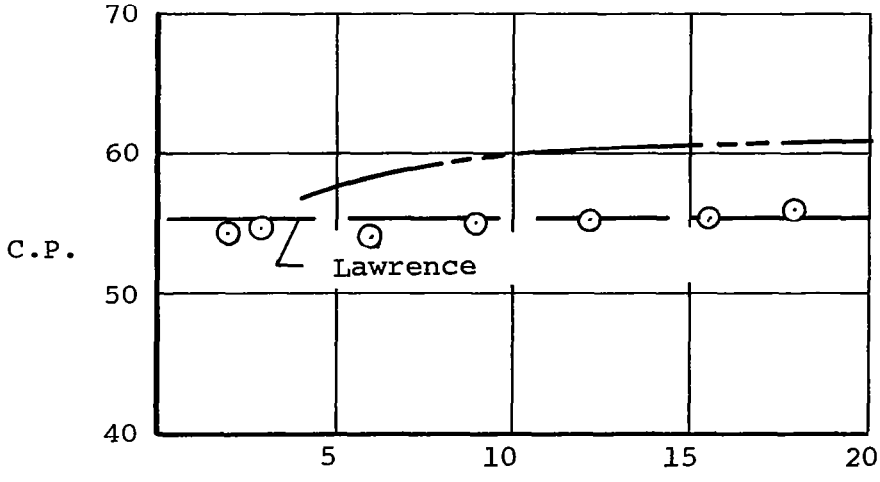

(c) Aspect ratio 2.0

Figure 14.- Concluded.

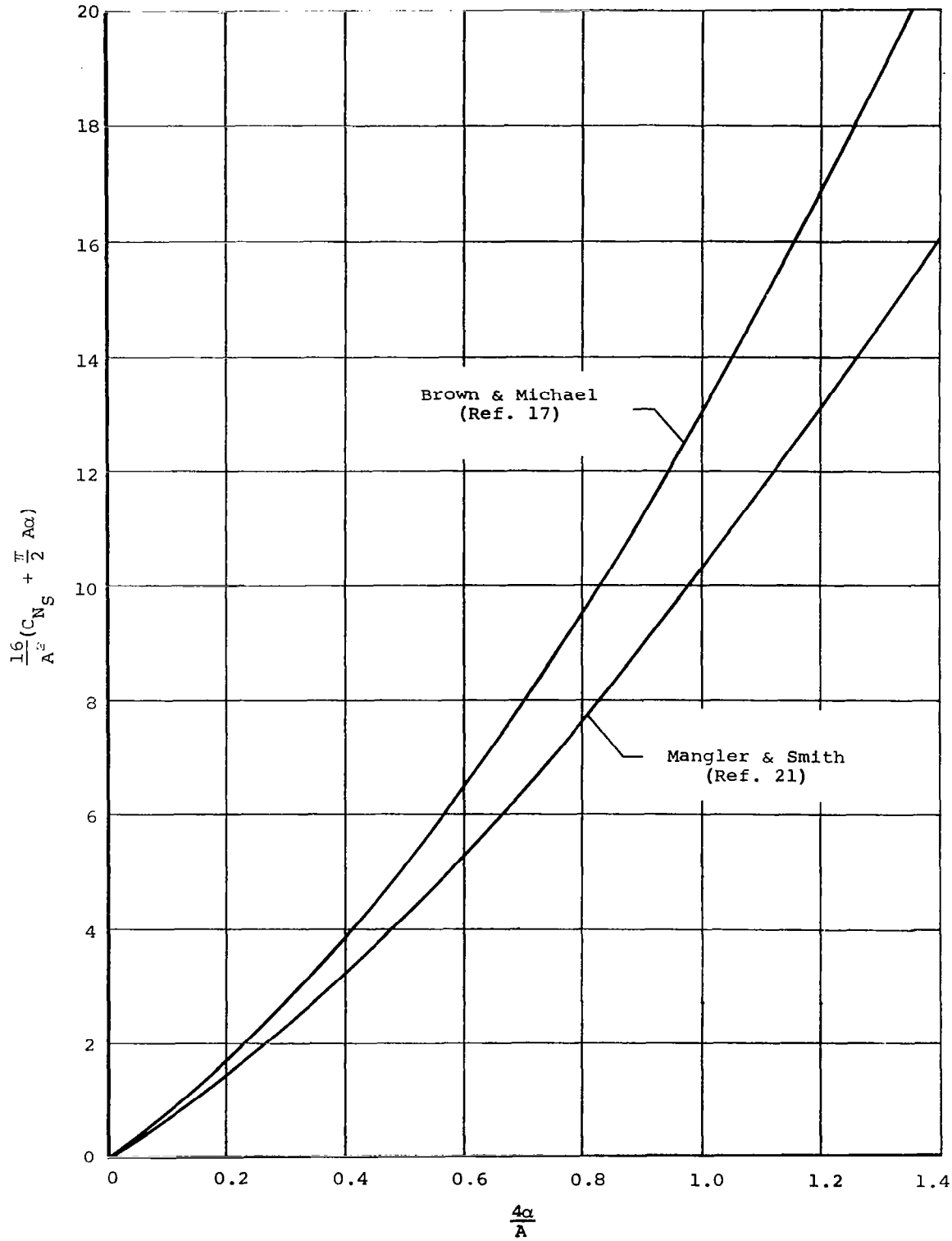

Figure 15.- Theoretical slender-body lift coefficient for delta wings with separated flow.

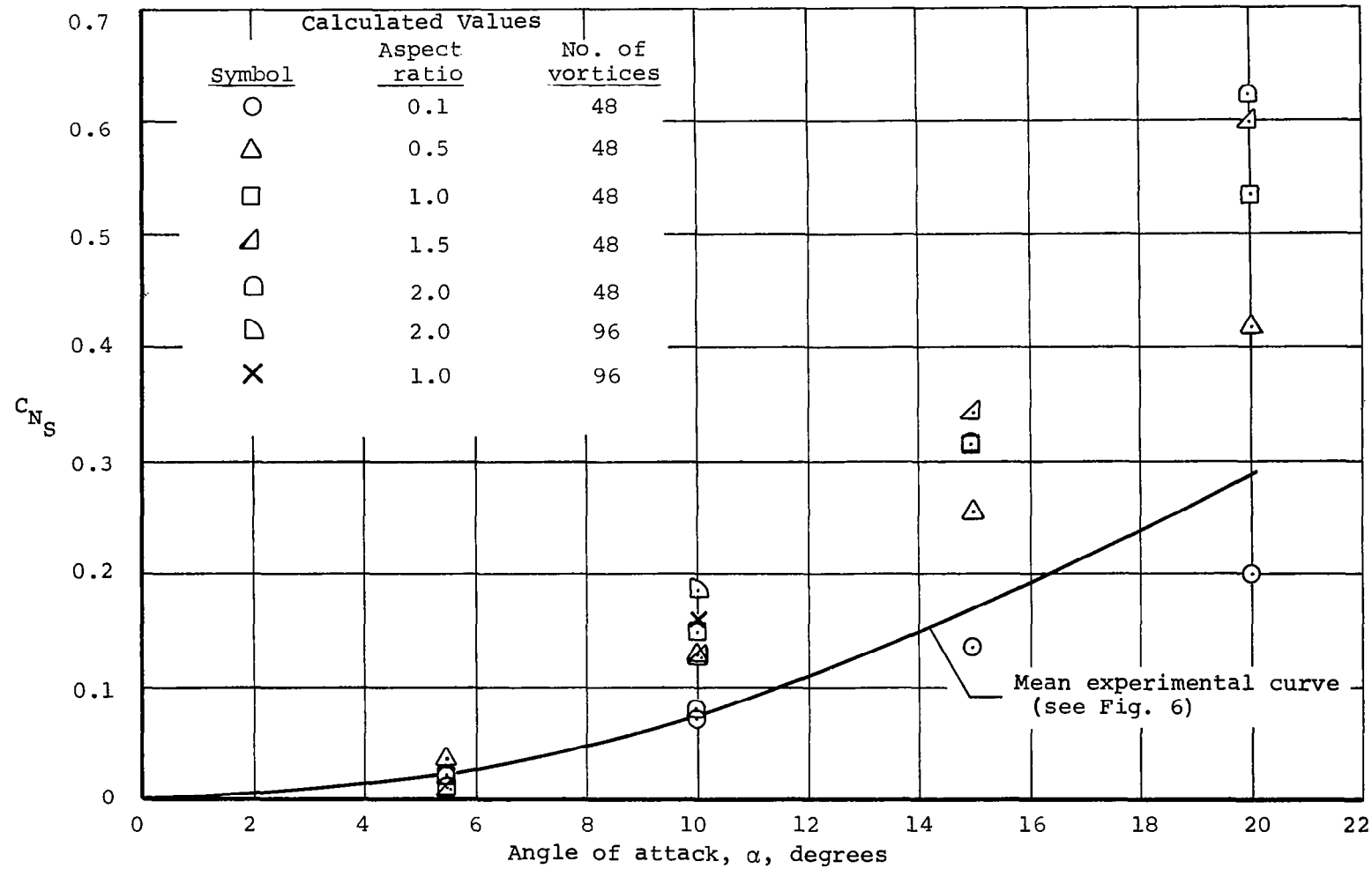

Figure 16.- Comparison of calculated and experimental separation normal force for delta wings.

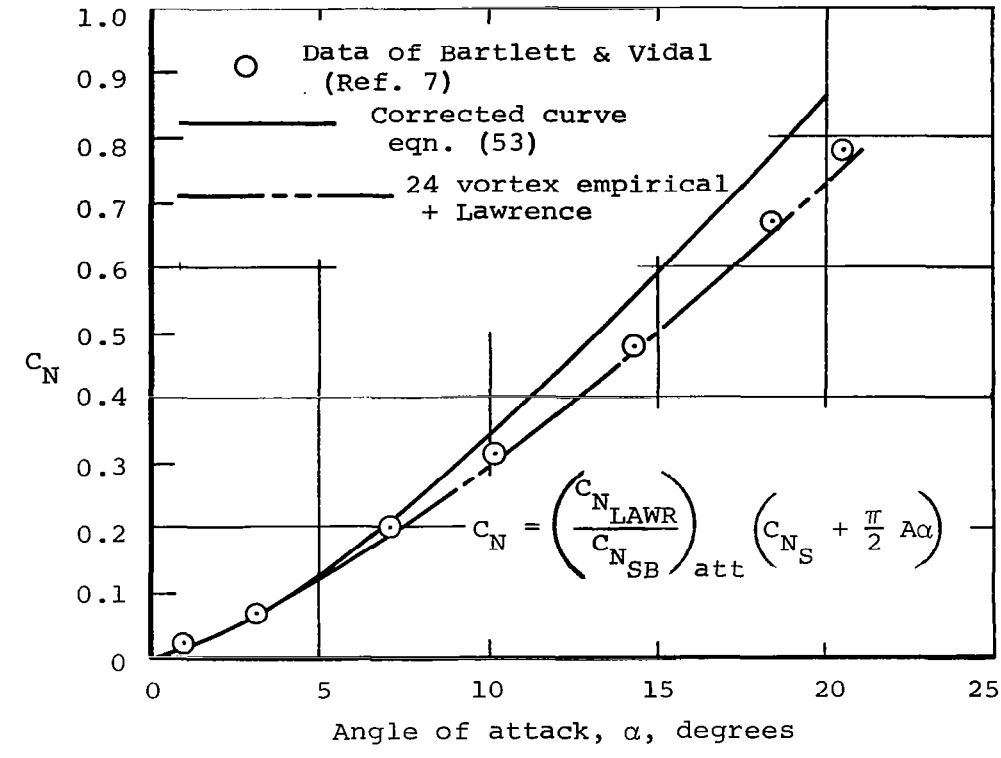

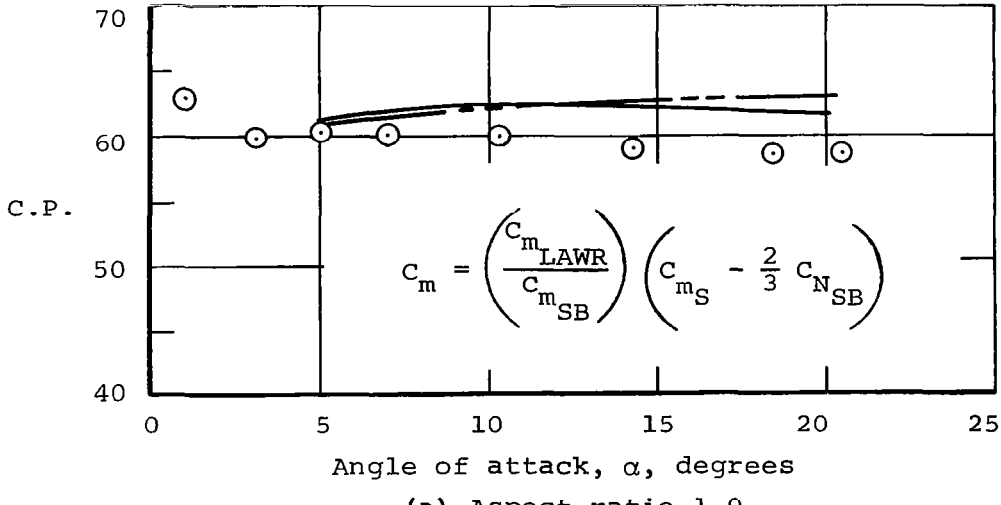

(a) Aspect ratio 1.0.

Figure 17.- Comparison of "corrected" normal force and center of pressure with experimental measurements for delta wings.

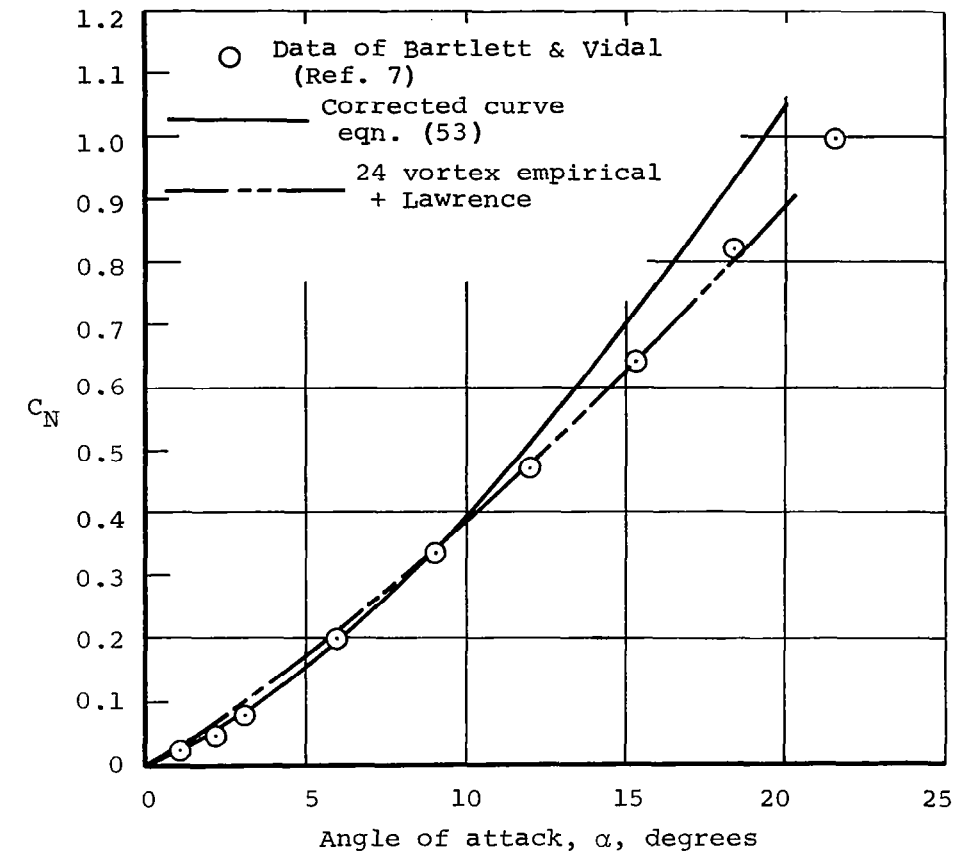

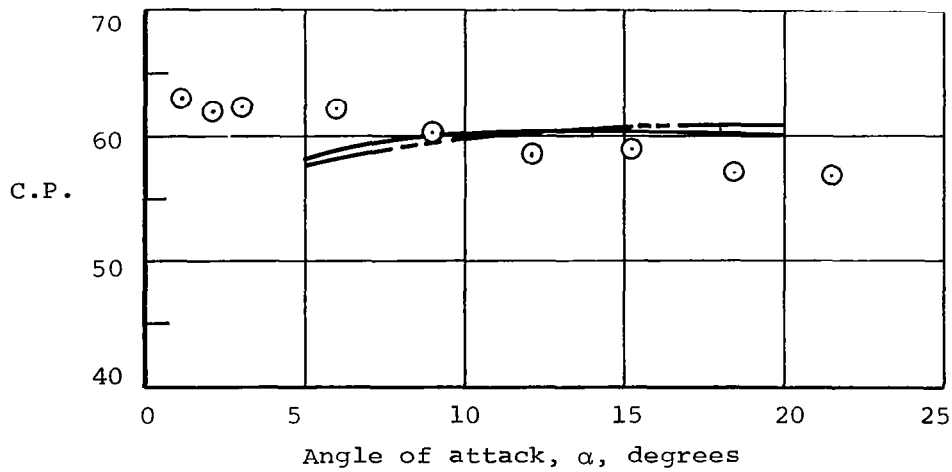

(b) Aspect ratio 1.5.

Figure 17.- Concluded.

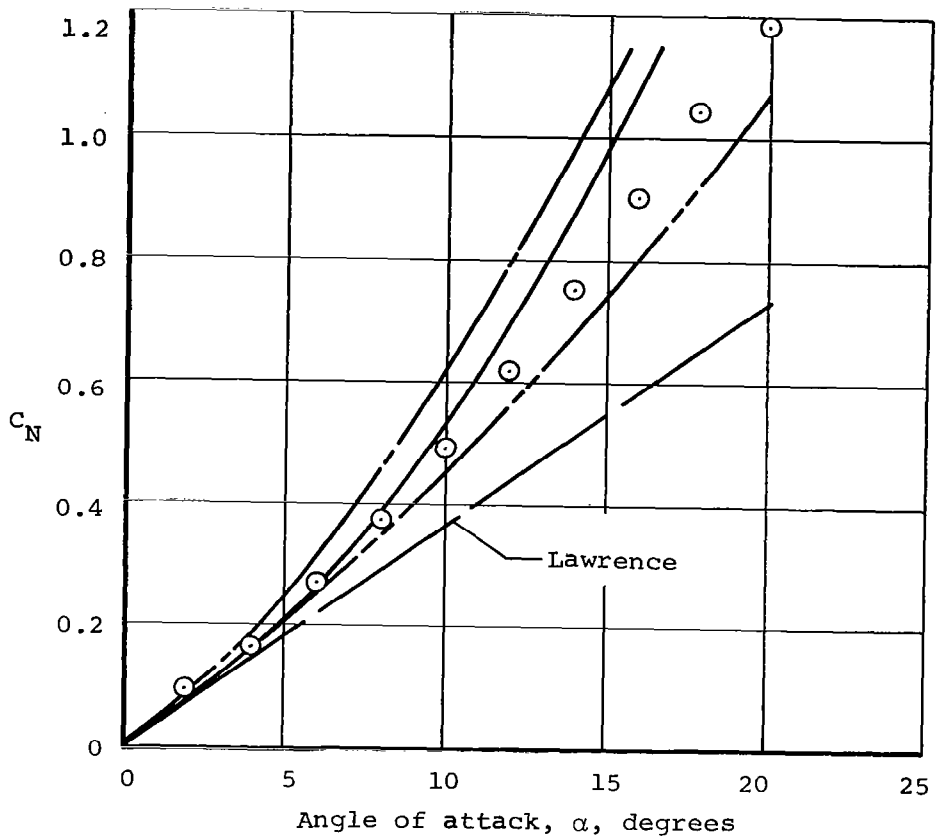

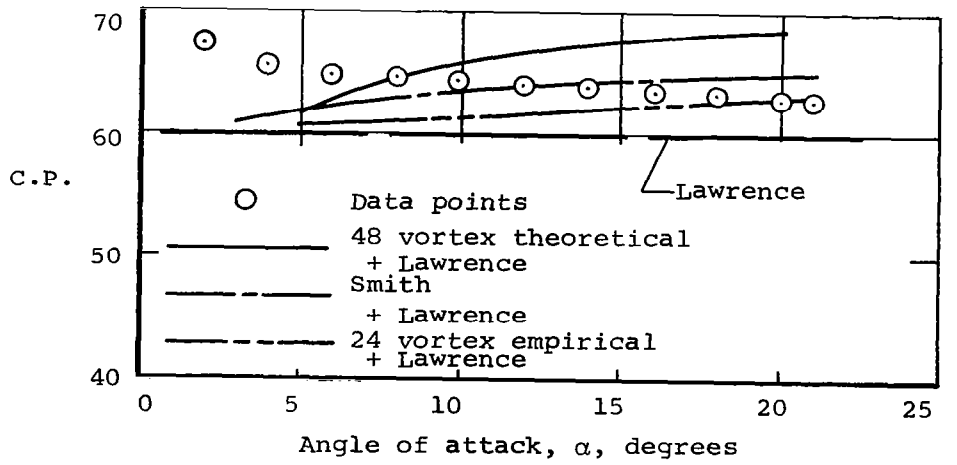

Figure 18.- Comparison of calculated normal force and center of pressure with experimental measurements for double-delta wing-body configuration.

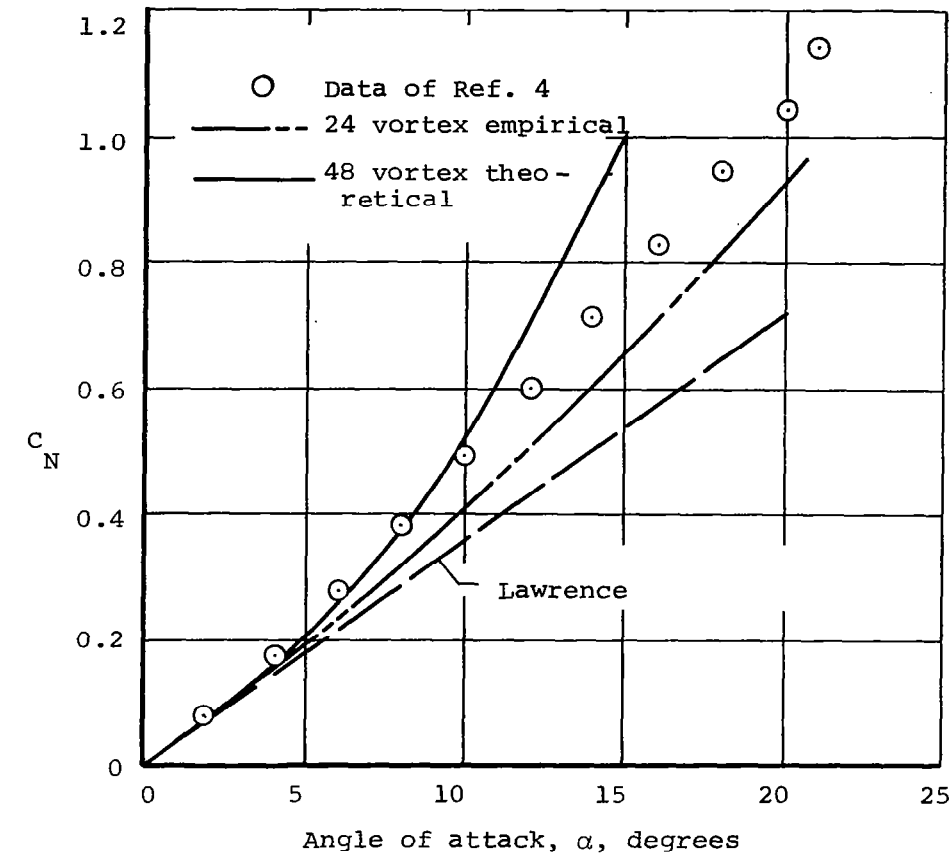

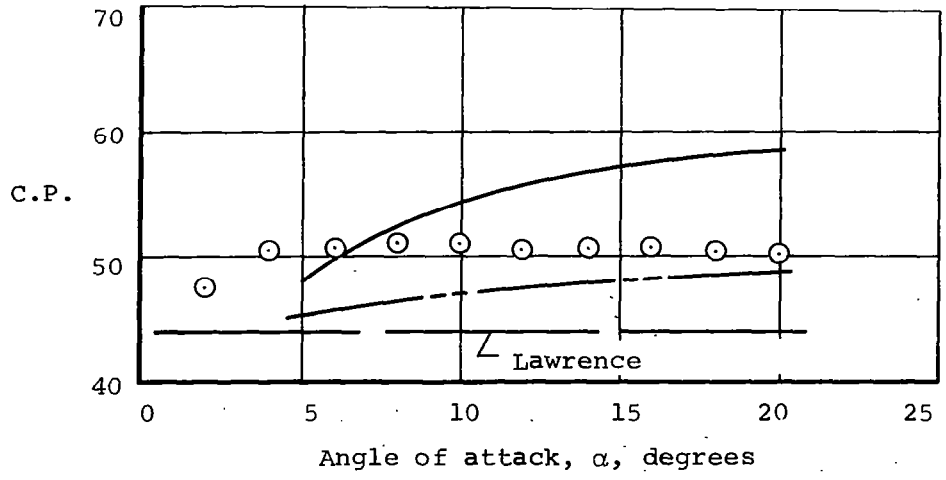

Figure 19.- Comparison of calculated normal force and center of pressure with experimental measurements for OGEE modified F5D wing-body configuration.

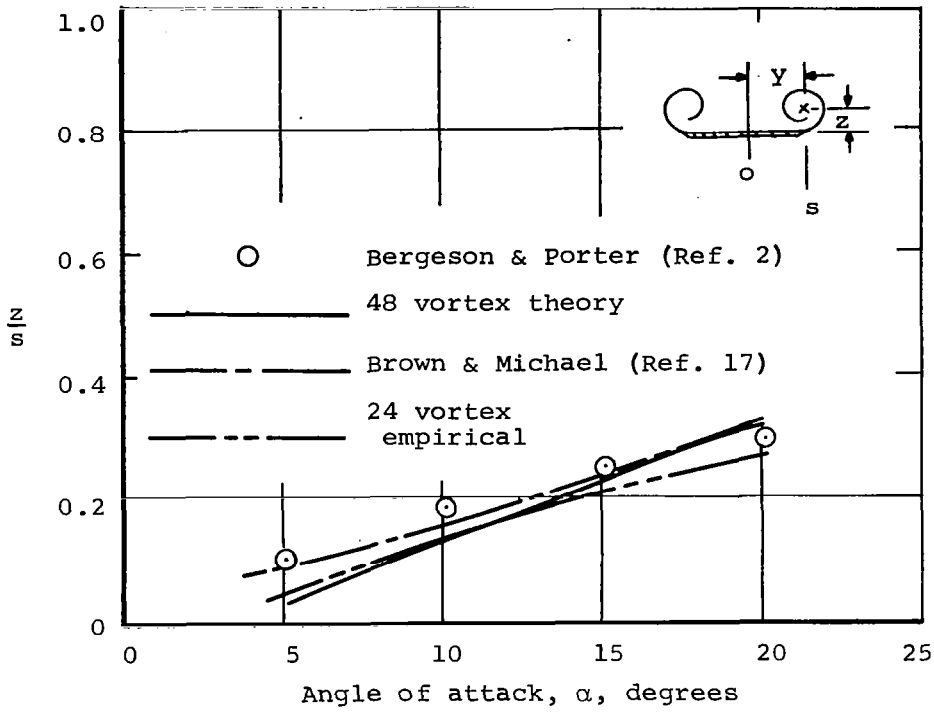

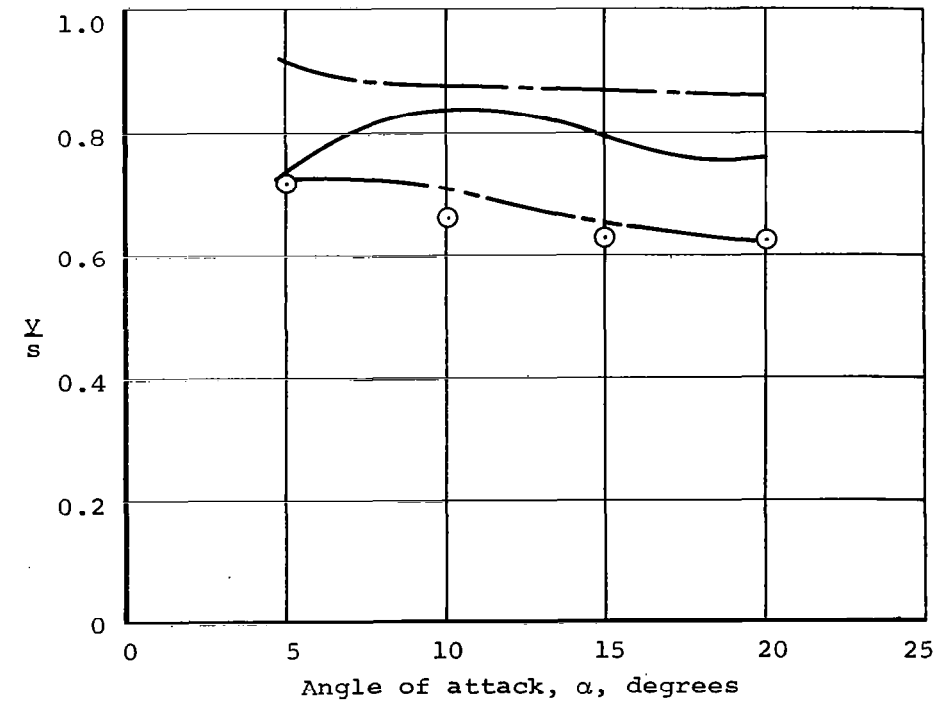

Figure 20.- Predicted and measured vortex locations on delta wing of aspect ratio 1.0.

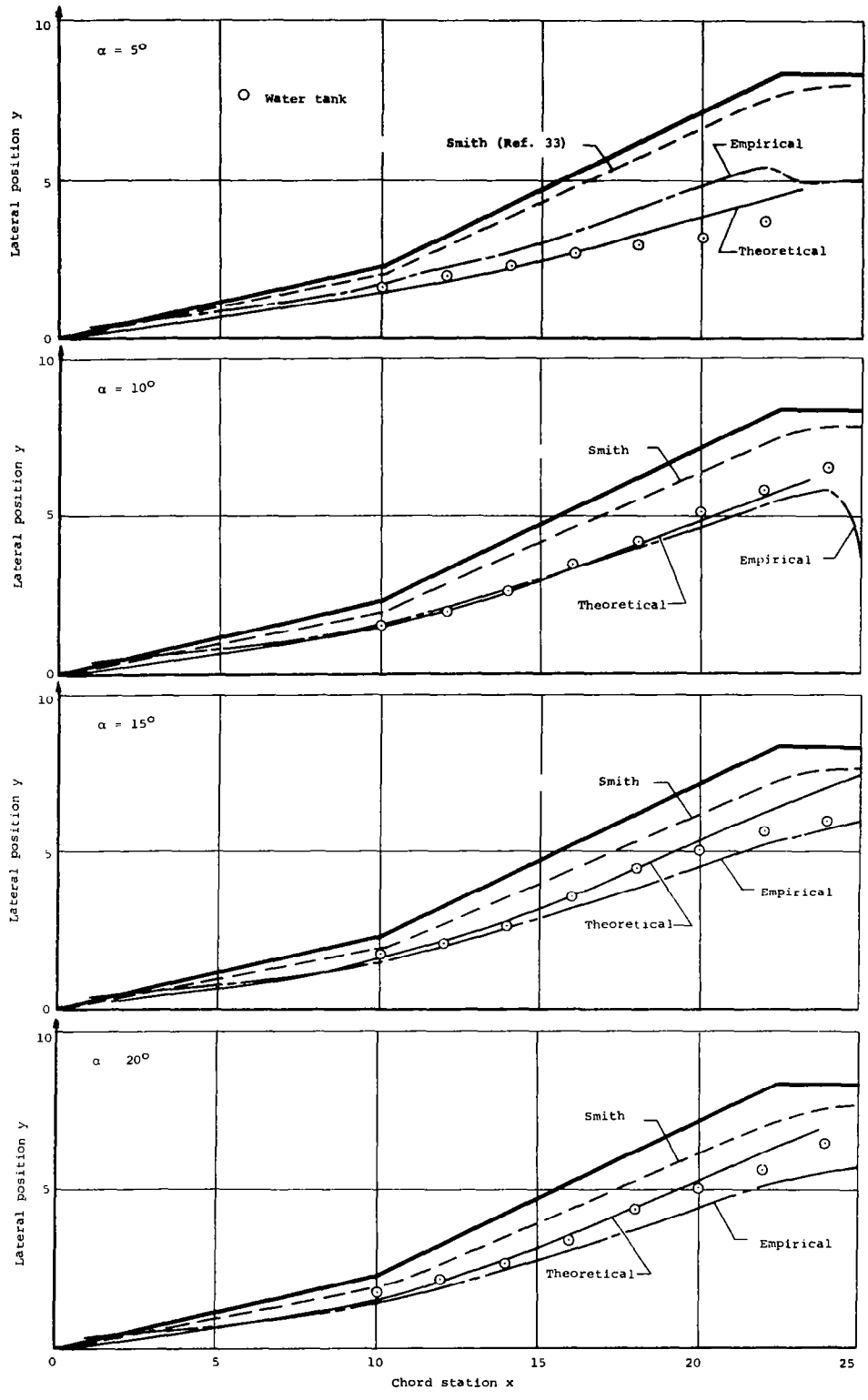

Figure 21.- Positions of separation vortices on a double delta wing.

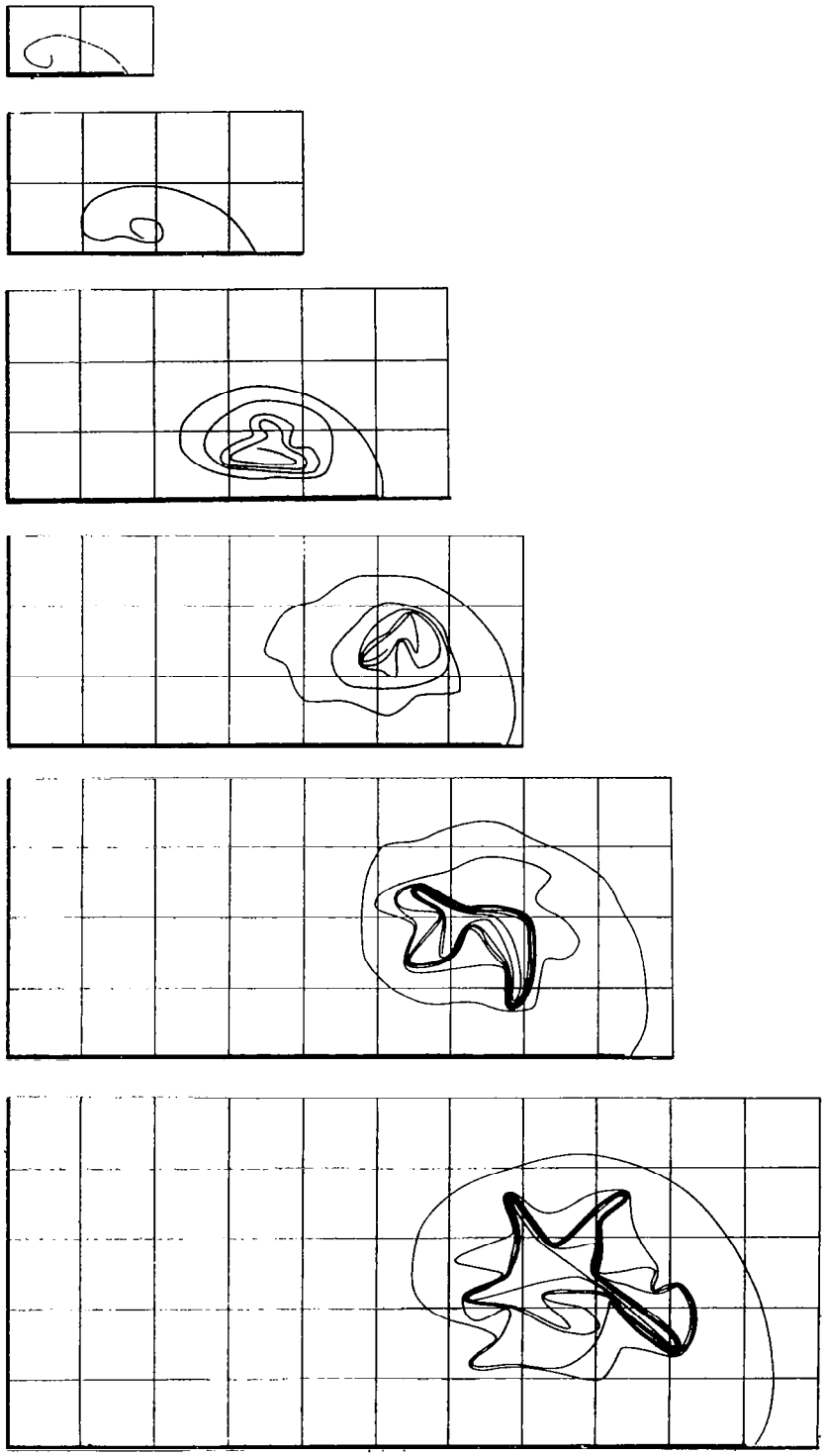

Figure 22.- Vortex sheet development on an aspect ratio 1.0 delta wing at 15° angle of attack - theoretical shedding rates.

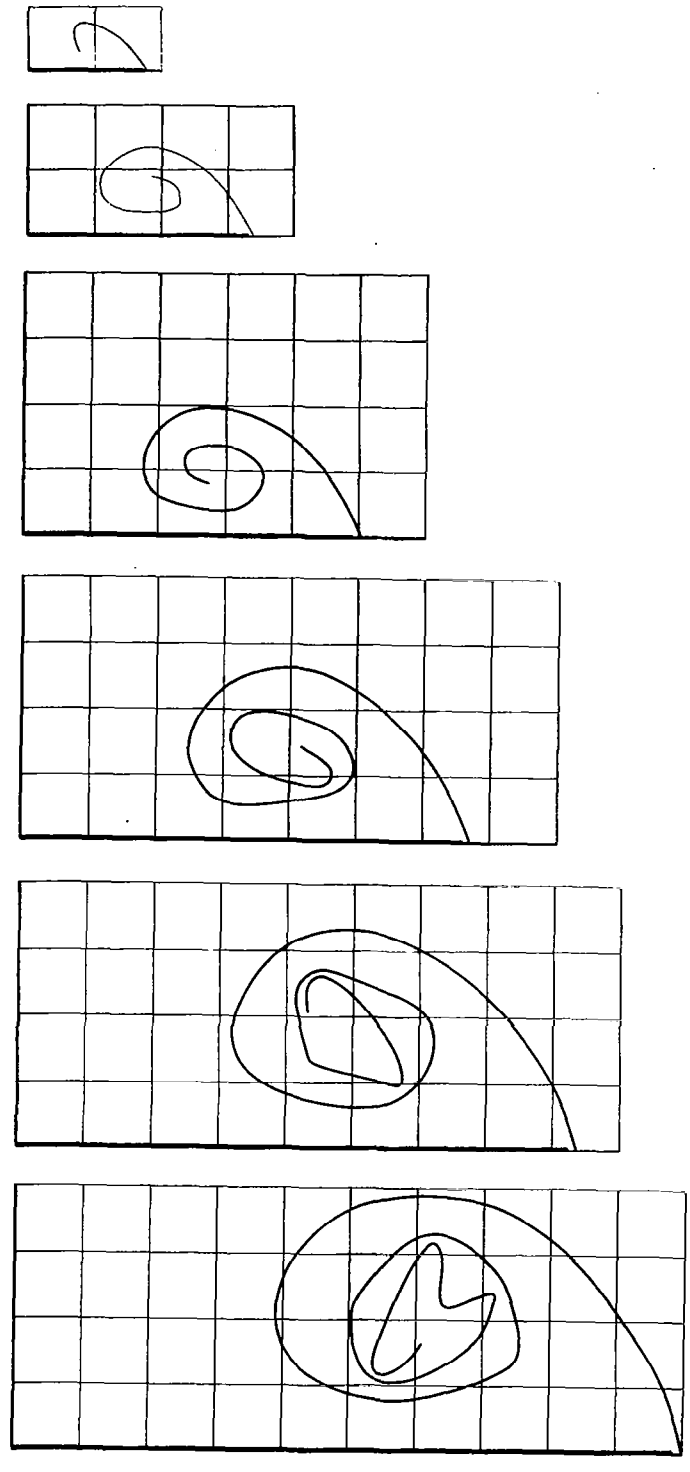

Figure 23.- Vortex sheet development on an aspect ratio 1.0 delta wing at 15° angle of attack - empirical shedding rates.

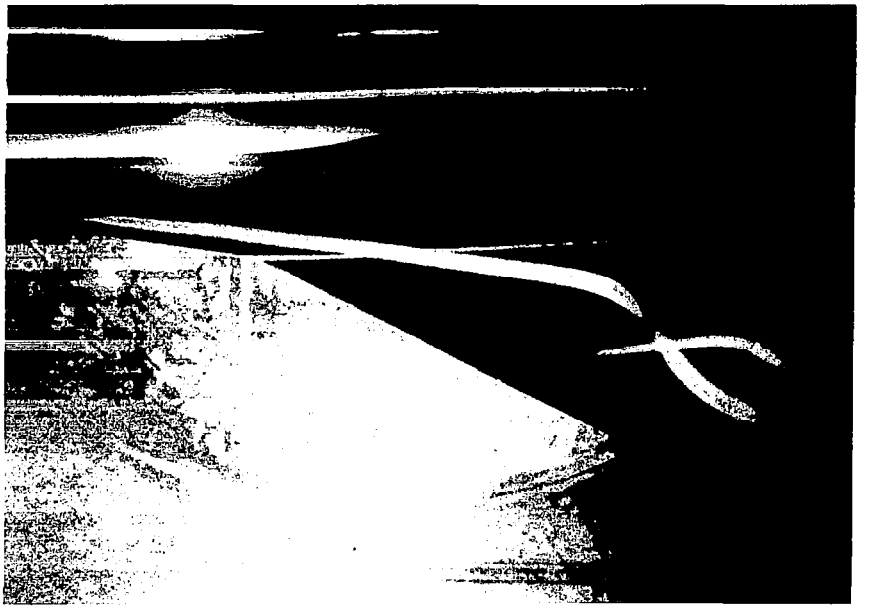

(a) Plan view.

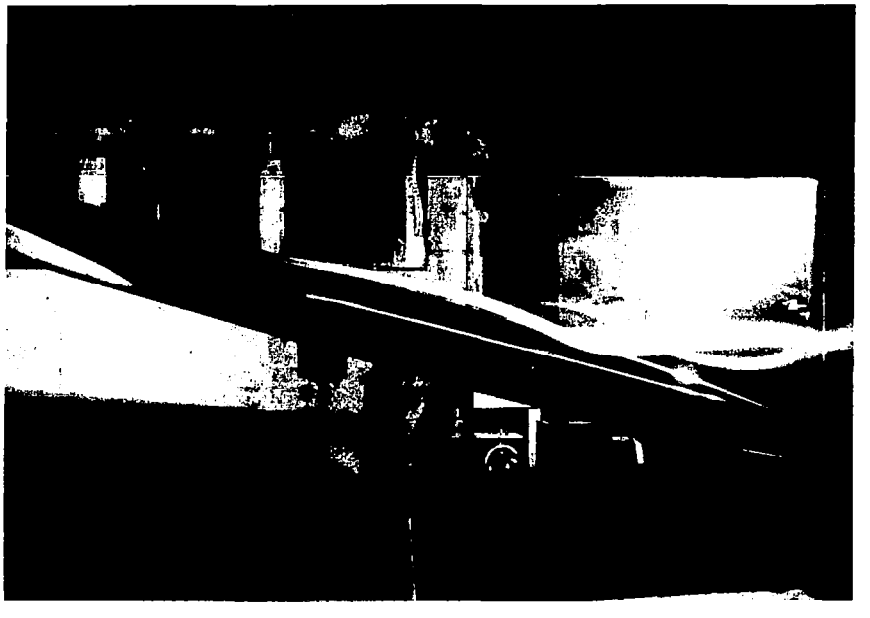

(b) Side view.

Figure 24.- Vortex patterns over double-delta wing-body combination as observed in Ames 7- by 10-foot wind tunnel ($\alpha = 16^{\circ}$).

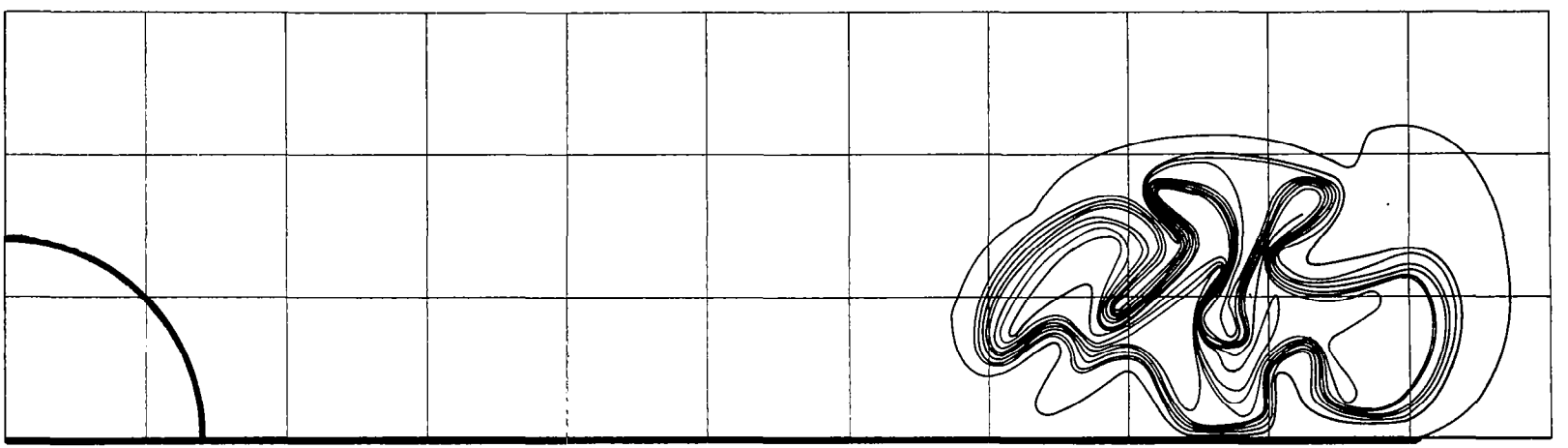

Figure 25.- Vortex sheet shape calculated by theoretical method at trailing edge of double-delta wing-body combination.

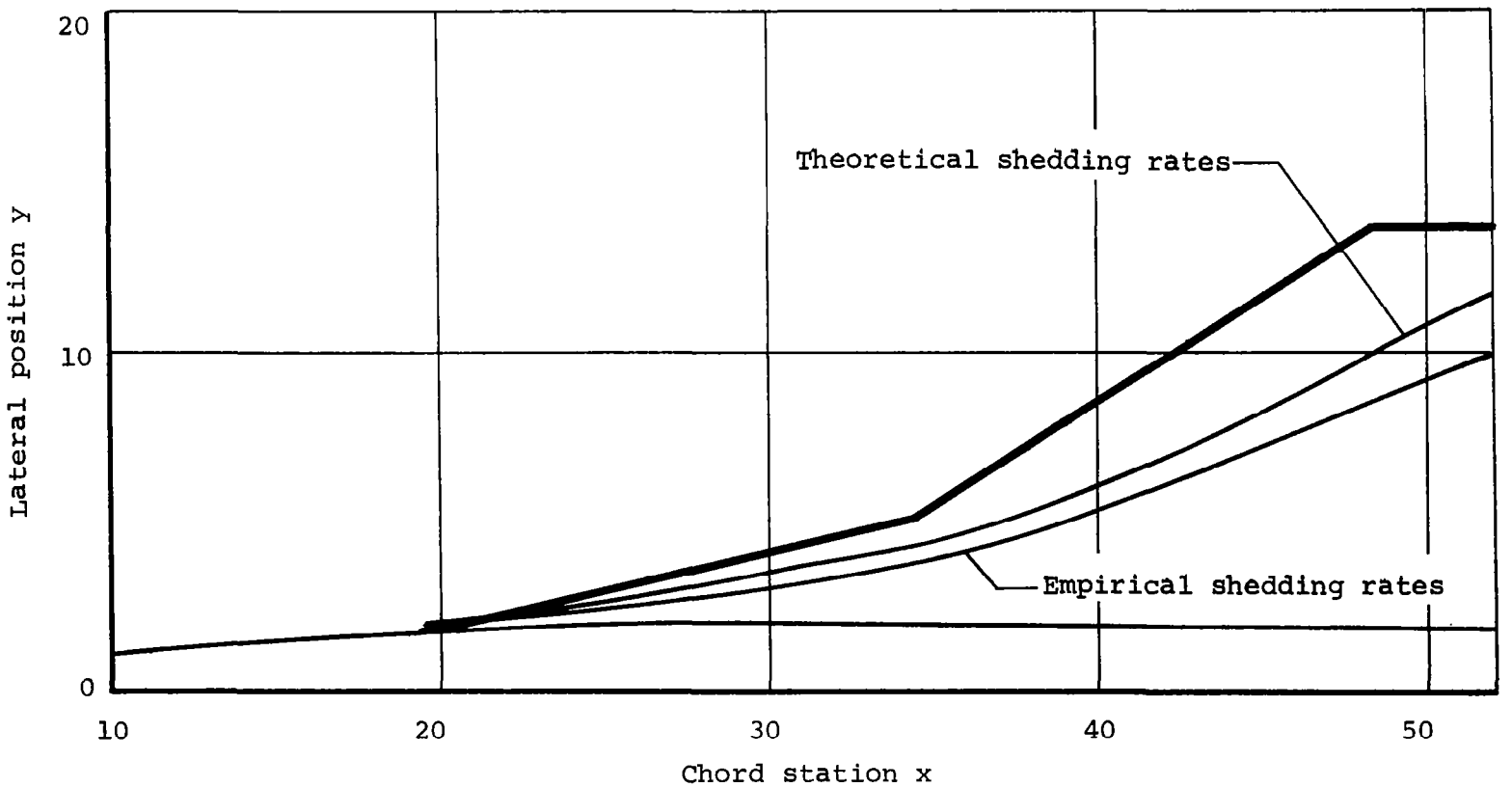

Figure 26.- Calculated lateral vortex center of gravity positions over double-delta wing at $\alpha = 15^{\circ}$.